ABSTRACT

Title of Document:	THE PHOTOCHEMISTRY OF POLYENYL RADICALS AND ITS APPLICATION TO UHMWPE FOR USE IN REPLACEMENT JOINTS
	Michael Jacob Kasser, Doctor of Philosophy, 2009
Directed By:	Professor Mohamad Al-Sheikhly, Department of Materials Science and Engineering

The use of UV light as an alternative to thermal treatments above the melting point (150 °C) to remove free radicals in irradiated UHMWPE was explored. It was found that, in contrast to the allyl free radical which is converted by 258 nm light to alkyl free radicals, polyenyl radicals are not converted to alkyl radicals by UV light. None-the-less, by sandwiching UV light treatments between low temperature thermal anneals (100 °C), it was possible to reduce free radical concentrations by 30%. This reduction was achievable for depths up to one millimeter. However, this reduction did not have a significant effect on oxidation due to an increase in oxidation susceptibility because of the concurrent increase in concentration of easily abstracted allylic hydrogens.

By photoirradiating for the optimal amount of time, it was possible, for the first time, to synthesize a polyethylene sample whose residual free radicals consisted

of almost entirely dienyl free radicals. This allowed unambiguous identification and simulation of dienyl free radical's EPR spectra to be a singlet containing nine peaks separated by 9 G hyperfine separation.

Detailed studies of photoirradiation of UHMWPE containing free radicals revealed that photoirradiation with a continuous spectrum above 200 nm causes the decay of diene unsaturations and allyl free radicals, a reduction in the overall amount of free radicals, and an increase in the degree of unsaturation of polyenyl free radicals. Upon longer photoirradiation times, polyenyl radicals were converted from lower to higher degrees of unsaturation. This effect was identical in the presence and absence of oxygen, but was suppressed by hydrogen gas. These results showed that the conversion does not occur by a linear alkyl radical addition mechanism wherein alkyl radicals migrate to stable polyene unsaturations and polyenyl radicals thereby increasing their order, as previously suggested. The valid mechanism appears to be the direct photoconversion of diene unsaturations to dienyl radicals and lower order polyenyl radicals to higher order polyenyl radicals.

THE PHOTOCHEMISTRY OF POLYENYL RADICALS AND ITS APPLICATION TO UHMWPE FOR USE IN ARTIFICIAL CARTILAGE

By

Michael Jacob Kasser

Dissertation submitted to the Faculty of the Graduate School of the
University of Maryland, College Park, in partial fulfillment
of the requirements for the degree of
Doctor of Philosophy
2009

Advisory Committee:
Professor Mohamad Al-Sheikhly, Chair
Professor Robert Briber
Associate Professor Srinivasa Raghavan
Professor Peter Kofinas
Professor Lourdes Salmanca-Riba
Professor Emeritus Joseph Silverman

Dedication

I would like to dedicate my dissertation to my wife, Shira, the mother of my children. I am fortunate to have someone so wise, caring, and helpful in my life. Without her constant support, feedback, and encouragement I would not have been able to complete my experiments or dissertation. “Sheli veshelcha, shelach hee.”

Acknowledgments

I would like to thank the many people who made this dissertation a reality. First and foremost, I would like to thank God for giving me the wisdom and perseverance to finish the job at hand. I would like to thank my advisor, Dr. Al-Sheikhly for his guidance, feedback, and criticism. His direction allowed me to complete my Ph.D. in a timely manner. I would like to thank Dr. Silverman who, despite being retired, always seems to be around to provide excellent perspective and guidance. I have benefited tremendously from the many discussions I have had with him. I would like to thank Mr. Vincent Adams for his technical help and expertise designing and performing experiments. I would also like to thank Dr. Alia Weaver. Her mentoring and assistance allowed me to become familiar with much of the equipment required to perform my experiments. I would like to thank Mrs. Amanda Forster for helping our lab acquire and giving access to much of the equipment required in my experiments. I would also like to thank Ali Mohamad for teaching me how to use MCNP5. I would also like to thank Biomet for providing the medical grade UHMWPE used in all of my experiments. Finally, I would like to thank my wife for her constant encouragement and support.

Table of Contents

List of Tables

List of Figures

Chapter 1: Introduction

Ultrahigh molecular weight polyethylene (UHMWPE) was first introduced in artificial joints by Sir John Charnley in the 1960s. Since then, a metal femoral bone stent articulating against a UHWMPE artificial cartilage has become the system of choice for artificial hips and knees. A schematic of these artificial joints can be seen in Figure 1[1] and Figure 2[2]. With correct implantation, the artificial joint can remove pain and restore mobility for arthritic patients. Currently, around one million total joint replacements, accounting for 1.8 billion dollars, occur annually world-wide[3-5], and this number is expected to continue to rapidly increase[6]. The average survivorship for implants is 75% at 25 years, although these numbers are lower for younger patients[3-5]. None-the-less, as implant reliability has improved, orthopedic surgeons have started to opt for joint replacement in younger, more active patients. This has created a need for implants that last longer, even under more challenging loading conditions, than traditional implants.

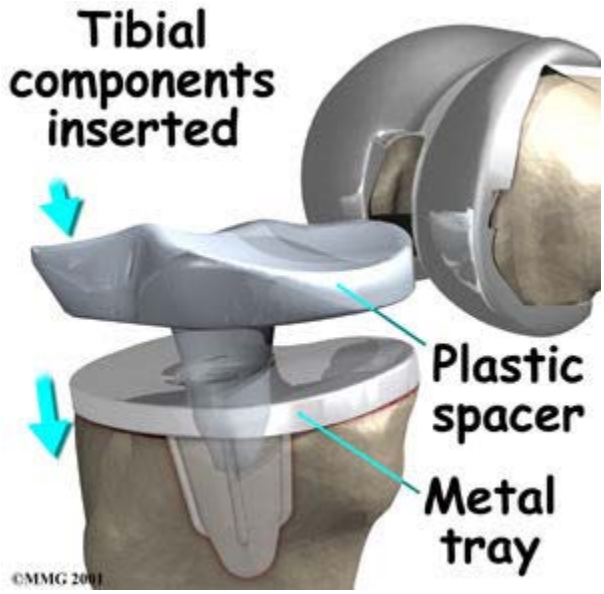

Figure 1. A schematic drawing of an artificial knee. The UHMWPE tibial tray is sandwiched between a metal tray and a metal capped femur.

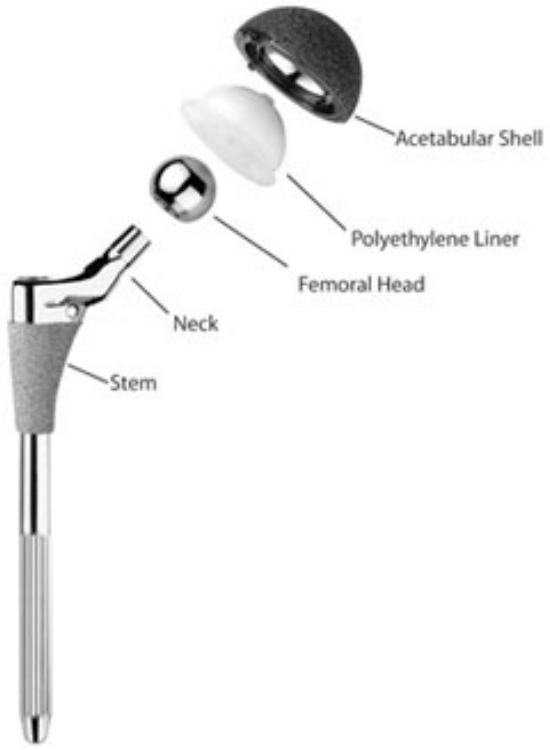

Figure 2. Parts of an artificial hip. A metal stem which is inserted into the femur ends with a metal femoral head that articulates against a hemispherical UHMWPE acetabular liner. The liner is often encased in a metal shell which is a attached to the hip bone.

1.1 Why UHMWPE?

UHMWPE is the material of choice in total joint replacement and is used in almost all knee replacements and the vast majority of hip replacements. Contemporary joint arthroplasty, wherein both sides of the joint are replaced by an engineered material, i.e. the bone is replaced by a metal and the cartilage is replaced by a plastic, was initially developed in the 1950's by Charnley[5]. Initially, polytetraflouroethylene was used because of its chemical inertness and low friction coefficient. However, these devices commonly failed within one to two years due to excessive creep deformation and wear[7]. UHMWPE was then tested because it exhibited excellent creep and wear resistance. The first hip prosthesis made from UHMWPE was implanted in 1962. Since then, it has become the material of choice in replacement joints due to its good biocompatibility, excellent creep and fatigue resistance, low friction coefficient, and high elastic modulus and wear resistance. However, UHMWPE can not be melt processed and parts must be machined. Therefore, in the 1970s and 1980s polyacetal (Delrin) liners, which can be injection molded and have a higher modulus of elasticity, were investigated. However, while their short-term results (5 years) were promising, significantly higher long-term failure rates were observed and their use was discontinued by the mid 1980s[7].

Other attempts to improve upon UHMWPE have included carbon-fiber-reinforced UHMWPE (Poly Two) and hot, isostatic pressed UHMWPE (Hylamer) which had an increased crystallinity content. These materials appeared promising because they had higher modulus of elasticity. However, Poly Two failed quickly *in vivo* via fatigue cracking because the carbon fibers served as stress concentrators and

crack initiation sites[5, 8]. Hylamer also performed poorly *in vivo* and exhibited higher wear rates than conventional UHMWPE, possibly due to increased susceptibility to oxidative degradation[5, 9].

While UHMWPE is essentially the only material used in replacement knees, other material systems, such as metal on metal and ceramic on ceramic, exist for replacement hips. Initially, these systems did not perform well due to poor manufacture or design. Recent improvements have shown that, when implanted correctly, these systems can work very well and exhibit extremely low wear rates[10]. However, their tolerances for misalignment are lower than UHMWPE[10], and they require more precise implantation. Additionally, use of metal on metal systems results in increased concentration of metal ions in the blood stream[11], the long-term affects of which are not completely known. Overall, the vast majority surgeons performing hip replacement surgery choose to implant a metal femoral head which articulates against an UHMWPE liner.

1.2 Structure of UHMWPE

UHWMPE is composed of extremely long, linear chains of saturated hydrocarbon whose moleuclar weight is between two to six million g/mol[12]. The chains often fold back on themselves forming crystals. However, due to the large number of physicals entanglements, not all of the chains can crystallize and UHMWPE's crystallinity ranges between 40-60%. These crystals are embedded in a matrix of amorphous polyethylene. Often, the long chains are stretched between two or more crystals, forming taut tie molecules. A schematic diagram of UHMWPE can be seen in Figure 3[13]. In general, UHMWPE excellent material properties are a result

of either its large molecular weight or its crystallinity. Excellent wear resistance and creep resistance are the result of the large molecular weight which results in many physical entanglements and tie molecules in the amorphous region. Crystallinity is responsible for the material's Young's modulus, and blunting fatigue cracks[14].

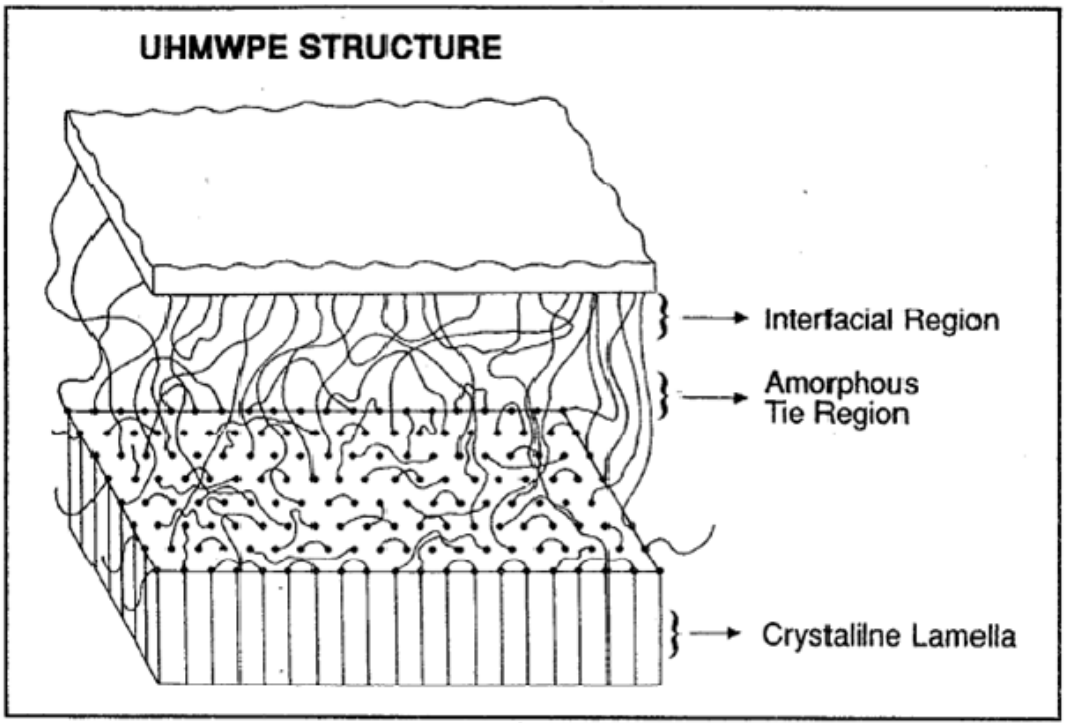

Figure 3. The microstructure of UHMPWE. Chains of saturated hydrocarbon fold back on themselves to create crystal lamella, while the amorphous region remains disordered. Often, a single chain will travel from one crystal to another, forming a taut tie molecule. The surface of the crystal is composed of folded chains.

Chapter 2: History of UHMWPE as Artificial Cartilage

2.1 Gamma Sterilization in Air and Subsequent Oxidation

Traditionally, UHMWPE liners were sterlized in air by gamma radiation from a ^{60}Co source and then stored in air permeable packaging. However, lack of reliability caused this practice to be exmained, and it was discovered that gamma sterlization and shelf-aging causes UHMWPE to oxidize[15-18], which dramatically reduces its wear and fatigue resistance[19-22]. The oxidation process is quite complex and not fully understood. Contrary to expectation, the peak oxidation level does not occur at the surface, but rather, it occurs one half to two millimeters below the surface in retrieved or shelf-aged implants. This can be particularly detrimental to tibial inserts whose peak loads occur one to two millimieters below the surace[23]. This complex oxidation profile can not be reproduced via accelerated aging unless increased levels of oxygen, typically five atmospheres, as well as increased temperatures are used[5, 24]. The oxidation profile is known to be a function of absorbed dose, dose rate, aging time, and concentration of oxygen during and after irradiation[15, 18, 21, 25]. The oxidation products include ketones, hydroperoxides, aldehydes, carboxylic acids, and alcohols[26-28]. At body temperatures, the hydroperoxides may be unstable and decompose into free radicals, creating a cascade oxidation process whose oxidation rate increases with time[20, 22]. Many models have been developed to explain the oxidation behavior[15, 21, 24, 29-31], but none are fully accepted. However, it is clear that oxidation results in chain scission which dramitically reduces the material properties of UHMWPE. Thus, it is well accepted that oxidation must be avoided or minimized.

2.2 Radiation Chemistry of Polyethylene

In order to avoid oxidation, manufacturers switched to sterlizing components with gas plasma or ethylene oxide. However, these components had higher wear rates because they lacked an unintended benefit of gamma sterlization, radiation-induced crosslinking which improves wear resistance[32-34]. When polyethylene is subjected to ionizing radiation, ions and exited states are formed[35],

$$PE \rightarrow PE^{+\bullet} + PE^{+*\bullet} + e^{-} + PE^{*} + PE^{**} \quad (2.1)$$

where PE is normal polyethylene, $PE^{+\bullet}$ is the polyethylene cation, $PE^{+*\bullet}$ is the excited cation, e^{-} is a free electron, PE^{*} is electronically excited polyethylene, and PE^{**} is superexcited polyethylene. Neutral free radicals are formed via the reactions

$$PE^{+\bullet} + PE \rightarrow PE^{\bullet} + PEH^{+} \quad (2.2)$$

$$PE^{**} \text{ or } PE^{*} \rightarrow PE^{\bullet} + H^{\bullet} \quad (2.3)$$

$$PE^{**} \text{ or } PE^{*} \rightarrow PE^{\bullet} + PE^{\bullet} \quad (2.4)$$

where $PE^{\bullet}$ is an alkyl radical and $H^{\bullet}$ is a hydrogen atom. The hydrogen atom can abstract another hydrogen from a nearby chain, resulting in an alkyl radical and hydrogen gas.

$$H^{\bullet} + PE \rightarrow H_2 + PE^{\bullet} \quad (2.5)$$

Cations can also decay via dissociation

$$PE^{+\bullet} \text{ or } PE^{+*\bullet} \rightarrow (PECH\text{-}CHPE)^{+\bullet} + H_2 \quad (2.6)$$

or by recombination with an electron.

$$PE^{+\bullet} + e^{-} \rightarrow PECH{=}CHPE + H_2 \quad (2.7)$$

Additionally, the cation resulting from dissociation can recombine with an electron

$$(\text{PECH-CHPE})^{+\bullet} + e^{-} \rightarrow \text{PECH=CHPE}\,, \tag{2.8}$$

where PECH=CHPE is a *trans*-vinylene unsaturation. Conjugated diene unsaturations are also formed as a direct radiolytic product[36]. Overall, upon irradiation with ionizing radiation, alkyl free radicals, *trans*-vinylene unsaturations, diene unsaturations, and hydrogen gas are formed[37-39]. The alkyl free radicals are unstable and quickly migrate via a hydrogen hopping mechanism[40, 41]. They can decay via one of three mechanisms: (1) two alkyl radicals on the same chain recombine, forming a *trans*-vinylene unsaturation, i.e. intramolecular recombination,

$$\text{PE}^{\bullet} + \text{PE}^{\bullet} \rightarrow \text{PECH=CHPE} \tag{2.9}$$

(2) two alkyl free radicals on adjacent chains recombine, forming a crosslink, i.e. intermolecular recombination,

$$\text{PE}^{\bullet} + \text{PE}^{\bullet} \rightarrow \text{PE-PE} \tag{2.10}$$

or (3) the alkyl radical migrates to an allylic position of an unsaturation, forming an allyl free radical if it is a vinylene[42],

$$\text{PE}^{\bullet} + \text{PECH=CHPE} \rightarrow \text{PE} + \text{PEC}^{\bullet}\text{HCH=CHPE} \tag{2.11}$$

or forming a polyenyl free radical if it is a polyene unsaturation. A schematic diagram of the alkyl, allyl, and polyenyl free radicals can be seen in Figure 4. While it is believed that radiation produces free radicals throughout the entire polymer, since the spacing between chains in the crystalline region (4.1 Å) is significantly larger than the carbon-carbon bond length (1.5 Å), crosslinking in the crystalline region is not favored[43]. While some alkyl free radicals form allyl free radicals in the crystalline region[44], most of the alkyl free radicals migrate to the crystal surface[45, 46] where they can also form crosslinks. Allyl and polyenyl free radicals are significanly more stable

than alkyl free radicals due to resonance stablization[47]. None-the-less, they do slowly decay over a period of months and years[47-49].

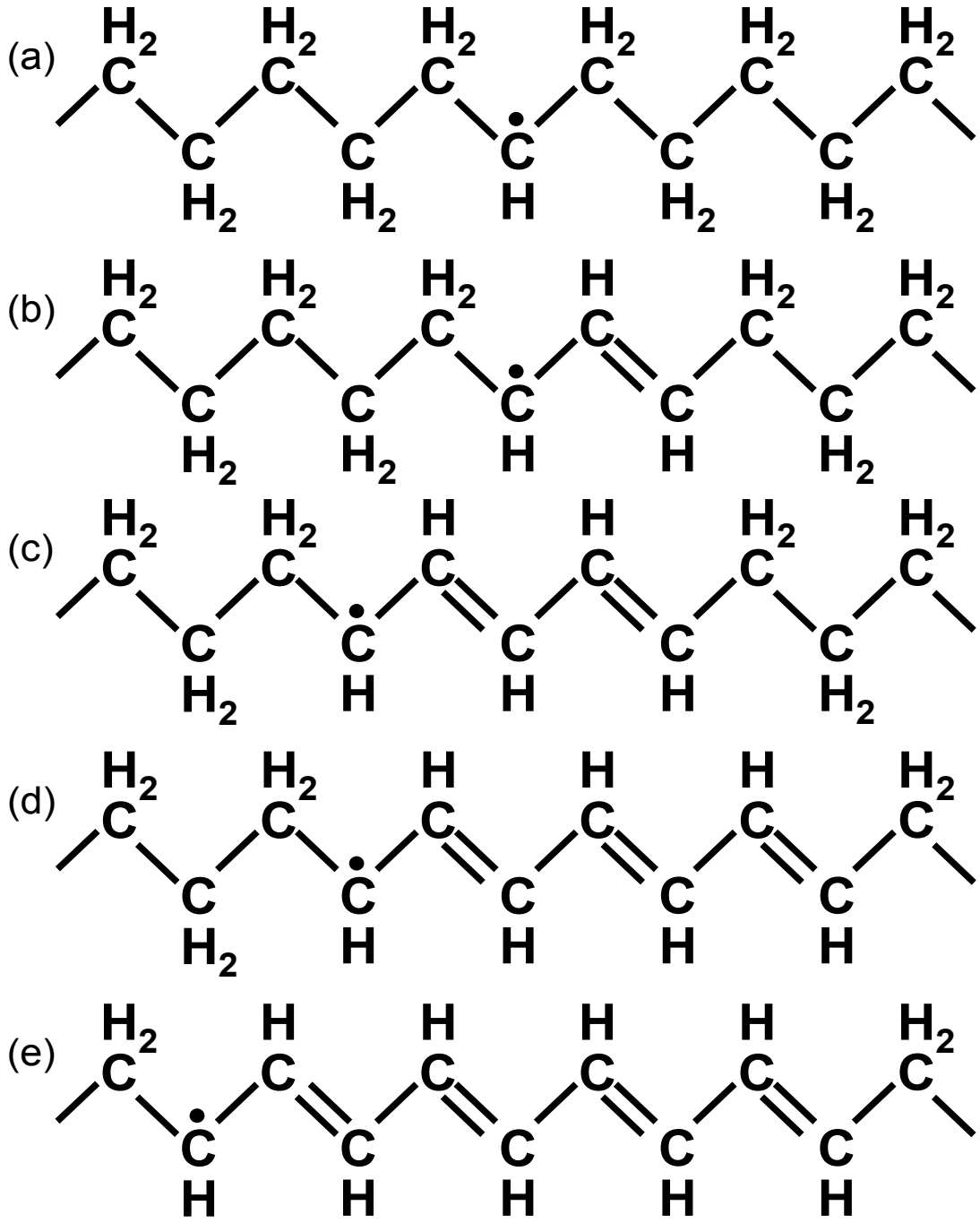

Figure 4. Schematic drawing of the (a) alkyl, (b) allyl, (c) dienyl, (d) trienyl, and (e) tetraenyl free radicals.

2.2.1 The Need to Avoid Oxygen

The above paragraph has assumed that there is no oxygen present at the time of irradiation. In the presence of oxygen, the alkyl, allyl or polyenyl radicals will quickly combine with oxygen, forming a peroxyl free radical.

$$PE^{\bullet} + O_2 \rightarrow PEO_2^{\bullet} \quad (2.12)$$

This reaction is extremely fast, with a measured reaction constant of 1.3×10^{-3} L mol^{-1} s^{-1} [29]. The peroxyl can abstract a hydrogen from a nearby chain forming a hydroperoxide and an alkyl free radical.

$$PEO_2^{\bullet} + PE \rightarrow PEOOH + PE^{\bullet} \quad (2.13)$$

This reaction is expected to be considerably slower since its gas phase reaction constant is 10^{10} times smaller than reaction (2.12)'s gas phase reaction constant[50]. This process will continue until the peroxyl free radical recombines with another peroxyl or with a carbon-centered free radical. It has been estimated that, in the presence of oxygen, one free radical generates 12 carbonyl and five hydroxy groups before decaying[51].

2.3 Crosslinked UHWMPE

In order to achieve the improved wear resistance that crosslinking provides without suffering the decrease in material properties that results from oxidation, manufactures have started to irradiate UHMWPE in an oxygen free environment and then subject it to a thermal treatment that removes or dramatically reduces free radicals. Various crosslinked acetabular liners were clinically introduced in 1998 and 1999[12, 52], but crosslinked tibial inserts have not seen widespread clinical use. The explanation why requires some background about artificial hip and knee failure

mechanisms as well as an understanding of the effect of crosslinking followed by thermal treatment on fatigue resistance.

2.3.1 Artificial Hip Failure Mechanism

Aseptic loosening of the acetabular liner secondary to wear is, by far, the most common failure mode for artificial hips[4, 53]. Finite element analysis has shown that the largest shear stresses occur at the surface of the liner[54]. Due to the combination of flexion/extension and abduction/adduction movements, these stresses are multidirectional, although the flexion/extension stresses are significantly higher than the abduction/adduction stresses[55]. The resulting plastic deformation causes the initially randomly oriented lamellae to align parallel to the major stress direction[56, 57]. While this strain hardens the material in the direction of primary loading, it softens the material in the perpendicular direction[58], leaving it susceptible to wear. SEM micrographs of the wear surface of UHMWPE liners run in hip simulators have shown that plastic deformation causes the formation of strain hardened fibrils perpendicular to the major loading direction[59]. Subsequent loading from the perpendicular direction cause the fibrils to break off, creating wear debris. Since the body can only slowly remove the wear particles, if the wear rate is sufficiently high, the wear debris can reach a critical concentration of 10 billion particles per gram of tissue[4]. This concentration triggers an autoimmune response which recruits osteoclasts that break up the bone opposite the liner. The replacement hip fails when enough bone is replaced with fibrous tissue, resulting in the loosening of the acetabular liner[60, 61].

2.3.2 Artificial Knee Failure Mechanism

The most common failure mode for artificial knees is fatigue cracking. Unlike hips, finite element analysis has shown that the peak stresses in knees occur one to two millimeters subsurface[62, 63]. Further, unlike hips that have conformal wear surfaces, the wear surfaces in knees are much less conforming and the applied load is distributed along a much smaller area[64]. This means that the stresses in knees are significantly larger than those in hips. These stresses are well above the yielding stress of UHMWPE and result in plastic deformation. One mode of plastic deformation is lamellar separation, a schematic of which is depicted in Figure 5[14]. Large strains cause the lamellae to continue to separate, rupturing the tie molecules and creating microvoids[65]. Subsequent perpendicular stresses cause the microvoids to propagate, forming fatigue cracks parallel to the surface. Eventually, the crack turns a corner and large pieces of the liner delaminate. While fatigue delamination is the primary failure mechanism, surface wear is still a concern and improved wear resistance is desired.

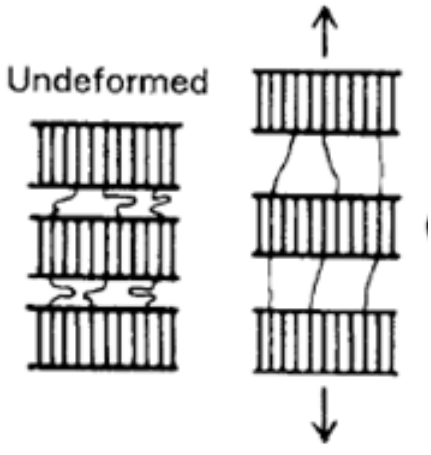

Figure 5. Schematic drawing of lamellar separation.

2.3.3 The Effect of Crosslinking on Wear and Fatigue Resistance

An effective way to reduce wear is to crosslink the implant. This improves wear resistance because the crosslinked amorphous region is much more rigid and prevents the lamellae from aligning[32, 34]. However, there are also some drawbacks to crosslinking. The most significant drawback is that it reduces fatigue resistance. This reduction is the combination of two factors, the latter of which is much more significant. First of all, crosslinking has made the amorphous region of the polymer more rigid[66]. Secondly, melting the polymer after crosslinking significantly reduces its crystallinity. This occurs because the crosslinks formed at the surface of the premelt crystals lock in place the chains that were previously in the crystal and do not allow them to recrystallize after melting[67]. Since most plastic deformation takes place in the crystalline region[68], less stress energy is being dissipated via plastic deformation and more stress energy goes into crack propagation[69]. The reduction in fatigue resistance has prevented the widespread use of crosslinked liners in artificial knees. Another drawback to crosslinked liners is that they are more rigid, and hence, less forgiving of misalignment than conventional liners. This may lead to increased rates of impingement and dislocation failures[70].

2.3.4 Crossfire Liners

One attempt to improve wear resistance without degrading fatigue resistance is *Crossfire* acetabular liners manufactured by Stryker. Instead of annealing the polymer above its melting temperature, an anneal at 120 °C which is slightly below the melting temperature is used. This reduces the free radical concentration to about 10% of the starting free radical concentration with only a small reduction in

crystalline content corresponding to the melting of small crystals[71]. While significant oxidation has been observed during accelerated oxidation tests[71] and *in vivo* service[72], this has not affected their short and medium term performance[73]. It remains to be seen if it will have deleterious long term effects.

2.4 Surface Modification of UHWMPE

One way to improve wear resistance without compromising fatigue and oxidation resistance comes from the realization that fatigue resistance is a bulk property while wear resistance is a surface property[74, 75]. Thus, if one would crosslink only the surface of the liner, the surface would have improved wear resistance while the bulk would maintain its fatigue resistance. Practically, this is easily achieved by irradiation with low energy (<1 MeV) electrons.

2.4.1 Surface Modification Required Depth

Since fatigue cracks are known to form one to two millimeters below the surface, it is clear that the electron's penetration depth should be less than one millimeter, but it is unclear exactly how deep the penetration depth should be. Determining the depth requires knowing the annual wear rate of highly-crosslinked UHMWPE and multiplying it by the expected service lifetime. Unfortunately, the wear rate of crosslinked UHMWPE is largely unknown. Many wear tests on hip simulators have given negative wear rates for highly-crosslinked liners[32, 53, 76], while other have not[34, 77]. This discrepancy likely arises from the fact that most wear measurements are gravimetric and there is an inability to accurately correct for lubricant absorption during the wear test. Measured *in-vivo* short- and medium-term

wear rates are quite varied, which is a result of a combination of factors. *In-vivo* wear measurements are performed by comparing a successive series of x-rays and measuring the penetration of the femoral head into the liner over time. Unfortunately, different doctors use differing measurement techniques (manual, computer-assisted, and radiostereometry). It is also difficult to compare one x-ray to another due to differences in patient position, exposure dose, and other factors at the time of the x-ray[73]. Most importantly, this technique measures the combination of creep and wear, and short-term studies are often inaccurate due to an inability to correct for the "bedding-in" effect that occurs over the first two years of implantation. While medium-term studies are long enough that they do not need to use penetration data from the first two years, it is still not clear if penetration during later years is a result of wear or of plastic deformation. For example, it has been shown that surface scratches on retrieved crosslinked components can be removed by melting, indicating that they are a result of plastic deformation, not wear[78]. Indeed, an experimentally validated wear model[79], as well as hip simulator experiments[34], predict that there will be no wear when there is sufficient crosslinking to reduce the molecular weight between crosslinks to less than 4000 g/mole. None-the-less, studies with a mean length of four or more years that did not use the penetration data from the first year have an average wear rate around 0.019 ± .055 mm/y with a range of 0.01 to 0.036 mm/yr[80-83]. As explained above, the lower values are likely to be more accurate, and I believe a predicted wear rate of 0.01 mm/yr to be reasonable. Given this wear rate, a liner whose surface has been crosslinked to a depth of half of a millimeter should last 50 years.

2.4.2 The Drawback of Surface Modification

Unfortunately, surface modification has a serious drawback. Due to the fact that only the surface of UHMWPE is modified, the liner must be machined to its final geometry before irradiation. If the free radicals remaining after irradiation are eliminated by heating the liner to above its melting temperature, as is usually done, upon cooling, the liner will likely deform from its initial shape due to residual stresses created during ram extrusion of bar stock. While this effect can be reduced by melting the bar stock before machining the liner, it can not be fully mitigated. Since UHMWPE implants need to be machined to tight tolerances, an alternative method to remove free radicals is required. This dissertation explores the possibility of using ultraviolet light photoirradiation as an alternate method to eliminate free radicals. A literature search has not revealed any previous attempt to use UV light to remove free radicals from polyethylene.

Chapter 3: Using Ultraviolet Light to Eliminate Free Radicals

3.1 Background

Due to resonance stabilization with an adjacent double bond, the unpaired electron in the allyl free radical is delocalized over three carbon atoms. In its ground state, the π-orbital electronic configuration of the allyl radical is $(b_1)^2(a_2)$, where b_1 is the bonding orbital and a_2 is the non-bonding orbital. It has been experimentally determined[84] that the allyl radical can be excited either by promoting a bonding electron, b_1, to a non-bonding orbital, a_2, or by promoting the non-bonding electron to the higher antibonding orbital, $\bar{b}_1$. These two transitions are depicted in Figure 6[84]. The transfer of the unpaired electron from a non-bonding orbital to an antibonding orbital requires about five eV, corresponding to a photon wavelength of 258 nm. The result of this transition is that the unpaired electron is no longer trapped in the allylic site[85] (reaction 3.1).

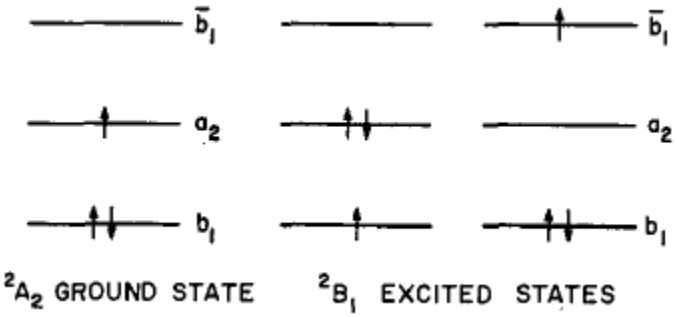

Figure 6. Simple π orbital molecular diagram for the allyl radical in its ground and excited states.

$$\sim CH_2\text{-}C^{\bullet}H\text{-}CH{=}CH\text{-}CH_2 \sim \xrightarrow{258nm} \sim CH_2\text{-}C^{\bullet}H\text{-}CH_2\text{-}CH{=}CH\text{-}CH_2 \sim \quad (3.1)$$

The transfer of a paired electron to a non-bonding orbital requires around three eV, which corresponds to a wavelength of 365 nm. The result is that the allyl radical disassociates[85].

$$\sim CH_2\text{-}C^{\bullet}H\text{-}CH{=}CH\text{-}CH_2 \sim \xrightarrow{365nm} \sim CH_2\text{-}C^{\bullet}H_2 + CH{=}CH\text{-}CH{=}CH\text{-}CH_2 \sim \qquad (3.2)$$

Ohnishi *et al.* experimentally observed reaction (3.1) by photoirradiating HDPE at liquid nitrogen temperatures with an unfiltered mercury lamp[86], while Shimada *et al.* experimentally observed reaction (3.2) by photoirradiating through a filter that removed wavelengths shorter than 360 nm[87]. Although not directly observed, it has been calculated by comparison of bond energies that, at the appropriate wavelengths, a similar transition to reaction (3.1) is energetically favorable for most (tetraenyl and lower) polyenyl radicals[88].

$$\sim CH_2\text{-}C^{\bullet}H\text{-}(CH{=}CH\text{-})_n CH_2 \sim \rightarrow \sim CH_2\text{-}C^{\bullet}H\text{-}CH_2\text{-}(CH{=}CH\text{-})_n CH_2 \sim \qquad (3.3)$$

The appropriate wavelengths have been determined by Bodily and Dole who reported ultraviolet absorption maxima for the allyl, dienyl, trienyl, tetraenyl, and pentaenyl free radicals[84-86] . Additionally, Waterman and Dole later reported approximate values of the molar absorptivity for the allyl and dienyl free radicals[89]. A table of ultraviolet absorption maxima for several free radicals and unsaturations can be found in Table I. In the work of Ohnishi and Dole, it was found that upon being warmed to room temperature, many of the photogenerated alkyl radicals decayed by migrating back to the allylic position of an unsaturation (the back reaction of (3.1)), but, overall, the amount of free radicals decreased, i.e. some of the alkyl radicals decayed by recombination or disproportionation.

Additionally, significant amounts of diene unsaturations were consumed and higher order polyene unsaturations and polyenyl radicals are produced during photoirradiation[36, 86]. This strongly suggests the following proposed[90, 91] reaction mechanism of the linear addition of alkyl radicals:

$$\begin{aligned}
&\sim CH_2\text{-}C^{\bullet}H\left(\text{-}CH_2\right)_a\text{-}C^{\bullet}H\text{-}\left(CH_2\right)_b\text{-}C^{\bullet}H\text{-}\left(CH_2\right)_c\text{-}CH{=}CH\text{-}CH{=}CH\text{-}CH_2\sim \rightarrow \\
&\sim CH_2\text{-}C^{\bullet}H\text{-}\left(CH_2\right)_d\text{-}C^{\bullet}H\text{-}\left(CH_2\right)_e\text{-}C^{\bullet}H\text{-}CH{=}CH\text{-}CH{=}CH\text{-}CH_2\sim \rightarrow \\
&\sim CH_2\text{-}C^{\bullet}H\text{-}\left(CH_2\right)_f\text{-}CH{=}CH\text{-}CH{=}CH\text{-}CH{=}CH\text{-}CH_2\sim \rightarrow \\
&\sim CH_2\text{-}C^{\bullet}H\text{-}CH{=}CH\text{-}CH{=}CH\text{-}CH{=}CH\text{-}CH_2\sim
\end{aligned} \tag{3.4}$$

where a through f are positive integers. In the first step of this reaction, an alkyl radical migrates to the allylic site of a diene unsaturation, converting the diene unsaturation into a dienyl radical. In the next step, another alkyl radical intramolecularly recombines with the dienyl radical, resulting in a triene unsaturation. This process repeats in the next step wherein another alkyl radical migrates to the allylic position of the triene, converting it to a trienyl radical. This process can continue, converting lower order polyene unsaturations and polyenyl radicals into higher order groups.

These results suggest the use of UV light to reduce the free concentration in UHMWPE. Stable allyl and polyenyl radicals can be converted into unstable alkyl radicals. These radicals can then decay intermolecularly to produce crosslinks or intramolecularly to produce higher order unsaturations via reaction (3.4). Since reaction (3.4) is of central importance, it will now be discussed in greater depth.

Number	**Polyenes**	λ_{max}, nm	**Polyenyls**	λ_{max}, nm
1	Vinylene	185	Allyl	258
2	Diene	229,236,245	Dienyl	285
3	Triene	264,275,288	Trienyl	323
4	Tetraene	310	Tetraenyl	359
5	Pentaene	340	Pentaenyl	396
0			Alkyl (secondary)	215

Table I: List of polyene unsaturation and polyenyl radical ultraviolet absorption maxima. Taken from [89].

3.2 The Alkyl Radical Addition Reaction Mechanism

For this reaction mechanism to be true, at first glance, several observable results should hold true: (1) there should be comparable concentrations of unsaturations and free radicals; (2) While the alkyl radical migration to the allylic site can occur either intra- or intermolecularly, the radical recombination to form a higher order unsaturation must occur intramolecularly (intermolecular recombination would result in the formation of a crosslink); (3) in order to increase the overall degree of conjugation of the system by one degree, the concentration of free radicals should be halved; (4) there should be a one-to-one correspondence between the decrease in unsaturations and increase in free radicals of the same degree, i.e. the decrease in diene unsaturation concentration should equal the increase in dienyl radical concentration. Conversely, there should be a one-to-one correspondence between the decrease in free radicals and an increase in unsaturations of one higher degree, i.e. the decrease in dienyl radical concentration should equal the increase in triene concentration. We will now examine these assumptions in more detail.

3.2.1 Free Radical and Unsaturation Concentrations

While reaction (3.4) seems to imply that similar concentrations of free radicals and unsaturations are to be expected, this need not be the case. Polyene unsaturations are transformed into polyenyl radicals via both the intra- and intermolecular migration of alkyl radicals, whereas polyenyl radicals are transformed into polyene unsaturations only via the intramolecular recombination of radicals. It is known that intermolecular migration is significantly faster than intramolecular migration, even in the crystalline region[92]. Therefore, in the presence of alkyl radicals, it is reasonable to expect polyenyl radicals to be much more stable than polyene unsaturations which would result in their having a significantly higher concentration than polyene unsaturations.

3.2.2 Intra- and Intermolecular Recombination

In order for a polyenyl radical to transform into an unsaturation of one higher degree, it must recombine with an alkyl radical intramolecularly. One may ask, if intermolecular recombination is so much faster than intramolecular recombination, why should this reaction occur at all instead of intermolecular recombination which results in crosslinking? There are at least two possible reasons why intermolecular recombination would be suppressed and intramolecular recombination would be enhanced. In order for two radicals to form a crosslink, they must get within 1.54 Å (the length of a carbon-carbon bond) of each other, which is often difficult due to steric hinderances[93]. It is for this reason that the presence of terminal unsaturations, such as vinyl or acetylene, which reduce the steric hindrances, dramatically enhance crosslinking[35, 94]. It is likely that the presence of the rigid double bond decreases the

free radical's flexibility which may increase steric hindrance and suppress crosslinking. It is also possible that intramolecular recombination is enhanced by the promotion of the π-electrons in polyene unsaturations and polyenyl radicals to an excited state by UV light.

3.2.3 Sources of Alkyl Radicals

Reaction (3.4) predicts a continuous decrease in the concentration of free radicals due to the intramolecular recombination of alkyl and polyenyl radicals. However, this assumes that there is a constant amount of alkyl radicals. If, instead, there would be continuous supply of alkyl radicals, the overall degree of conjugation of the system could increase without a significant change in the overall concentration of free radicals. It, therefore, becomes imperative to identify possible sources of alkyl radicals. One source is ionizing radiation, such as high energy electrons, which primarily results in alkyl radicals created via the breaking of carbon-hydrogen bonds. While most of these radicals quickly decay into crosslinks or form allyl radicals, some can still be present at the start of photoirradiation which usually took place around half an hour after the electron beam irradiation. Another source is the photoconversion of allyl radicals into alkyl radicals (reaction 3.1 and 3.2). Both of these sources are limited and will only be significant at the start of photoirradiation. A possible source of alkyl radicals is the photoconversion of polyenyl radicals to alkyl radicals (reaction 3.3), but this source would also be limited. Another source of alkyl radicals is the photodecay of oxidation products or peroxyl radicals. A schematic of these reactions can be seen in Figure 7. In the presence of air, alkyl and other carbon-centered free radicals quickly combine with oxygen to form peroxyl radicals. UV

light can reverse this process, converting a peroxyl radical back to alkyl radical, although chain scission occurs during this process[85, 88, 95, 96]. The peroxyl radical can abstract a hydrogen from a nearby polymer chain, resulting in a hydroperoxide and an alkyl radical. Hydroperoxides are known to be unstable under UV light photoirradiation, and decompose into alkoxy and hydroxy radicals[94, 95]. These radicals can then abstract a hydrogen from a nearby chain, resulting in the formation of water or alcohol, respectively. Thus, in the combined presence of UV light and air, one alkyl radical can result in the formation of three alkyl radicals. This reaction sequence can be responsible for a continuous creation of alkyl radicals when adequate oxygen is present. Additionally, if ketone groups are present, they will decompose under UV light, either via Norrish type I reaction, resulting in the formation of two alkyl radicals and carbon monoxide, or by the Norrish type II reaction, resulting in a main chain break and a vinyl group[97, 98].

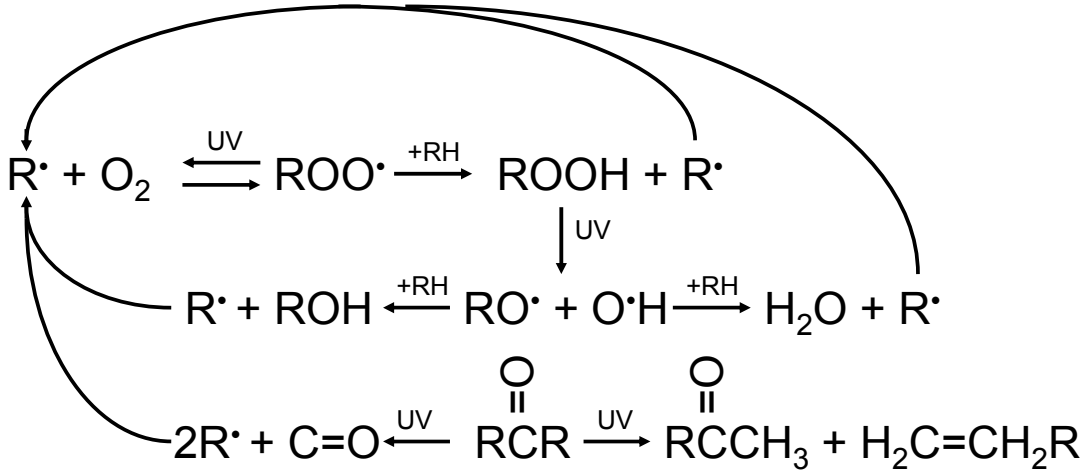

Figure 7. Possible pathways for the generation of alkyl radicals via the photodecomposition of oxidation products. Hydroperoxides photodecay into water, alcohol and two alkyl radicals. Ketones can decay via the Norrish type I reaction, generating two alkyl radicals, or via the Norrish type II reaction, resulting in main chain break and a vinyl group.

3.2.4 One-to-one Polyene/Polyenyl Conversion

Reaction (3.4) implies that there should be a one-to-one conversion of polyene unsaturations to polyenyl radicals and vice versa. In practice, this conversion may be difficult to observe for two reasons: (1) the molar absorptivity for many of these species is unknown; (2) most species are being simultaneously created and destroyed. These difficulties will be addressed when analyzing experiments.

3.3 Desired and Undesired Photoreactions

In order to achieve the minimum concentration of long-lived radicals while maintaining the mechanical properties, it becomes important to first clarify which reactions are desired and which reactions should be suppressed. While both reaction (3.1) and (3.2) will convert stable allyl radicals into unstable alkyl radicals, reaction (3.2) is less preferred because it results in chain scission which would degrade the mechanical properties of UHMWPE. Fortunately, unless lower wavelengths of light are filtered out, this reaction is not expected to play a major role because the allyl free radical's molar absorptivity at 285 nanometers, ~7000 M^{-1} cm^{-1} [85, 89], is significantly greater than its coefficient at 365 nanometers, ~25 M^{-1} cm^{-1} [99]. However, reaction (3.2), may be of interest since, unlike reaction (3.1) it does not result in the increase of higher order polyene unsaturations and polyenyl radicals[87].

The presence of oxygen or oxidation products should be avoided since, as discussed above, they generally result in the creation of more free radicals and main chain scission. However, unlike reaction (3.2), these reactions occur between 250 to 360 nanometers and have large absorptivities[85, 100, 101]. Thus, the only way to

minimize these reactions is to minimize the content of oxygen in polyethylene during electron beam and ultraviolet light irradiation.

Chapter 4: Methods

4.1 Materials

4.1.1 UHMWPE

All experiments were conducted using medical grade UHMWPE GUR1050 that was ram extruded into 1.75" diameter rods. These rods were then machined into smaller discs. According to the manufacturer, this batch of UHMWPE possesses a density of 931 kg/m^3 yield stress of 21.4 MPa, an ultimate tensile stress of 50.5 MPa, and an elongation at break of 362%. UHWMPE is defined by ASTM D4020 to have molecular weight of at least 3.1 million g/mole. The discs were usually microtomed, using a sledge microtome (Leica RM2255, Houston, TX), into films of 200-500 μm. When required, one millimeter films were created by polishing one side of the disc flat using 450 grit sandpaper and then machining excess material away using a milling machine. No cutting fluid was used during machining to avoid contaminating the sample. Instead, the sample was cooled by blowing compressed nitrogen to minimize oxidation during machining. The thickness of the films was measured using a digital thickness gauge (Mitutoyo, Aurora IL).

Films were annealed in a mechanical convection oven (GCA Model 18EM) which was retrofitted with a digital temperature control. In order to maintain an inert environment, the films were inserted into a glovebox filled with high purity nitrogen and sealed in packets of aluminized polyethylene.

4.1.2 Electron Beam Irradiation

Unless otherwise stated, all irradiations were performed using a 7 MeV electron beam at the University of Maryland, College Park. UHMWPE films were irradiated to a dose of 101 ± 4 kGy, at 60 pulses per second with an average dose per pulse of 8 – 10 Gy. Dosimetry, using calibrated Far West dosimeter films, was performed *in situ* using the following procedure. An initial dosimetry run, consisting of four films in a square configuration, was performed to determine the absorbed dose relationship between the films. An EPR tube containing an UHMWPE film was reproducibly positioned directly in front of one of the films (Figure 8). Absorbed dose in the UHMWPE film was then calculated by measuring the adjacent Far West film and assuming an identical dose relationship as measured in the dosimetry run. The 100 kGy dose was fractionated into three runs in order to increase the accuracy of dosimetry and to avoid substantial heating of the tube during irradiation. Preliminary experiments demonstrated that this procedure resulted in an increase in temperature of less than 10 °C.

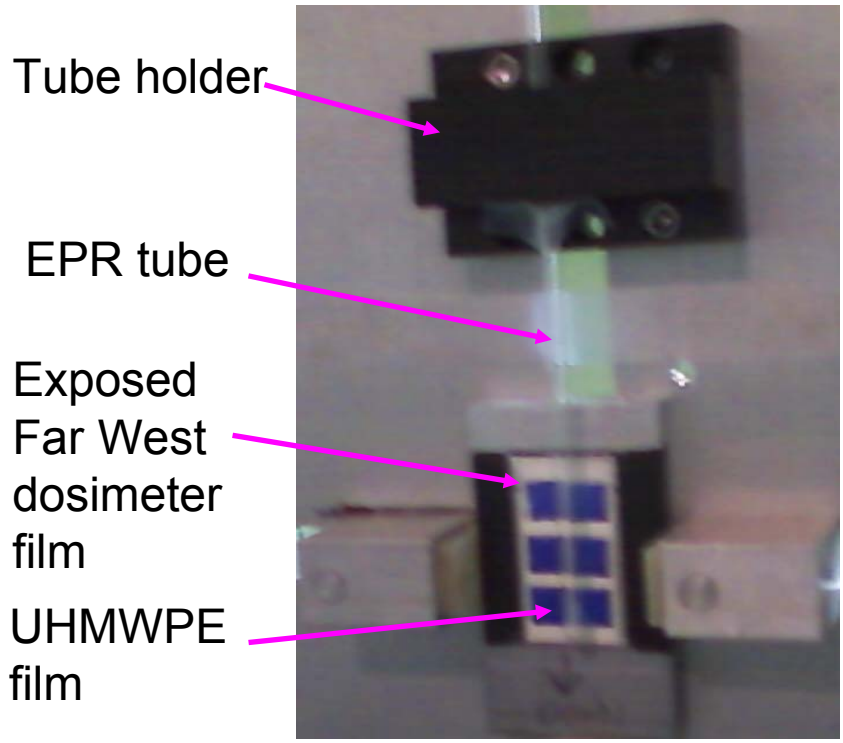

Figure 8. Dosimetry setup. An EPR tube containing an UHMWPE film is reproducibly positioned directly in front of a Far West dosimeter film. An irradiation without the tube is initially performed to determine the dose relationship between the films. Subsequent irradiations are performed with the tube in place and Far West films on only the left-hand position.

Irradiation environment was controlled by varying the environment in the EPR tube containing the UHMWPE film. For nitrogen irradiations, the film and a resealable EPR tube (J-Young EPR tube, Wilmad Labglass, Buena, NJ) were loaded into a glovebox filled with high purity nitrogen gas (Airgas, Hyattsville, MD). The film was inserted into the tube and the tube was sealed while in the glovebox. For a hydrogen environment, a regular suprasil tube containing a film was evacuated overnight to 10^{-8} torr, backfilled with hydrogen gas to 150 torr, and then flame sealed. Following irradiation, the sample was inverted and the tip of the EPR tube was annealed with a propane torch until it glowed red, removing the free radicals created in the tube during irradiation. Preliminary experiments demonstrated that no measurable increase in temperature occurred in the other end of the tube containing

the sample. Subsequent reversion transferred the sample to the tube's radical-free tip which was later inserted into the EPR cavity for measurement.

4.1.3 Electron Penetration Depth as Determined by Monte Carlo Simulations

As mentioned in section 2.4.1, an irradiation depth of 0.5 millimeters is desired in order to improve the wear resistance without adversely affecting fatigue resistance of UHMWPE. The question arises as to what electron energy and sample orientation should be employed to achieve the desired penetration depth. When penetrating a dense medium, high energy electrons lose energy via elastic and inelastic collisions with nuclei and bound electrons. During this process, photons and ionized electrons are created. Photons (whose yield is small and whose mean free path is many times that of the electrons) primarily interact with matter via Compton scattering, the photoelectric effect, and pair production. Which interaction occurs is probabilistic in nature but depends on many factors including the incident particle's energy and trajectory. Therefore, the penetration depth of high energy electrons in a material is a statistical problem that is well suited to be solved via the random sampling methods employed by Monte Carlo simulations. Essentially, the computer tracks an incident electron's history by selecting what interactions occur via randomly generated numbers that are weighted to correspond to the probability of the interaction. This process is repeated a large number of times until a statistically meaningful tally is obtained.

Monte Carlo simulations were performed using Monte Carlo N-Particle[1*], to optimize incident electron energy and sample orientation. Simulations showed that

[1*] X-5 Monte Carlo Team, MCNP- A General Monte Carlo N- Particle Transport Code, Version 5, LA-UR-03-1987, Los Alamos National Laboratory, April 2003.

the desired absorbed energy profile could be obtained using a monoenergetic 330 keV electrons and a plane sample orientation. The simulations were then experimentally validated by irradiating a stack of alternating 50 μm UHMWPE films and 50 μm Far West dosimeter films. This allowed two, independent dosimetry methods, Far West film dosimetry and *trans*-vinylene content (ASTM F2381), to be used. Irradiations were performed at NIST using monoenergetic van der Graaff machine. A comparison of experimental and simulation results can be seen in Figure 9. All results are in good agreement. The gradual decrease in absorbed dose may have the added benefit that it will minimize internal stresses resulting from differing mechanical properties of the crosslinked and non-crosslinked UHWMPE[102].

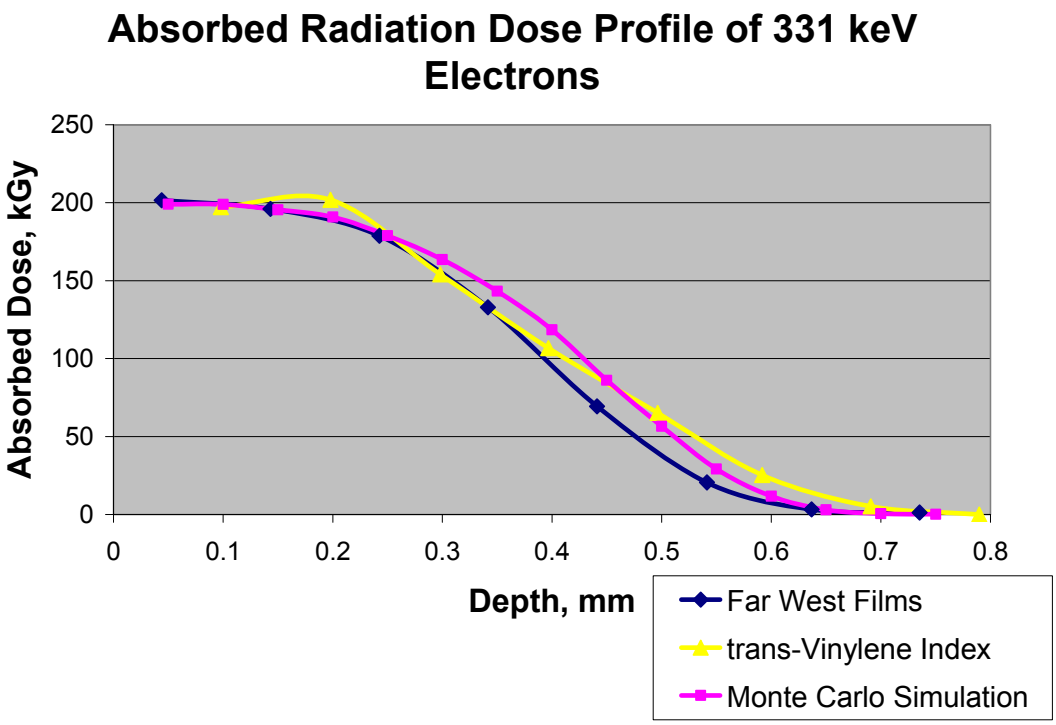

Figure 9. Comparison of the absorbed radiation dose profile as measured by Far West Films, trans-vinylene concentrations, and predicted by Monte Carle simulations. Both the trans-vinylene measurements and Monte Carlo simulation were normalized to a known dose as measured by Far West dosimeter films. Measurements were made by irradiating a stack of

alternating Far West films and 50 micrometer UHMWPE films with a monoenergetic 331 keV electron beam.

4.1.4 UV Lamp

A 325 W short arc xenon lamp (Schoeffel Instruments Corp., Westwood, NJ) was used as an ultraviolet light source. Unless otherwise noted, the distance between the lamp to the sample was around 44 cm. This lamp emits a continuous spectrum from the ultraviolet to the infrared. Initially, the spectral output of the lamp was characterized using a monochromator and a photodetector (Kratos Analytical GM252, Manchester, U.K.). However, since the photodetector was not calibrated, it could only give the relative spectral distribution. In order to measure absolute energy output of the lamp, a calibrated Blak-Ray UV meter (Blak-Ray Model J221, Upland, CA), which detects light between 300-390 nm, was used. Due to the high intensity of the lamp, a neutral density filter that reduces the light to about one fifth needed to be used. After correcting for the meter's wavelength sensitivity as provided by the manufacturer, the lamp's absolute output between 300-390 nm at 44 cm was measured to be 5200 ± 340 $\mu W/cm^2$. This is an average of three separate measurements. This value was then used to back-calculate absolute output at other wavelengths (Figure 10). When lower light fluxes were required, a lower power compact short-arc xenon lamp (ILC) was used.

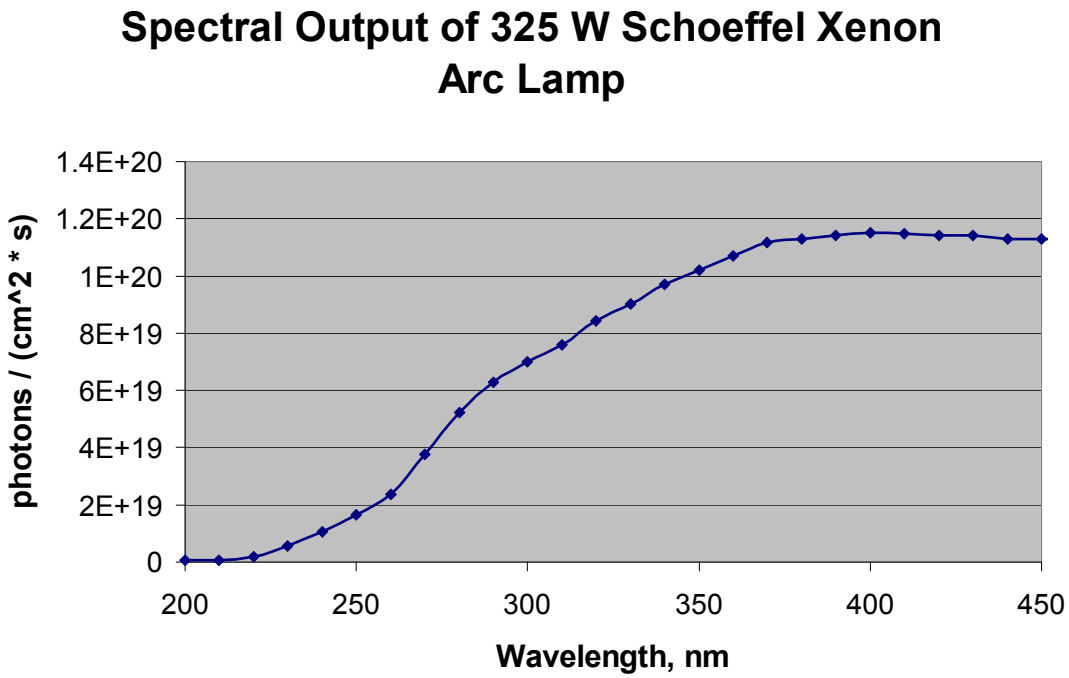

Figure 10. The measured spectral distribution, in photon fluence, of the 325 W xenon arc lamp.

4.1.5 Monochromator

For some experiments, a high intensity monochromator (Bausch & Lomb, Cat. #33-86-27, Rochester, NY) was used to isolate single wavelengths of light. The monochromator was not calibrated and the estimated uncertainty is ±2 nm. Additionally, in order to increase power output, the monochromator was reduced from a double-slit to a single-slit operation, which widens the spectral distribution of the light. However, the uncertainties are inconsequential given the relatively broad nature of ultraviolet absorption.

4.2 Characterization Techniques

4.2.1 Electron Paramagnetic Resonance

Since Electron Paramagnetic Resonance (EPR) is a relatively rare technique, a brief background describing how EPR works is deemed appropriate. EPR is similar to NMR, except instead of detecting the spin of unpaired protons, it detects the spins of unpaired electrons, also known as free radicals. In a magnetic field, unpaired spins will align parallel to the magnetic field. A specific amount of energy, supplied by a photon in the microwave frequencies, can be absorbed by the electron, flipping its spin to antiparallel. This phenomena is described by the equation

$$\Delta E = \hbar \nu = g \mu_0 B \tag{4.1}$$

where ΔE is the energy required to flip the spin, $\hbar$ is Plank's constant, $1.055 \times 10^{-34} J \cdot s$, ν is the microwave frequency, g is the g-factor which is approximately 2, μ_0 is the Bohr magneton, $9.264 \times 10^{-24} J \cdot T^{-1}$, and B is the total magnetic field.

An EPR spectra is generated when a constant microwave frequency is applied to a sample while the magnetic field is swept. In solids, there are a variety of factors that change the energy required to flip the spin[46]. Thus, instead of getting a sharp peak, a broader absorption peak is observed. Additionally, the magnetic field at the free radical is not the same as the magnetic field produced by the magnet. In most systems, the free radical is near enough to an unpaired nuclear spin, like that of a hydrogen atom, which applies a small magnetic field, B_I, to the free radical. Thus, the total magnetic field applied to the free radical is

$$B = B_0 \pm B_I \tag{4.2}$$

where B is the total magnetic field, B_0 is the magnetic field produced by the magnet, and B_I is the magnetic field produced by nuclear spin. B_I can be positive or negative since the nuclear spin can either oppose or add to the magnet's applied magnetic field. This means that there are now two applied magnetic fields at which the free radical will absorb microwave energy, effectively splitting the absorption peak into two identical peaks. As the number of identical hydrogen atoms increase, the number of peaks increases, following Pascal's triangle. This phenomenon is known as the hyperfine interaction, and the magnitude of the splitting is known as the hyperfine splitting constant. Naming nomenclature is that hydrogens attached to the atom containing the unpaired electron are designated α, one atom off are β, two atoms off are γ, etc. In practice, only the α and β protons are close enough to exert a measurable difference in magnetic field. Take, for example, the alkyl free radical, Figure 11[103]. It has four identical β protons, which create a pentet (five peaks) with intensity ratios 1:4:6:4:1. These peaks are further split by the one α proton, forming a 1:5:10:10:5:1 sextet. The magnitude of the splitting is H_β = 33.1 G and H_α = 22.4 G.

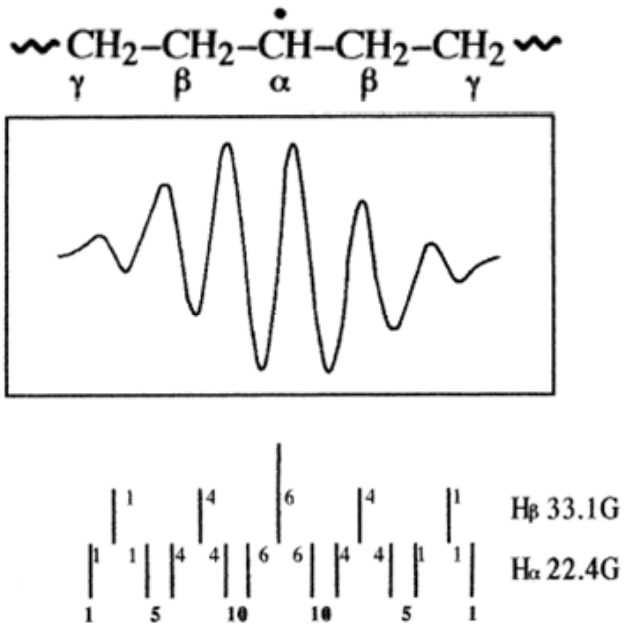

Figure 11. The structure, EPR spectra, and hyperfine splitting of the alkyl free radical.

There are essentially two functions performed by ESR, indentifying and quantifying free radicals. Free radical identification can be performed by looking at differing g-factors, number and relative intensity of peaks, and hyperfine separation. However, identification can be complicated by the presence of more than one specie and the fact that many different species have similar spectra. Quantification of free radicals can be accomplished by double integrating a spectra since the free radical concentration is proportional to peak area (in order to reduce noise, spectra are commonly first derivatives).

As mentioned above, in the absence of oxygen, there are three types of free radicals that commonly occur in irradiated polyethylene, the alkyl, allyl and polyenyl free radical. The spectrum of the alkyl free radical is well known and can be seen in Figure 11 above. It consists of a symmetrical sextet and can accurately be simulated via the hyperfine separation constants given above. This is because a sample

containing only alkyl free radicals can easily be created by irradiating at liquid nitrogen temperatures. Additionally, the alkyl radical spectrum is significantly wider than that of the other spectra, which allows accurate identification of the radical even when other radical species are present[42, 104]. This fact will be exploited throughout this dissertation.

The spectrum of the allyl radical is not as well known. While it is accepted to consist of a septet superimposed on a broad singlet Figure 12[30], there is considerable discrepancy in the literature about its hyperfine separation and proper simulation parameters[28, 30, 103, 105-109] since they often depend on variables such as instrument settings and sample morphology.

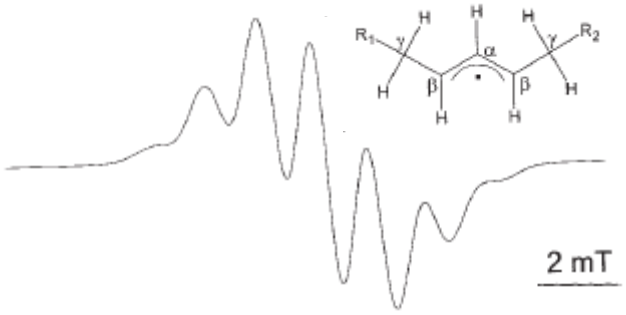

Figure 12. The structure and spectra of the allyl free radical

While, in reality, polyenyl are a family of free radicals, i.e. dienyl, trienyl, tetraenyl, etc., they are often lumped together since it is believed that their EPR spectra is a simple singlet. The loss of hyperfine structure is not due to lack of interacting hydrogens, but to the inability of the instrument to resolve the narrowing hyperfine separation[110]. However, more accurate spectra simulations have been achieved by assuming that the dienyl and trienyl free radical possess some hyperfine

structure[105]. It is also believed that the singlet's linewidth decreases with increasing degree of unsaturation[110].

In the presence of oxygen, alkyl, allyl and polyenyl radicals quickly become peroxyl free radicals via the reaction

$$R^{\bullet} + O_2 \rightarrow RO_2^{\bullet} \qquad (2.12).$$

The peroxyl's EPR spectrum is a simple singlet without any hyperfine structure, which makes it difficult to distinguish from the polyenyl free radical. However, there are two differences between them which can be used to differentiate them. One, by suppressing the motion averaging of the C-O bond by going to low temperatures, the peroxyl singlet becomes an asymmetrical spectrum with three peaks[111] while polyenyl radicals do not. Two, the peroxyl free radical does not exhibit power saturation, even at microwave powers up to 100 mW[51], while the polyenyl free radical does.

In practice, irradiated polyethylene contains various combinations of the free radicals described above depending on irradiation dose, thermal history, environment, and sample morphology. Since the spectra of the different radicals overlap, the experimentally observed spectrum is quite complicated. Attempts to examine only one species, or a ratio of species, from such spectra have included power saturation techniques[51, 105, 112], differing radiation doses[110], differing spectra widths[42, 104], and relative peak heights[113]. Currently, the most accurate way to interpret complex spectra involves simulating them, which requires knowledge of each radical's relative concentration, hyperfine constants, and linewidth. Most often, educated guesses resulting in best fits are made for these parameters, since, aside from alkyl radicals at low temperature, individual species cannot be examined.

Unless otherwise noted, all EPR spectra were acquired on a ESP300 spectrometer (Bruker Biospin, Billerica, MA) using the following instrument parameters: microwave frequency of 9.42 GHz, microwave power of 0.5 mW, frequency modulation of 100 kHz, modulation amplitude of 6.23 G, receiver gain of 50,000, center field at 3350 G, a sweep width of 300 G, a conversion time of 2.54 ms, and a time constant of 2.54 ms. It was verified that the modulation amplitude as well as conversion time to time constant ratio did not distort the signal. At 0.5 mW, some power saturation did occur for only the alkyl radicals, but this power was used despite this due to improvement in signal quality. Thirty scans were added to improve signal to noise ratio. Double integrations were performed using the same software that controls the instrument following the integration procedure described in Bruker Technical Note 6. Spectra simulations were performed using WINSIM software which can be downloaded for free from NIEHS webpage.

4.2.2 Ultraviolet-Visible Spectroscopy

Ultraviolet-Visible spectroscopy (UV-Vis) has been used to indentify free radicals and unsaturations in polyethylene films[31, 81, 85, 87]. While UV-Vis is not as sensitive as EPR for free radical detection, it allows distinct identification of different radical specie since they absorb at different wavelengths. For UV-Vis, the absorption peaks are unusually sharp, possibly due to extremely high molar absorptivity. Unfortunately, the molar absorptivity for all unsaturations and free radicals are not known, but those that are are listed in Table II. It is important to note that free radicals and unsaturations “one degree up” often absorb in the same region. For example, the allyl free radical[114] and diene unsaturation both exhibit absorbance

around 258 nm, while the dienyl free radical and triene both exhibit absorbance around 275 nm. Aside from free radicals and unsaturations, oxidation products also absorb ultraviolet light between 200-400 nm, but their absorption is much broader and weaker[91, 115].

Specie	Wavelength, nm	Molar Absorptivity (L/mole/cm)	Reference
trans-*trans*-diene	236	~25,000	[36]
Triene	274	~41,800	[36]
Tetraene	310	58,900	[116]
Alkyl	215	1,800	[89]
Allyl	258	7,300	[89]
dienyl	285	29,000	[89]

Table II: List of some unsaturations and free radical molar absorptivity.

Unless otherwise noted, all UV-Vis measurements were made using a Cary-3 spectrophotometer (Varian, Palo Alto, CA) between 200 to 550 nm. A film holder was modified by inserting a piece of aluminized polyethylene containing a slit that was slightly smaller than the PE films being measured. This ensured that light was transmitted only through the films, but it did cause a large change in absorbance when the instrument switched from a UV to visible light source at 348 nm. This change was manually corrected for by adding or subtracting this change. For measurements in an air environment, PE films of comparable thickness were inserted into both the measurement and reference beam. For measurements in a nitrogen environment, the sample film was loaded into the glovebox, placed in a film holder which was machined to fit into a glass cuvette and sealed with a tight-fitting rubber stopper. The reference sample was contained in a similar film holder in a glass cuvette, but was exposed to air. Occasionally, up to three scans were averaged to reduce noise.

4.2.3 Fourier Transform Infrared Spectroscopy

Fourier Transform Infrared (FTIR) spectroscopy is capable of detecting many chemical bonds present in polyethylene. The absorption peaks that are affected either by ionizing radiation, subsequent oxidation, or photoirradiation are listed in Table III.

Peak, cm^{-1}	**Assignment**
909	Vinyl
965	*Trans*-vinylene
990	Vinyl/*Trans-trans*-diene/Triene
1370	C-H
1720	Oxidation Products

Table III: Infrared absorption peaks of interest

UHMWPE is fabricated by the Zeigler-Natta catalyst process which results in the presence of one vinyl group at the end of each polymer chain. Since the chains in UHMWPE are extremely long, the concentration of vinyl groups is usually below detection limits. Additionally, ionizing radiation is known to consume vinyl groups[117, 118], further reducing the vinyl concentration. However, vinyl groups can be detected when polyethylene is photoirradiated in the presence of oxygen. The formation of vinyl groups is often attributed to the photodecay of ketone groups via the Norrish type II reaction[119]

$$\sim CH_2\text{-}(C{=}O)\text{-}CH_2\sim \xrightarrow{h\nu} \sim CH_2\text{-}(C{=}O)\text{-}CH_3 + H_2C{=}CH_2\sim . \qquad (4.3)$$

Trans-vinylene is a direct product of ionizing radiation[120] and increases linearly with dose for up to 150 kGy[121, 122]. It is usually independent of irradiation environment[123], temperature, or sample crystallinity[117, 124], and can be used to determine absorbed dose in UHMWPE, see, for example, ASTM F 2381. While *trans*-vinylene could be formed after irradiation via the intramolecular recombination of alkyl radicals, this is not usually observed[38], likely because intermolecular

recombination, which results in crosslinks, is considerably faster than intramolecular recombination[125], even in the crystalline region[92, 126].

The assignment of the peak occurring at 990 cm^{-1} is not entirely clear. Dole *et al.*[36] initially assigned it to the *trans-trans*-diene unsaturation. Additionally, comparison to model compounds containing trienes[127], imply that it could also correspond to triene, and, presumably, higher order unsaturations as well. However, it has also been assigned to the vinyl group in photo-oxidation studies[26, 97]. I believe the latter assignment is the correct one for several reasons: (1) samples that were electron beam irradiated and allowed to oxidize in air contained the diene unsaturation, as measured by UV-Vis, but did not contain this peak; (2) samples that were electron beam irradiated then photo-oxidized in air did not contain the diene unsaturation, as measured by UV-Vis, but did contain this peak; (3) both the 909 and 990 cm^{-1} peak decreased upon irradiation, consistent with vinyl, not polyene unsaturation, behavior; (4) the samples that contained the 990 cm^{-1} peak also had increased peaks at 1640 cm^{-1}, which has also been assigned to the vinyl group[128].

Finally, a variety of oxidation products, such as ketones, aldehydes, hydroperoxides, carboxylic acids, and esters, absorb in the range from 1675 to 1765 cm^{-1}. Unfortunately, their peaks are not well-resolved and individual species quantification is impossible without deriviterization by NO and SF_4[129, 130]. Nonetheless, a standardized method to assess the overall oxidation in retrieved UHMWPE implants has been developed and is detailed in ASTM F 2102. Briefly, an oxidation index is calculated by dividing the area under the peak at 1720 cm^{-1} to the area under the peak at 1370 cm^{-1}. Since the absorption at 1370 cm^{-1} is due to C-H

bonding which depends on only film thickness and does not change upon irradiation or oxidation. This is an effective way to normalize the absorption due to oxidation products to the films thickness, allowing easy comparison between different films.

Unless otherwise noted, all FTIR measurements were performed on a Nicolet Magna-IR 550 Spectrometer, Series II (Thermo Scientific, Waltham, MA) using the following settings: 2 cm^{-1} resolution, mirror velocity 0.4747, aperture open 60%, CO_2 and H_2O correction enabled, and 64 scans were summed. Before taking a background spectrum, the chamber was flushed with nitrogen for at least two minutes. All measurements were performed under nitrogen flushing which reduced, but did not eliminate, background noise. Additionally, the parallel film surfaces which are created by microtoming result in the creation of interference fringes characteristic of the film's thickness known as Fourier rippling[131]. These fringes can often distort or mask peaks at lower wavenumbers. When possible, this effect was mitigated by roughening the film's surfaces by polishing it against 450 grit sandpaper[122]. However, this dramatically reduced UV light transmission due to surface scattering so it could only be done for samples that did not require accurate UV-Vis measurements.

4.2.4 Differential Scanning Calorimetry

Differential Scanning Calorimetry (DSC) is a powerful technique capable of measuring the crystalline content in semicrystalline polymers. Additionally, the peak melting temperature and width of the melting peak sheds qualitative insight into the size distribution and perfection of the crystals. Because of this, DSC can also be used to detect the presence of oxidation since oxidation results in chain scission which allows previously stretched chains to fold into new crystals. These crystals are

smaller and less perfect that the original crystals and appear as an "oxidation shoulder[132]" on the melting peak. DSC has also been used to measure lamellar thickness[132, 133] and even gel content[134].

All measurements were performed on a Q2000 DSC (TA Instruments, New Castle, DE) in hermetically sealed aluminum pans with an empty aluminum pan as a reference. Samples were heated from 25 °C to 160 °C at a heating rate of 10 °C per minute. The percent crystallinity was then measured by dividing the area by 291 J/g which is the enthalpy for completely crystalline polyethylene.

Chapter 5: Thickness Experiment

5.1 Objectives

The first objective of this experiment is to quantify the extent that the photoconversion of stable free radicals to unstable free radicals can be used to reduce the concentration of free radicals in irradiated UHMWPE. Preliminary experiments demonstrated that lowest free radical concentrations were achieved when a UV light treatment was both preceded and followed by a thermal treatment. A second objective is to verify that there is adequate ultraviolet light penetration in UHMWPE required to remove free radicals generated from a 330 keV electron beam. While the saturated hydrocarbon backbone does not absorb ultraviolet light[135], extensive scattering occurs, mainly due to the crystalline regions[136]. Additionally, the development of unsaturations, which absorb ultraviolet light, is expected to decrease ultraviolet light penetration over time[135]. A third objective of this experiment was to determine if 100 °C thermal treatments preserve a greater amount of crystallinity than 120 °C thermal treatments.

5.2 Procedure

UHMWPE films of approximately 200, 500, and 1000 μm thickness were irradiated in a nitrogen environment as detailed in section 4.1.2. For each thickness, six to eight films were fabricated. Three to five films were subjected to UV light and thermal treatments in a nitrogen environment while three control films were subjected to only identical thermal treatments. For the 200 μm films, the procedure was a two hour thermal anneal at 100 °C, followed by a one hour UV light treatment, followed

by a two hour thermal anneal at 100 °C. This process was repeated three times, resulting in four thermal treatments totaling eight hours and three UV light treatments totaling three hour. For the 200 μm films two different UV light treatments were explored, an unfiltered photoirradiation, and photoirradiation through a Corning glass filter #3965 which filters out wavelengths below 320 nm. The filtered UV treatment was explored despite the fact that it is expected to result in chain scission via reaction (3.2) since previous results[87] have shown that it did not increase the degree of unsaturation of free radicals. However, it was found to be less effective than unfiltered UV light treatments and was not explored for other thicknesses. For the 500 μm films, a four hour thermal anneal at 100 °C, followed by a one hour UV light treatment, followed by a four hour thermal anneal at 100 °C was performed. This process was repeated three times, resulting in four thermal treatments totaling 16 hours and three UV light treatments totaling three hours. For the 1000 μm films, a four hour thermal anneal at 100 °C, followed by a two hour UV light treatment, followed by a four hour thermal anneal at 100 °C was performed. This process was repeated three times, resulting in four thermal treatments totaling 16 hours and three UV light treatments totaling six hours.

EPR measurements were taken immediately after electron beam irradiation in order to measure the initial free radical concentration. In general, EPR measurements were concluded 25-30 minutes after the start of electron beam irradiation. Additional EPR measurements were taken at the conclusion of each thermal treatment and UV treatment. The EPR spectra were visually analyzed to qualitatively determine the type of free radicals present. The doubly integrated area was calculated to determine free

radical concentrations and divided by the initial area to determine the percent of free radicals remaining. For each data point, three identical measurements were taken, wherein the EPR tube was removed and replaced in order to quantify the uncertainty resulting from sample positioning (>4%). At the conclusion of treatments, the UV-Vis spectra were taken in order to determine the types of free radicals and unsaturations present.

For DSC measurements a completely new set of samples, consisting of four different types of sample, were created. The four sample types were: virgin UHMPWE, irradiated only, irradiated and annealed at 100 °C for four hours, and irradiated and annealed at 120 °C for four hours. Three samples were made for each sample thickness (200, 500 and 1000 μm) and sample type, giving a total of 36 samples. The samples were irradiated and stored in aluminized polyethylene pouches filled with nitrogen in order to minimize oxidation before DSC measurements.

5.3 Results

5.3.1 Free Radical Concentration

A comparison of the decrease in free radical concentration between the UV treated and control samples for all thicknesses can be seen in Figure 13. The error bars correspond to the standard deviation between the three (or only two for the case of filtered UV) samples. The decay for all samples is best described ($R^2 = 0.96 \pm 0.02$) by second-order kinetics, as is shown in Figure 14, indicative of radical-radical recombination. It can be clearly seen that, except for the first data point which was not preceded by a UV treatment, the combination of thermal and UV treatments

reduces the concentration of free radicals to greater extent than thermal treatments alone. The results of the final concentrations are tabulated in Table IV.

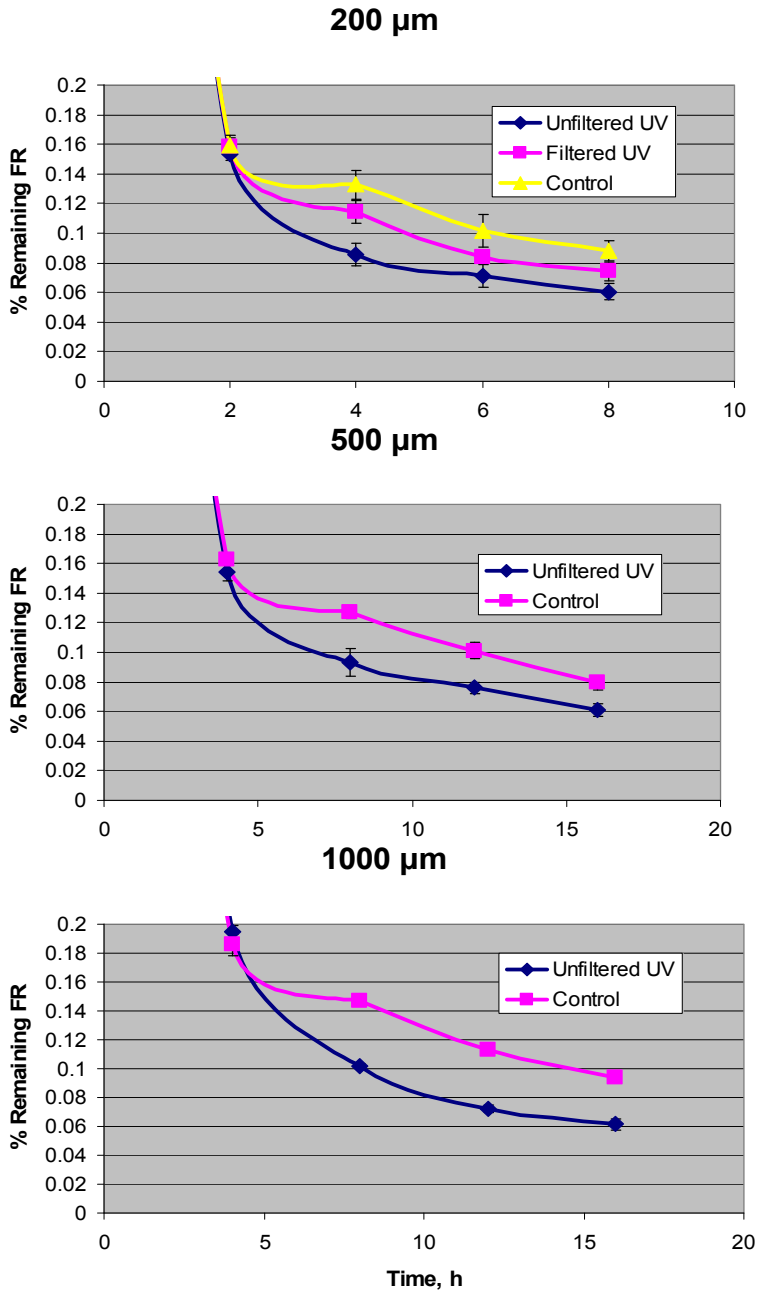

Figure 13. Decay of free radicals for 200, 500 and 1000 micron films. Note that the first data point for UV treated films is identical to control films because, unlike the other data points, it is not preceded by a UV treatment.

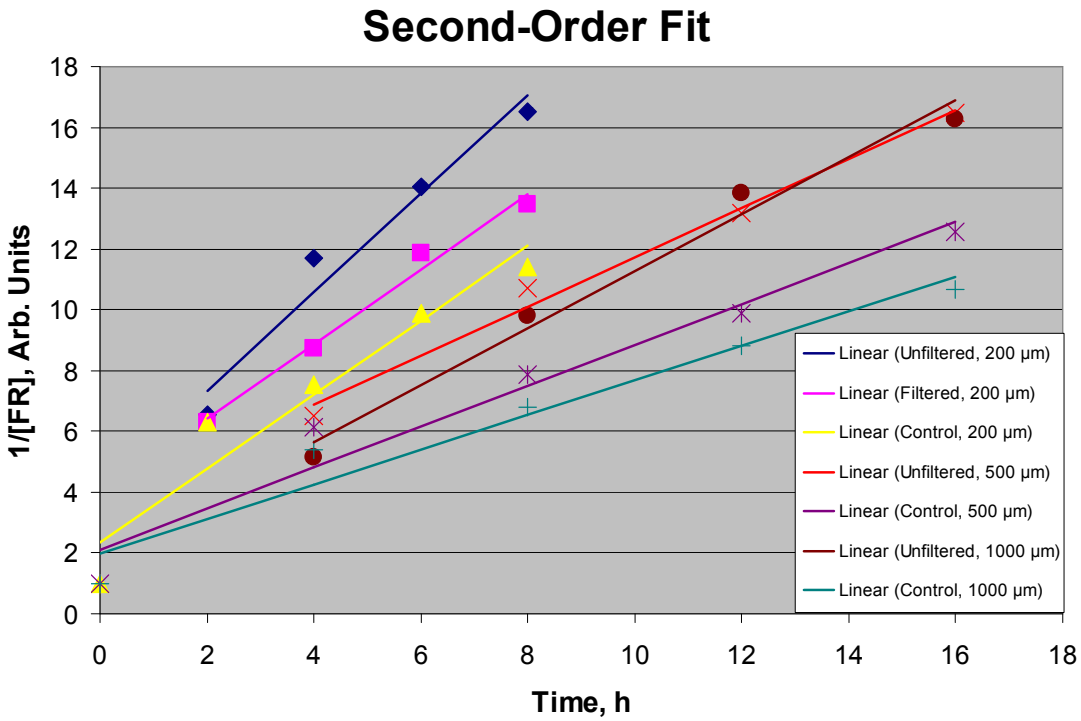

Figure 14. Plot of ln[FR] versus time for the decay of free radicals in UHMWPE films of different thickness that were subjected to unfiltered, filtered, and no UV photoirradiation. The slope of the linear trendline gives the relative reaction constant.

Sample	Thickness, μm	Starting [FR], arb. Units	Final [FR], arb. units	% Remaining	% Reduction
Unfiltered UV	203 ± 12	347 ± 26	20.8 ± 1.5	6.3 ± 0.6	33
Filtered UV	202 ± 15	340 ± 20	24.3 ± 0.3	7.2 ± 0.4	20
Control	203 ± 11	350 ± 24	31.1 ± 0.8	8.9 ± 0.7	
Unfiltered UV	532 ± 28	260 ± 12	16.7 ± 3.8	6.4 ± 1.5	16
Control	535 ± 25	256 ± 12	19.5 ± 1.7	7.6 ± 0.8	
Unfiltered UV	1030 ± 23	214 ± 10	13.1 ± 0.5	6.1 ± 0.4	34
Control	1017 ± 12	207 ± 4	19.4 ± 1.0	9.4 ± 0.5	

Table IV: Comparison of starting and final free radical (FR) concentrations between UV treated and control samples. Free radical concentrations are normalized by sample weight and received radiation dose.

5.3.2 EPR Spectra Evolution

The spectral evolution of control samples for all thicknesses, aside from the initial spectra which are discussed below, were essentially identical and can be seen in Figure 15. The initial six-peaked, mostly-alkyl spectrum decays to a five peak spectrum which likely correspond to the five strongest peaks of the allyl free radical, although there is likely a contribution from polyenyl radicals as well. All the peaks in the spectrum decay evenly with increasing annealing time. The spectral evolution for the samples treated with light of wavelengths greater than 320 nm were almost identical to the control sample, Figure 16, although they decayed more quickly than the control samples. The only significant difference was that after a UV treatment some alkyl radicals were present as evidenced by the presence of a weak outermost peak and the broadening of the next nearest peak. The spectral evolution for samples treated with unfiltered UV light was considerably different, and the spectral evolution for the 200, 500 and 1000 μm samples can be seen in Figure 17, Figure 18, and Figure 19, respectively. Upon the initial UV light treatment, the familiar "control" spectra is converted into a roughly six-peaked spectrum, corresponding to a sample consisting of mostly alkyl radicals, although other radicals are clearly present. The subsequent thermal anneal converts the spectra into a singlet containing at least six hyperfine peaks about 9 G apart. This is an unusual spectrum which is discussed in more detail below. Subsequent UV and thermal treatments do not significantly alter the spectra, although overall peak height and hyperfine peak heights are reduced. Additionally, the presence of weak outermost peaks can often be seen following a UV

light treatment, indicating the presence of alkyl radicals. This effect becomes less pronounced with subsequent photoirradiation.

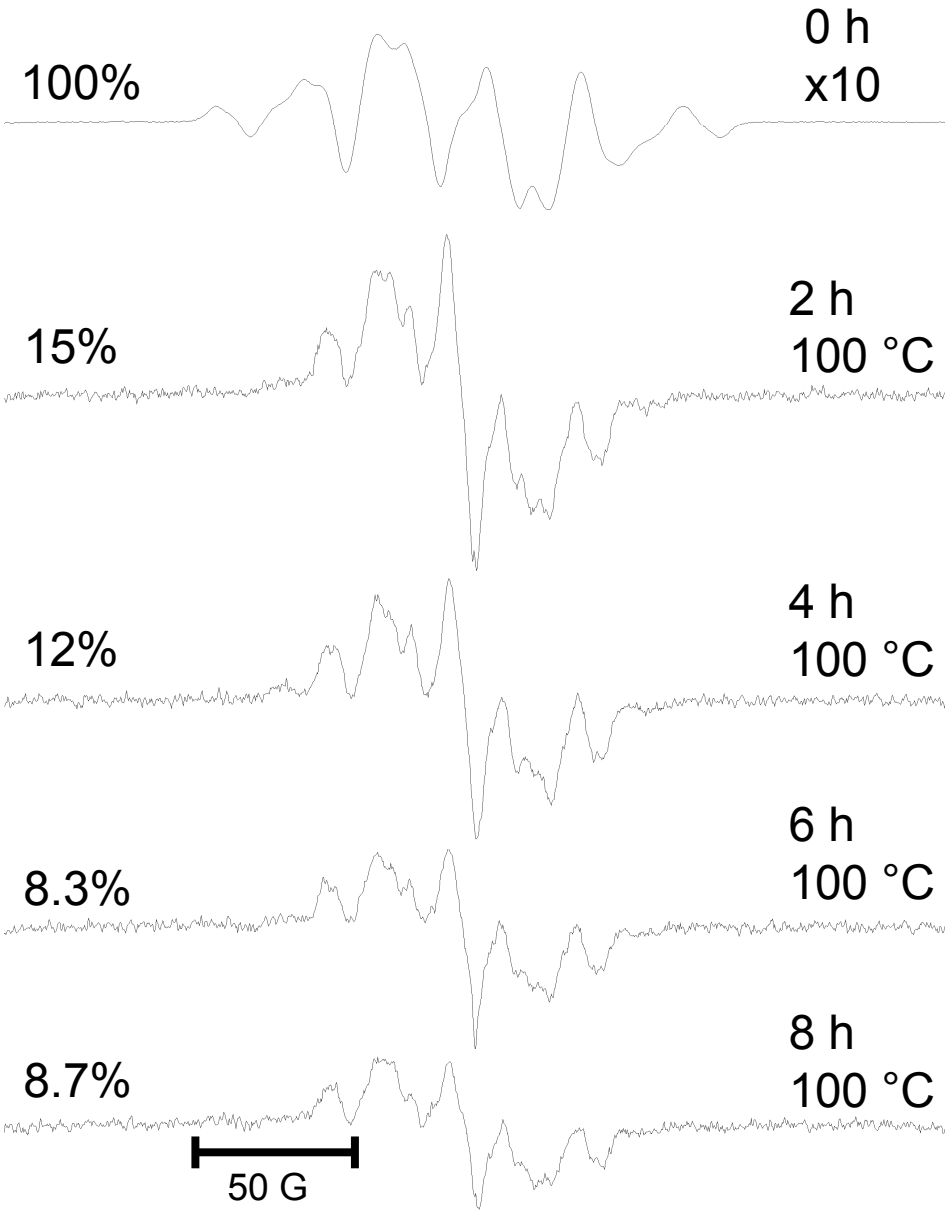

Figure 15. EPR spectra and the percent of free radicals remaining of a 200 micron sample subjected to 100 C thermal treatments. Please note that all experimental EPR spectra throughout the entire thesis have the same horizontal scale.

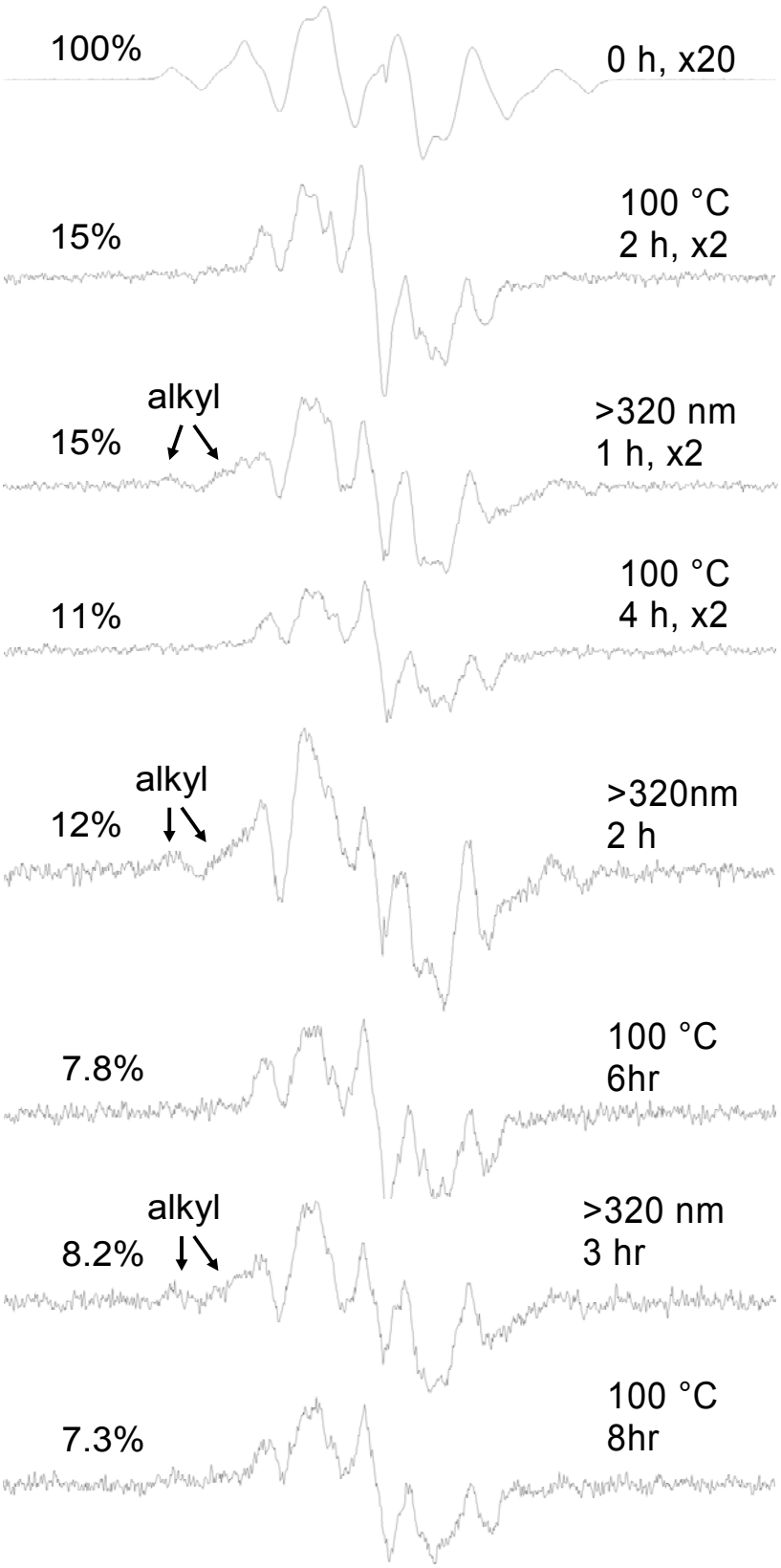

Figure 16. EPR spectra and percent of free radicals remaining of a 200 micron sample subjected to 100 C thermal treatments and photoirradiation with light of greater than 320 nm wavelength.

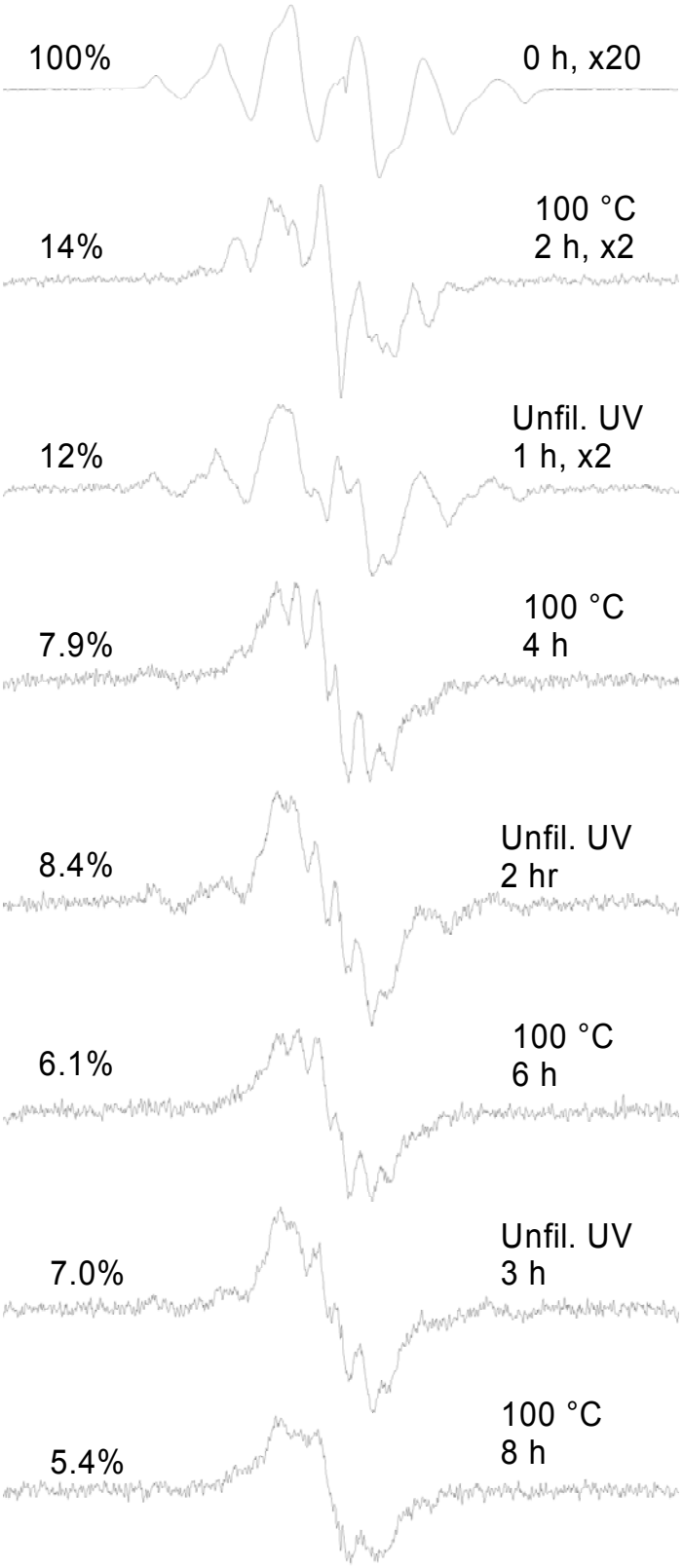

Figure 17. EPR spectra of a 200 micron film subjected to 100 C and unfiltered UV light treatments.

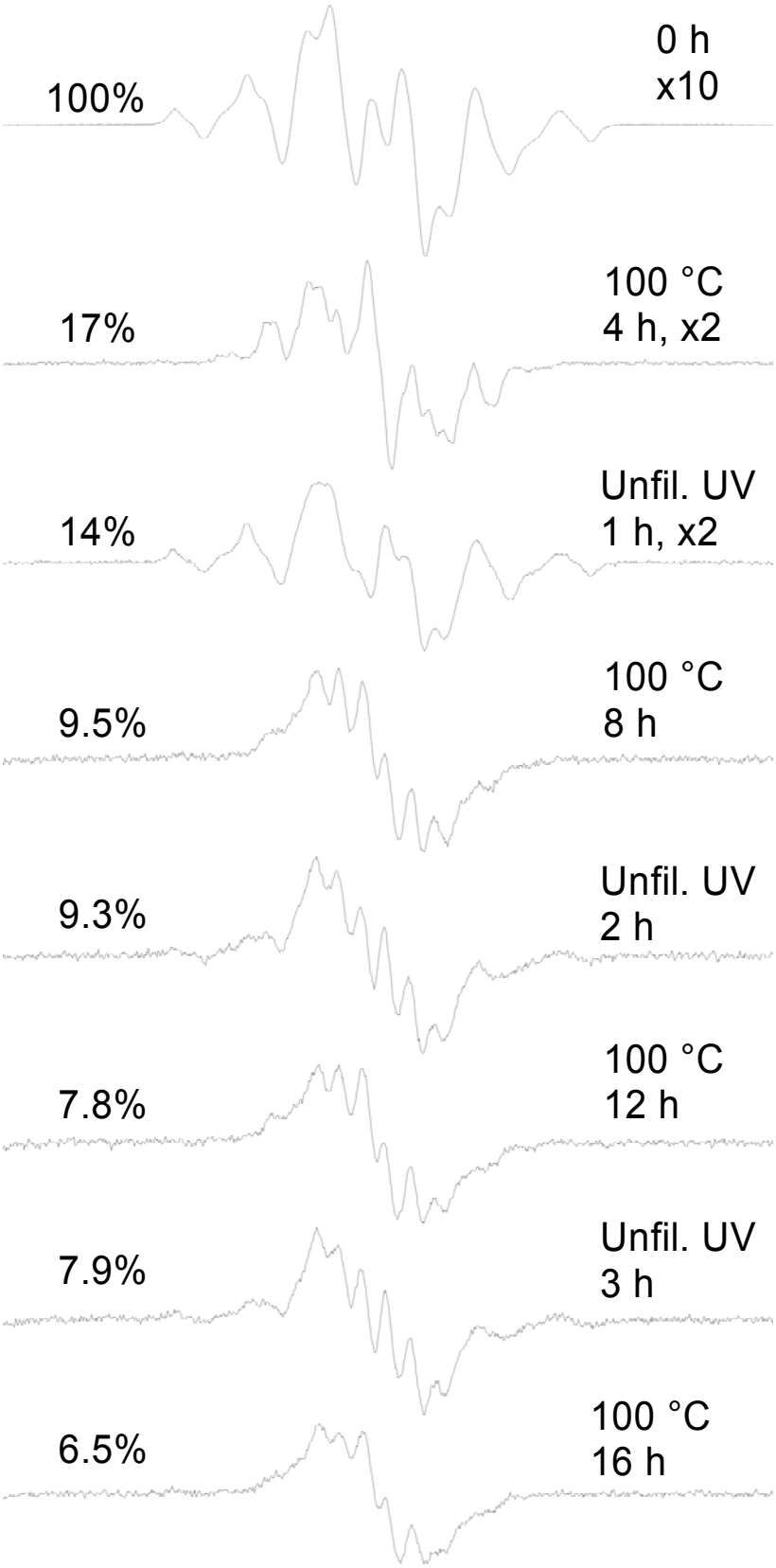

Figure 18. EPR spectra and percent of free radicals remaining of a 500 micron film subjected to 100 C and unfiltered UV light treatments.

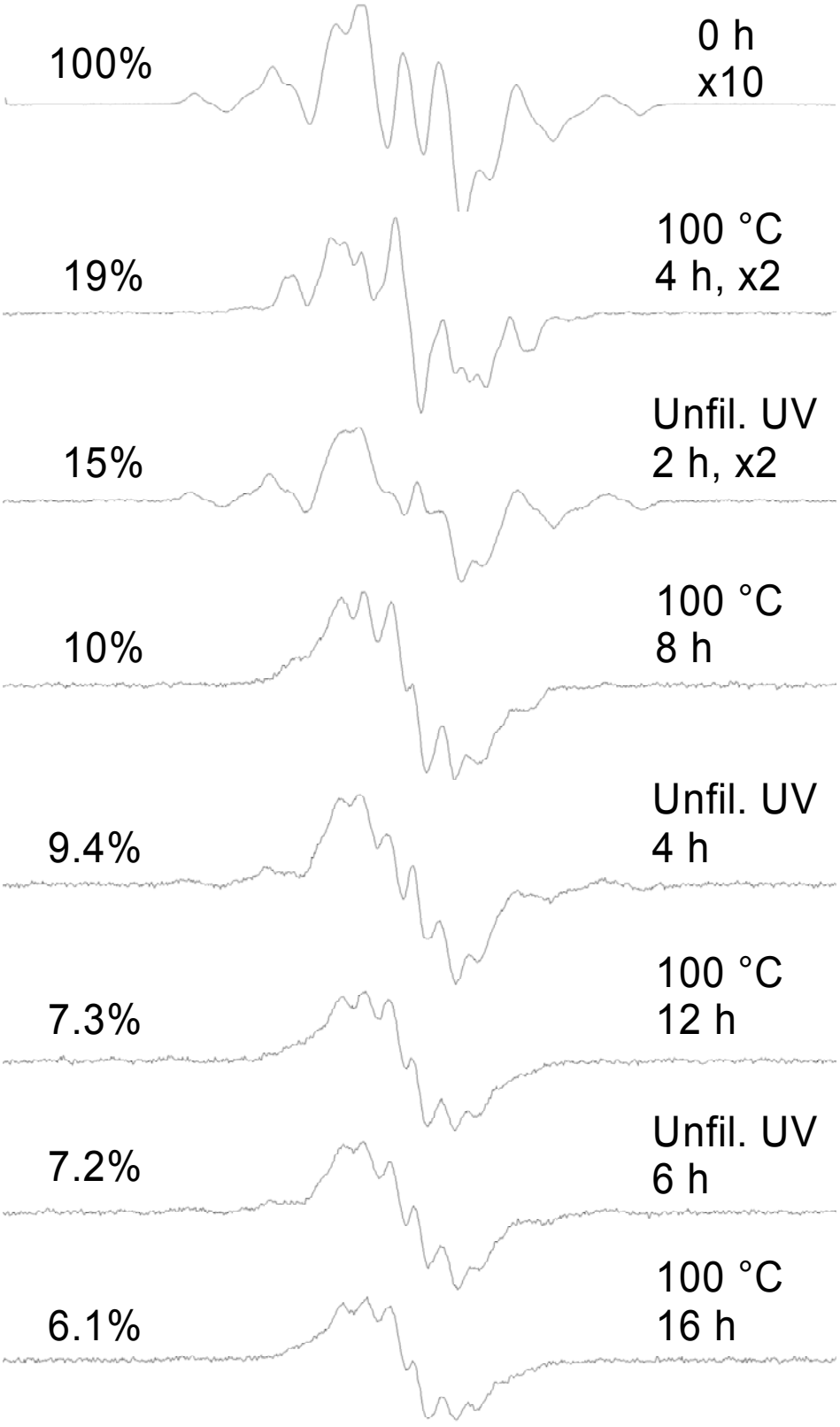

Figure 19. EPR spectra and percent of free radicals remaining of a 1000 micron film subjected to 100 C and unfiltered UV light treatments.

5.3.3 UV-Vis Results

At the conclusion of all thermal and UV treatments, the UV spectra were collected in a nitrogen environment. However, the 500 and 1000 μm films exhibited excessive light scattering and meaningful spectra could not be attained. Therefore, only spectra from the 200 μm are discussed. The UV spectra for the 200 μm films can be seen in Figure 20. Similar to the EPR spectra, the control and >320 nm samples had similar spectra while the unfiltered UV sample had a different spectrum. It is clear that all of the films contain a comparable concentration of diene unsaturations, but the presence of a shoulder for the control and >320 nm sample at 258 nm indicates that they possess significantly more allyl radical than the unfiltered UV sample. Conversely, the much larger peak at 285 nm for the unfiltered UV sample as compared to the other samples indicates that it contains much more of the dienyl radical than the other films. The shoulder at 275 nm may be attributed to the presence of triene, but, upon comparison to the allyl radical which also has a shoulder in the diene unsaturation region[114], may also be attributed to the dienyl radical. This point is to be clarified in future experiments (section 7.4.2). The unfiltered UV sample also has a very weak absorbance at 323 nm which may indicate the presence of some trienyl.

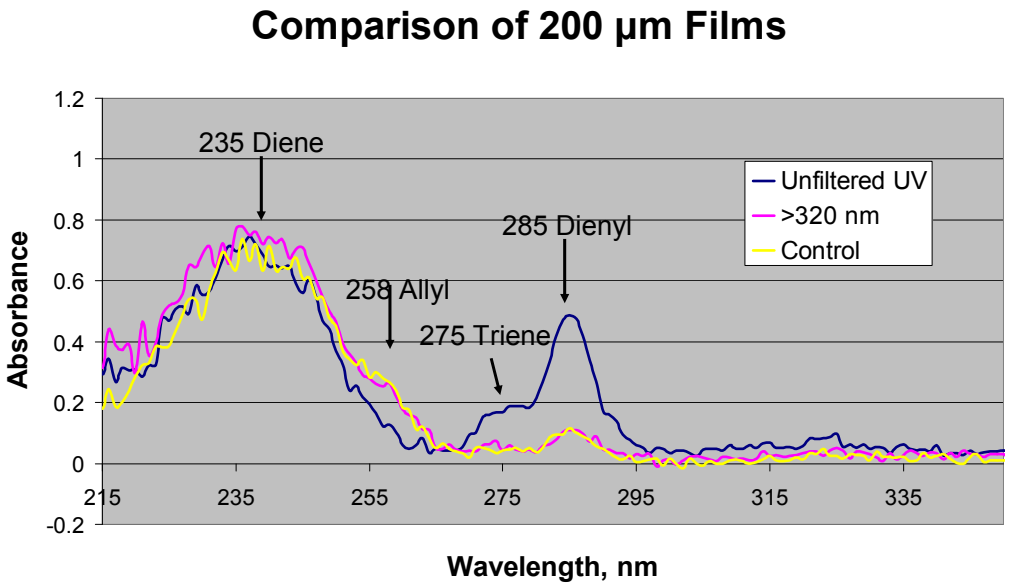

Figure 20. Comparison of the UV spectra of 200 micron films at the conclusion of all thermal and UV treatments. Non-photoirradiated and photoirradiated with >320 nm light sample had similar spectra containing allyl and some dienyl free radicals. Photoirradiated with unfiltered UV light has much less, if any, allyl and much more dienyl.

5.3.4 DSC Results

A comparison of the crystalline content and melting temperature for UHMWPE of different thicknesses that have undergone various radiation and thermal treatments can be seen in Figure 21. It is clear that ionizing radiation increases both the crystallinity and melting temperature. This has been attributed to ionizing radiation preferentially breaking taut tie molecules which relieves stress in the crystal[13]. This increases the crystal's perfection and, hence, its melting temperature. The broken tie chains are now free to crystallize, which increases the crystallinity of the sample[37]. It would also seem that crystallinity increases slightly with film thickness.

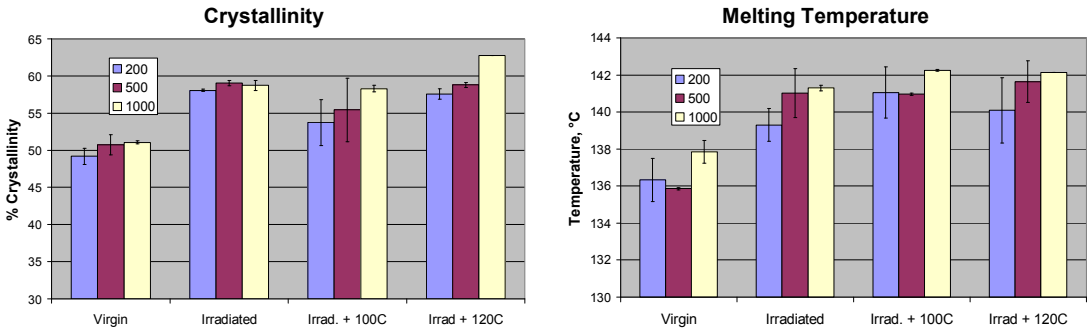

Figure 21. Change in crystallinity and melting temperature upon irradiation and thermal treatments for films of UHMWPE of various thicknesses.

5. 4 Discussion

5.4.1 The Effect of Thickness

It is interesting to compare the initial EPR spectra of films of differing thickness, Figure 22. In the 200 μm film, the initial spectra are of an almost pure alkyl spectrum, while the spectra of thicker samples become increasingly complicated. While the initial spectra are different, the spectra are nearly identical after an anneal at 100 °C, implying that the difference between spectra is caused by differing amounts of unstable alkyl radicals. Close comparison of the spectra shows that their largest difference is the presence of the central peak (depicted by the arrow in Figure 22) which is very pronounced in the spectra after the anneal. As mentioned above, this peak is likely attributed to the presence of the allyl radical. Comparison of the starting free radical concentrations in Table IV, which were normalized to sample weight and starting dose, reveals that the initial concentration decreases as sample thickness increases. Since an equal concentration of free radicals should have been created in all the samples independent of film thickness, these results imply that the unstable alkyl free radicals live longer in thinner samples. A higher ratio of unstable alkyl radical to stable allyl radicals in the thinner films also explains the difference in

EPR spectra. The difference in radical stability between the samples may be attributed to differences in sample morphology. It is known that the process of microtoming can increase the orientation and crystallinity of a semicrystalline polymer[137]. While an increase in crystallinity was only observed in pre-oriented samples, the ram extrusion process causes some degree of alignment[138]. Increases in crystallinity decrease the decay rate of radicals. The effects of microtoming decrease as sample thickness increases[137], and not be detectable in the 1000 μm films which were machined. However, DSC results (Figure 21) showed that thinner films had comparable or lower crystallinity and crystal perfection than thicker films. A close comparison of the thermographs for different film thicknesses, Figure 23, shows that upon irradiation, only the 200 μm films have a substantial increase and sharpening of the crystal distribution. While subsequent thermal treatments broaden this distribution, the initial crystal distribution may be responsible for the slow initial decay of alkyl radicals.

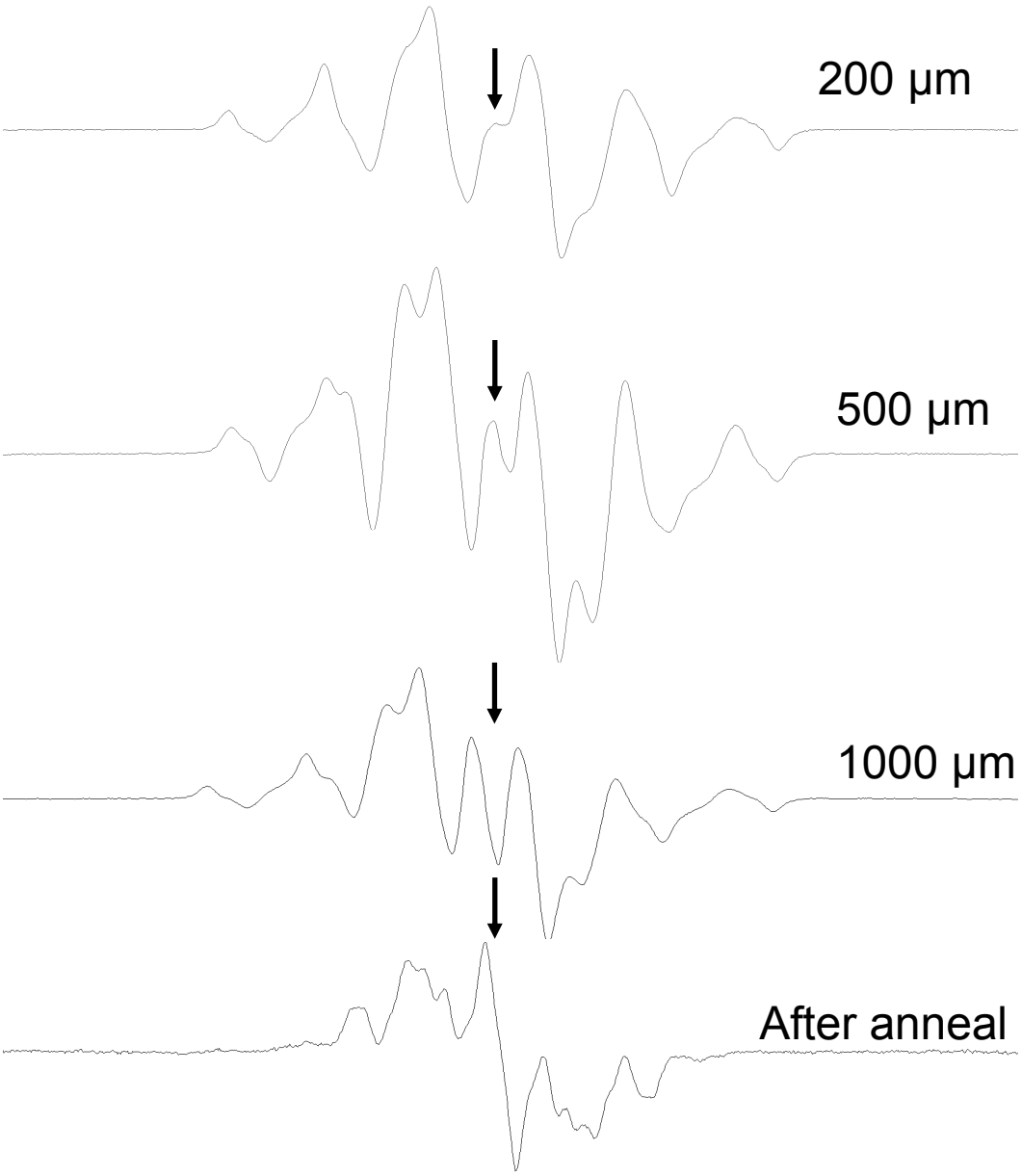

Figure 22. Starting EPR spectra of 100 kGy irradiated polyethylene films of differing thickness. Please note that while the horizontal scale is identical, the vertical is not.

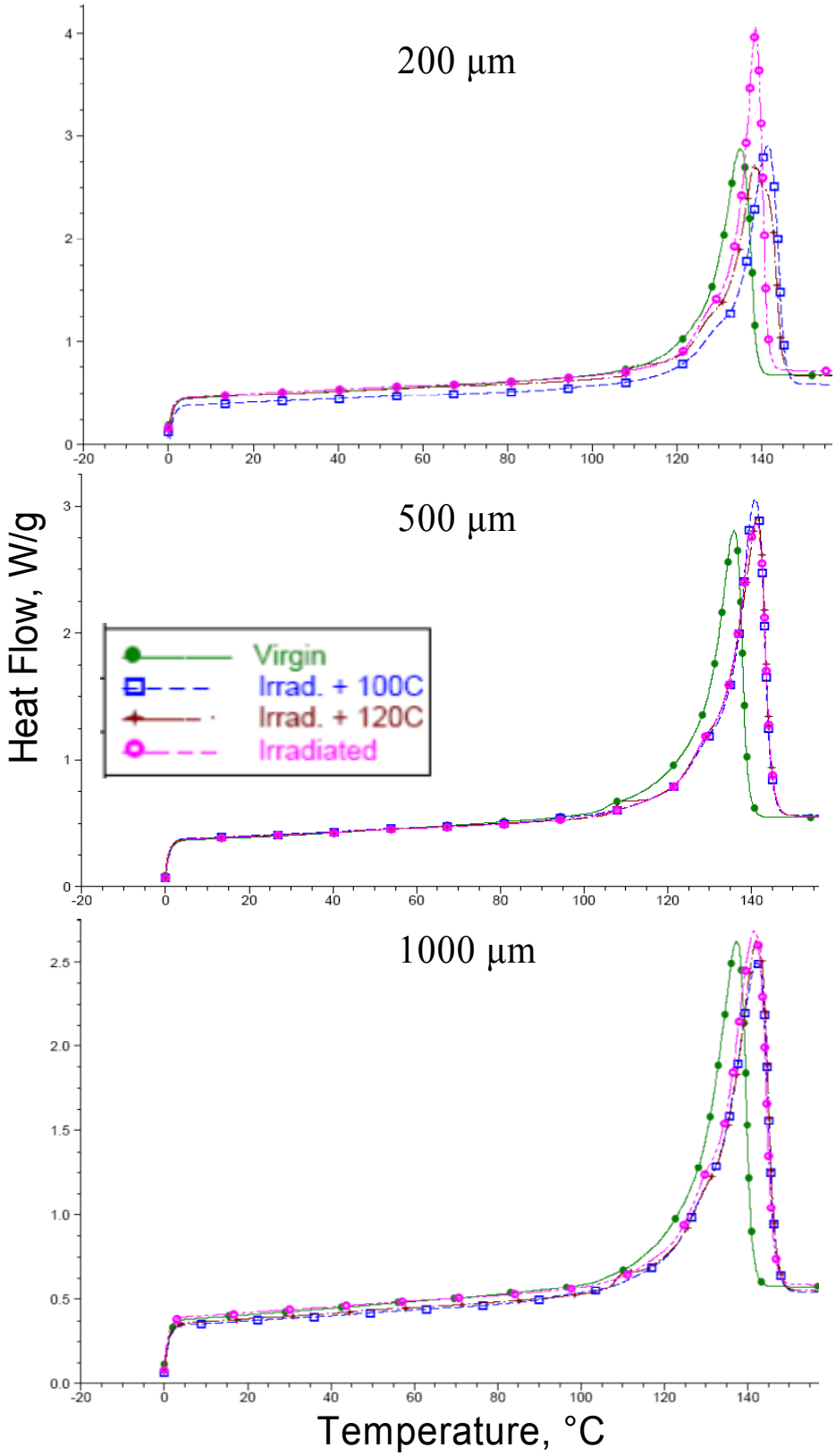

Figure 23. Effect of irradiation and subsequent thermal treatment on the DSC thermographs of UHMWPE films of different thicknesses. Note the substantial increase and sharpening of the crystal distribution in the 200 micron films upon irradiation.

5.4.2 Free Radical Decay

From Table IV, it is clear that while thermal treatments alone can reduce the free radicals concentration 9% of its initial value, when combined with unfiltered UV treatments, the free radical concentration can be further reduced to 6% of its starting value, which is a 33% reduction. While the 500 μm films did not achieve this reduction, it is believed that this is a result of inadequate UV treatments. This conclusion is supported by the fact that the 1000 μm achieved comparable free radical concentrations to the 200 μm films when longer (two hours) UV treatments were used. These results demonstrate that the UV treatment is effective to depths up to 1000 μm.

The reason that the combination of UV and thermal treatments cannot completely eliminate all free radicals is that while UV light effectively converts stable allyl radicals to unstable alkyl radicals via reaction (3.1), it has almost no effect on dienyl radicals, as is demonstrated in chapter 8. Therefore, it is impossible to completely eliminate all the free radicals.

The use of light of wavelengths greater than 320 nm to reduce free radicals was also explored. Although this treatment was expected to result in chain scission via reaction (3.2), it was explored since it was not expected to result in the creation of dienyl radicals which undermine the effectiveness of unfiltered UV light treatments. Further, assuming that most of the alkyl radicals generated via reaction (3.2) result in crosslinking, the overall molecular weight of the polymer would not be significantly changed despite the chain scission.

While UV treatment with wavelengths longer than 320 nm does reduce free radical concentration, for a given irradiation time, it is not as effective as unfiltered UV light photoirradiation, and was not explored for thicker films. Close examination of the EPR spectra evolution, Figure 16, reveals that after each UV light treatment alkyl radicals are created. In contrast to unfiltered UV light, the amount of created alkyl radicals does not decrease with UV photoirradiation time. These results imply that, in contrast to unfiltered UV light, three hours photoirradiation of light greater than 320 nm is insufficient to convert a significant portion of allyl radicals. This is to be expected upon comparison of the molar absorptivity at 258 nm, 700 L/mole/cm[85], to the molar absorptivity at 365 nm, 2.5 L/mole/cm[99]. This conclusion is supported by the fact that the UV spectra above 320 nm are nearly identical to the control spectra. It is somewhat surprising that even minimal conversion of the allyl radical results in a substantial reduction (20%) in the final free radical concentration. It is also possible that the alkyl free radicals are created via the decay of oxidation products created via the microtoming process[139], but this would result in an increase in free radical concentrations, not a reduction, as was observed.

5.4.3 The Dienyl Radical Spectrum

As mentioned above, an unusual EPR spectrum was observed after an unfiltered UV photoirradiation followed by a thermal treatment. A more detailed view of this spectrum can be seen in Figure 24. At least six peaks are clearly visible, but there are two more weak outer peaks depicted by the red arrows. The average location of these peaks did not significantly vary (>0.4 G) with film thickness or UV and thermal treatments, as can be seen in Table VI. The average separation between the

peaks is 9.0 ± 1.0 G. This hyperfine separation is too small to be attributed to the allyl radical whose separation is reported to vary between 12 to 18 G[107, 140, 141]. This structure also cannot be attributed to some combination of the alkyl and allyl free radicals since after a thermal treatment there are clearly almost no alkyl radicals present. Previous experiments demonstrated that it also cannot be attributed to a peroxyl free radical because it power saturates[51] and does not change upon cooling to -163˚C[103, 142]. Examination of the UV spectra (Figure 20) reveals that mostly dienyl radicals are present. Spectral simulations shown below confirm this assignment. A subtle change in the spectra is observed when comparing the spectra following a thermal treatment with one following a UV treatment, best seen by the change in height of P3. This difference is likely due presence of additional free radicals, such as allyl radicals in the case of thermal treatments (a decay product of the photoconverted alkyl radicals) or alkyl radicals in the case of UV treatments (created via the photoconversion of allyl radicals). The presence of these radicals can clearly be seen in Figure 24 as peaks that lie outside the dienyl radical (the allyl radical peak in Figure 24 is in the same location as the outermost peak of the control samples shown in Figure 15). As expected, these outer peaks become less pronounced with increasing thermal and UV treatments as more and more allyl radicals are photoconverted to dienyl radicals or non-radicals species.

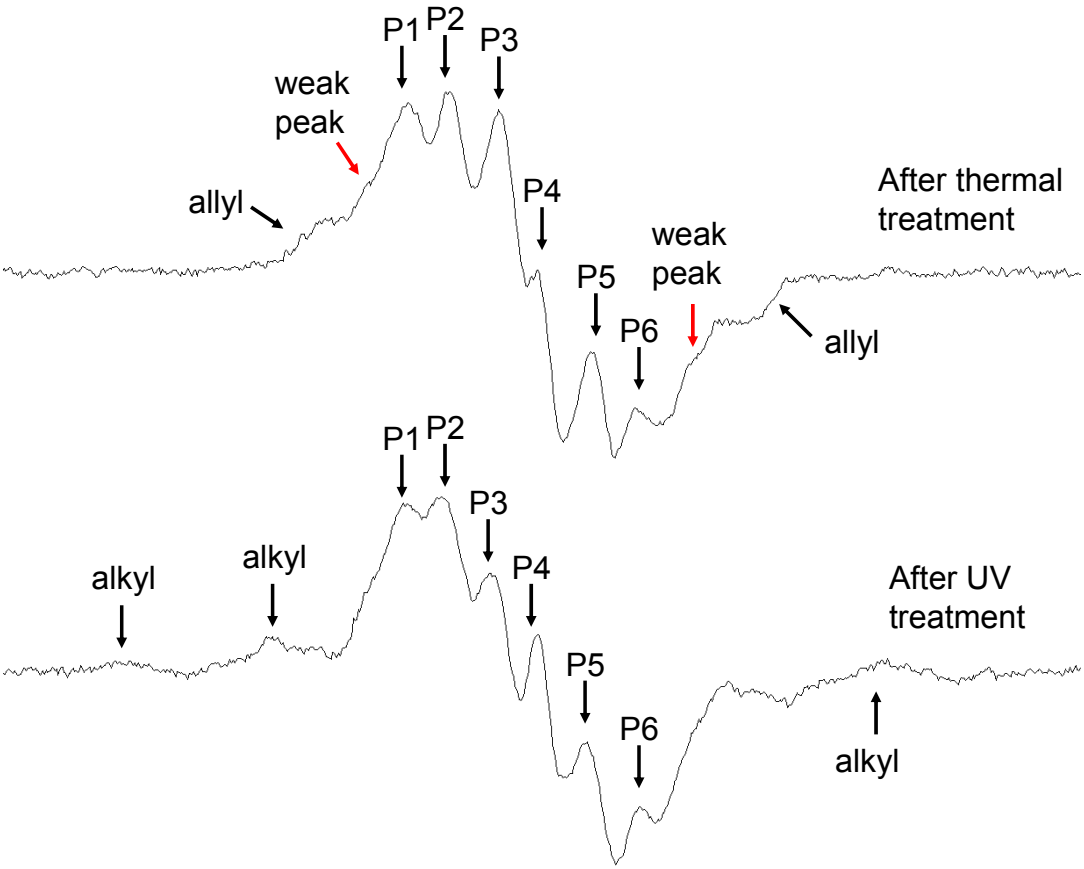

Figure 24. The EPR spectra of the dienyl radical with six peaks of 9 G hyperfine separation clearly marked. Two outer weak peaks are also marked. In addition to the dienyl radical, allyl radicals are present after a thermal treatment and alkyl radicals are present after a UV treatment.

P1, G	P2, G	P3, G	P4, G	P5, G	P6, G
3332.3±0.2	3340.0±0.3	3349.2±0.4	3357.4±0.4	3367.6±0.3	3377.4±0.1

Table V: Location of the six largest peaks in the EPR spectra of the dienyl radical.

Having identified the dienyl radical spectrum, it becomes possible to accurately simulate it. A schematic drawing of the dienyl free radical can be seen in Figure 25. Due to resonance stabilization, the free radical is distributed over five carbon atoms. Various calculations have shown that the electron density is symmetrical about the central carbon, but different for different carbons[143]. It is therefore reasonable to assume that there are three different α protons. It is also reasonable to assume that there are four identical β protons adjacent to the free

radical. Based on these assumptions, the dienyl radical was accurately simulated using WINSIM (Figure 26) and the simulation parameters are summarized in Table VI. Simulations were performed for only dienyl radical spectra immediately following a UV treatment, when it is reasonable to assume that only alkyl and polyenyl, but no allyl, radicals are present. These spectra were chosen over ones possibly containing allyl radicals since the simulation parameters are well-known for the alkyl but not the allyl radical. The individual species in the simulations can be seen in Figure 27. The values and uncertainties given in Table VI are the average and standard deviation of the results from all simulations whose correlation factor (a measure of how accurately the simulation matches the experimental spectrum) was greater than 98%. The average correlation for all considered simulations was 98.7%. It is worthwhile to note that the hyperfine coupling constants for the two pairs of α protons are quite close and the spectra can also be accurately simulated by assuming one α_1 and four α_2 protons. Two trends were noticed during simulation, the correlation factor was lower for thinner films and the relative concentration of alkyl radicals is reduced by repeated UV treatments. The lower correlation values for the thinner samples is likely the result of low signal-to-noise ration associated with the weak signal produced by the relatively few radicals contained in the smaller sample. On average, the percentage of alkyl radicals decreased from 49±5% after the initial photoirradiation to 27±4% for subsequent irradiations. The decrease in alkyl radicals is to be expected as there are less allyl radicals to photoconvert with increasing UV treatments.

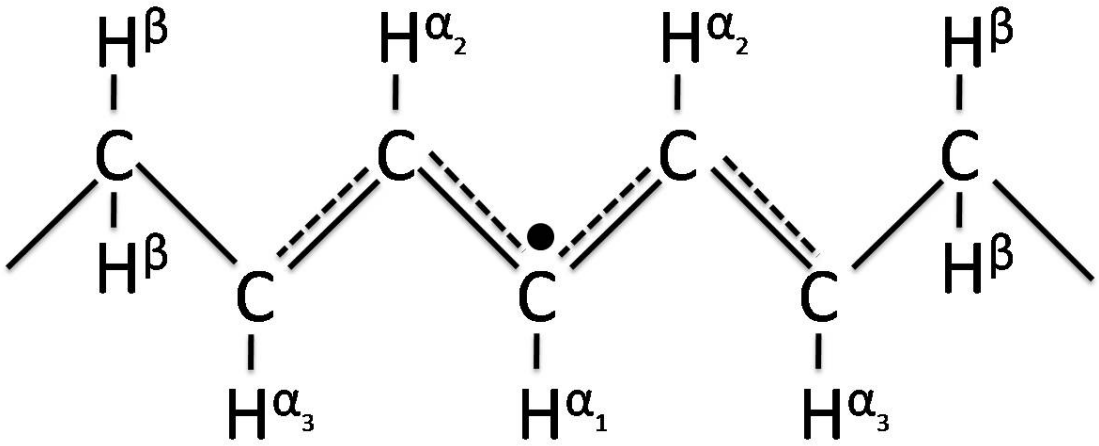

Figure 25. A schematic drawing of the dienyl free radical.

Figure 26. Simulation of experimental dienyl radical. The darker, noisier experimental spectrum is overlayed on the lighter, smooth simulation spectra. Simulated spectra is a combination of an alkyl and a singlet with 9 G hyperfine separation assigned to the dienyl radical.

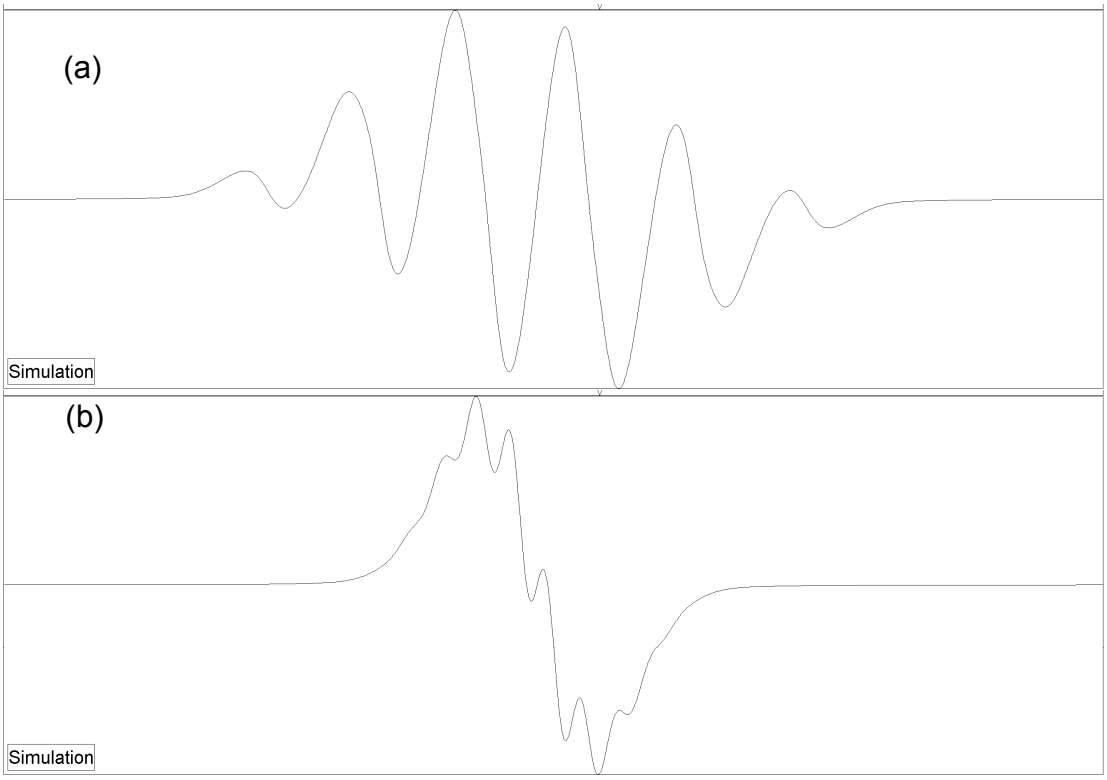

Figure 27. Individual species in the simulated spectrum above. (a) alkyl radical and (b) singlet with 9 G hyperfine separation assigned to the dienyl radical. Note the presence of weak shoulders also contained in experimental spectra.

Radical	Linewidth, G	$H_{\alpha 1}$, G	$H_{\alpha 2}$, G	$H_{\alpha 3}$, G	H_{β}, G
Alkyl	8.4±0.6	23.6±1.4	N/A	N/A	30.7±0.3
Dienyl	5.4±0.2	9.6±1.3	8.3±0.7	8.1±0.4	10.2±0.3

Table VI: Simulation parameters for the spectra simulated in Figure 26. There are two α protons and four β protons for the alkyl radical and one α_1, two α_2 and α_3, and four β protons for the dienyl radical.

5.5 Conclusion

This experiment demonstrated that unfiltered UV light combined with thermal treatments can be used to decrease the concentration of free radicals in irradiated UHMWPE to levels that are about two thirds of what can be achieved using thermal treatments alone. This treatment is effective to depths of at least one millimeter if sufficiently long photoirradiation times are used. However, it is impossible to eliminate all free radicals with UV light treatments because unfiltered UV light not

only does not convert polyenyl radicals, it creates more dienyl radicals. The use of UV light of wavelengths greater than 320 nanometers was also investigated because it does not increase the concentration of dienyl radicals. However, due to lower absorptivity, adequately long photoirradiation times were not explored and only marginal decreases in free radical concentrations were achieved. Theoretically, this technique should be able to eliminate all allyl radicals without converting them to polyenyl radicals, but at the cost of chain scission.

It was also found that the initial decay of alkyl radicals was slower in thinner samples. DSC showed that this effect could not be attributed to differences in crystallinity caused by microtoming. DSC also showed that annealing at 100 °C does not preserve a higher crystallinity content as compared to an anneal at 120 °C.

The most significant finding of this study was the identification and simulation of the dienyl radical. This demonstrates that the assumption that the dienyl radical is a smooth singlet is incorrect. Rather it is a singlet containing six strong hyperfine peaks 9 G apart. These results allow for more accurate spectral simulations for polyethylene irradiated to high doses.

Chapter 6: UV Treatment Effect on Oxidation

6.1 Objectives

While the previous experiment demonstrated that the combination of UV light and thermal treatments can reduce the free radical concentration, it is still unclear if this reduction will have any meaningful effect on the long-term performance of artificial cartilage. While oxidation reduces the mechanical properties such as fatigue resistance[144, 145] and wear resistance[146], a large reduction in mechanical properties does not occur until a critical oxidation index of 1-1.5 is reached[22]. Therefore, it is important to investigate if the reduction in free radicals leads to a significant reduction is subsequent oxidation. Both accelerated and non-accelerated aging were employed in the current study because the higher temperature required by accelerated testing activates oxidation pathways that may not be accessible in the body, such as the thermal decomposition of hydroperoxides which may[147] or may not[148] be stable at body temperatures.

A second objective of this study is to investigate if starting free radical type has an effect on subsequent oxidation. From the UV spectra of the UV treated films (Figure 20), it is clear that most of the remaining free radicals are dienyl radicals while for thermally treated films majority of the remaining radicals are allyl radicals. Therefore, the oxidation behavior of films that were annealed in a nitrogen environment for four hours at 120 °C and had a starting free radical concentration similar to that of the UV treated samples were also explored.

6.2 Procedure

200 μm films were irradiated to a dose of 100 kGy in a nitrogen environment. Four different sets of samples were created: irradiated and no thermal treatment; irradiated then annealed at 120 °C for four hours; sequential anneals at 100 °C and one hour UV treatments as described in the previous experiment; and only sequential anneals at 100 °C. Three samples for each condition were created to allow for statistical variation. Once all the samples were created they were simultaneously exposed to air at room temperature for up to 800 hours. At various time intervals, their EPR, UV and FTIR spectra were measured. The EPR and UV measurements were taken in air, but the FTIR measurements were taken in nitrogen to decrease background noise caused by variations in the concentration of CO_2 in air. UV measurements were taken for only the first 350 hours of oxidation since no spectral changes were observed past 200 hours. At this time, the films were roughened with sandpaper to reduce Fourier rippling and increase the accuracy of FTIR measurements. Measurements were taken for up to 800 hours of oxidation. Following the prolonged exposure to air, accelerated testing was performed on the same films by placing the films in a convection oven at 80 °C for 18 days. This treatment has been reported[24] to simulate five years of *in vivo* oxidation.

6.3 Results

6.3.1 Free Radical Concentration

The decrease in overall free radical concentration upon exposure to air can be seen in Figure 28. The scatter in the data is likely caused by errors in the baseline

correction which can be significant when measuring weak EPR signals. For all the annealed samples, the decay is best fit ($R^2 = 0.90$) by first-order kinetics with a reaction constants of relative value 1, 1.27, and 1.33 s^{-1} for the films that were sequentially annealed at 100 °C and UV treated, annealed at 100 °C , and annealed at 120 °C, respectively. The decay data for the non-annealed samples best fits ($R^2 = 0.91$) second-order kinetics with a reaction constant of 2.7 s^{-1}. Absolute decay constants can not be calculated because absolute radical concentrations are not known. The difference in results is likely caused by the fact that, unlike the other samples, the non-annealed sample initially contains a large number of alkyl radicals which decay differently than the oxidation of stable carbon centered radicals. The starting free radical concentration for the films annealed at 120 °C and sequentially annealed at 100 °C and UV treated were comparable. The films annealed at 100 °C had a slightly higher starting concentration and the films that were not annealed had a considerably higher starting concentration.

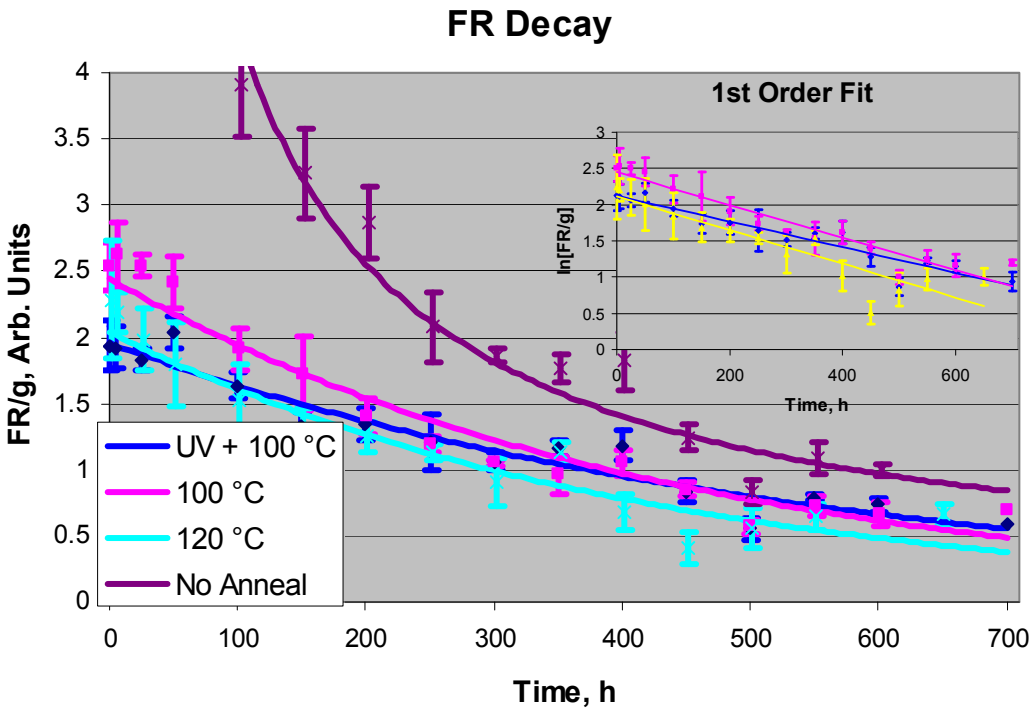

Figure 28. Free radical decrease upon exposure to air for films that were not annealed, annealed at 100 °C for four hours, annealed at 120 °C for four hours, and sequentially annealed at 100 °C and UV treated. All annealed samples were best fit by a first-order decay, whereas the non-annealed samples best fit a second-order decay. Inset: Plot of ln[FR] versus time with linear trendlines used to calculate rate constants. Note that the decay for the non-annealed sample is not shown since it best fit second-order decay.

6.3.2 EPR Spectra Evolution

The EPR spectra evolution for non-annealed, annealed at 100 °C , and sequentially annealed at 100 °C and treated with unfiltered UV light can be seen in Figure 29, Figure 30, and Figure 31, respectively. Despite having different initial free radical species and concentrations, all of the samples had a similar progression. After exposure to air for 200 hours a combination of a singlet and a pentet is clearly visible. These radicals will be assigned in the discussion section. Upon further exposure to air, the pentet decays and only a sharp singlet remains. The decay to a sharp singlet

seems to occur more quickly for the samples that were UV treated. This singlet will be discussed in more detail in section 6.4.3.

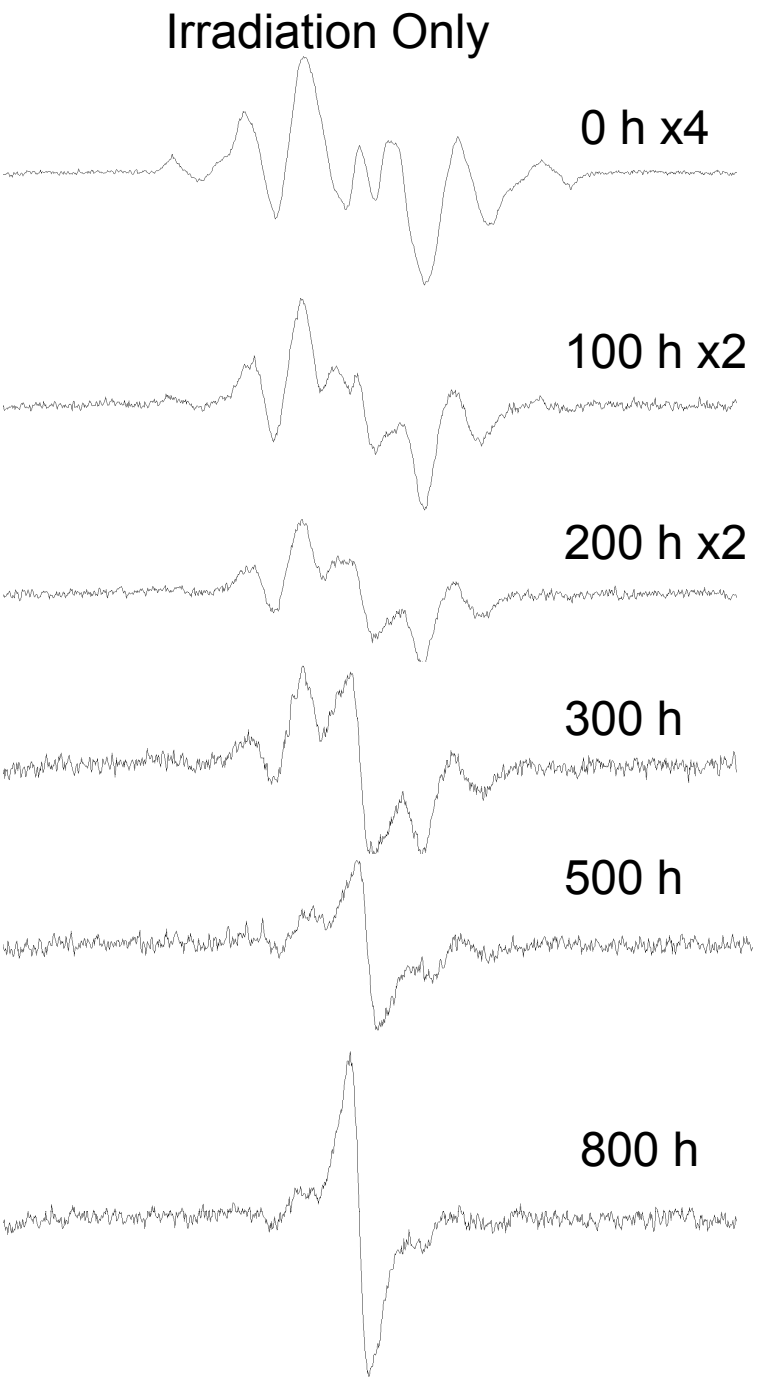

Figure 29. EPR spectra evolution upon exposure to air for samples that were not annealed.

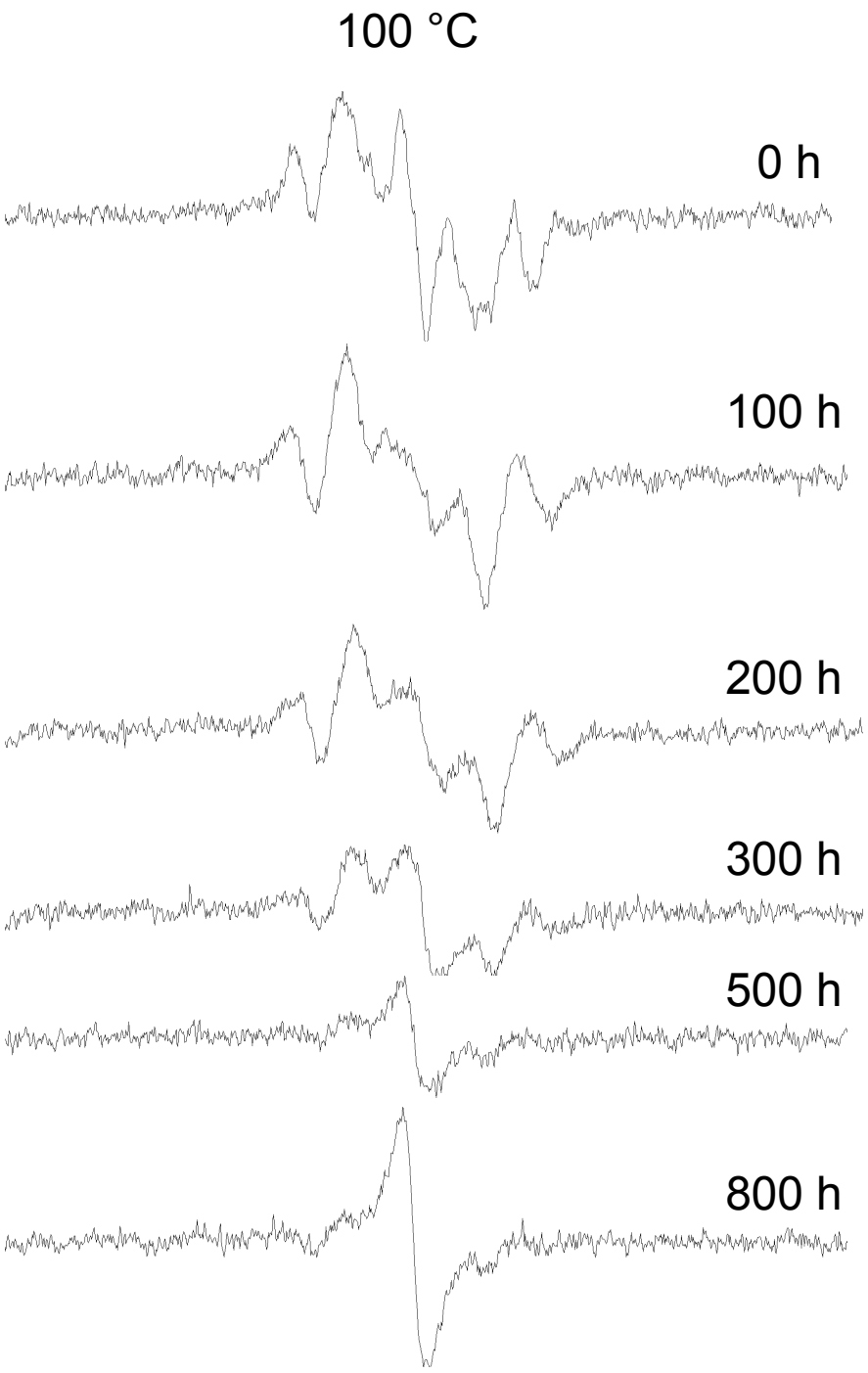

Figure 30. EPR spectra evolution upon exposure to air for samples that were annealed at 100 °C.

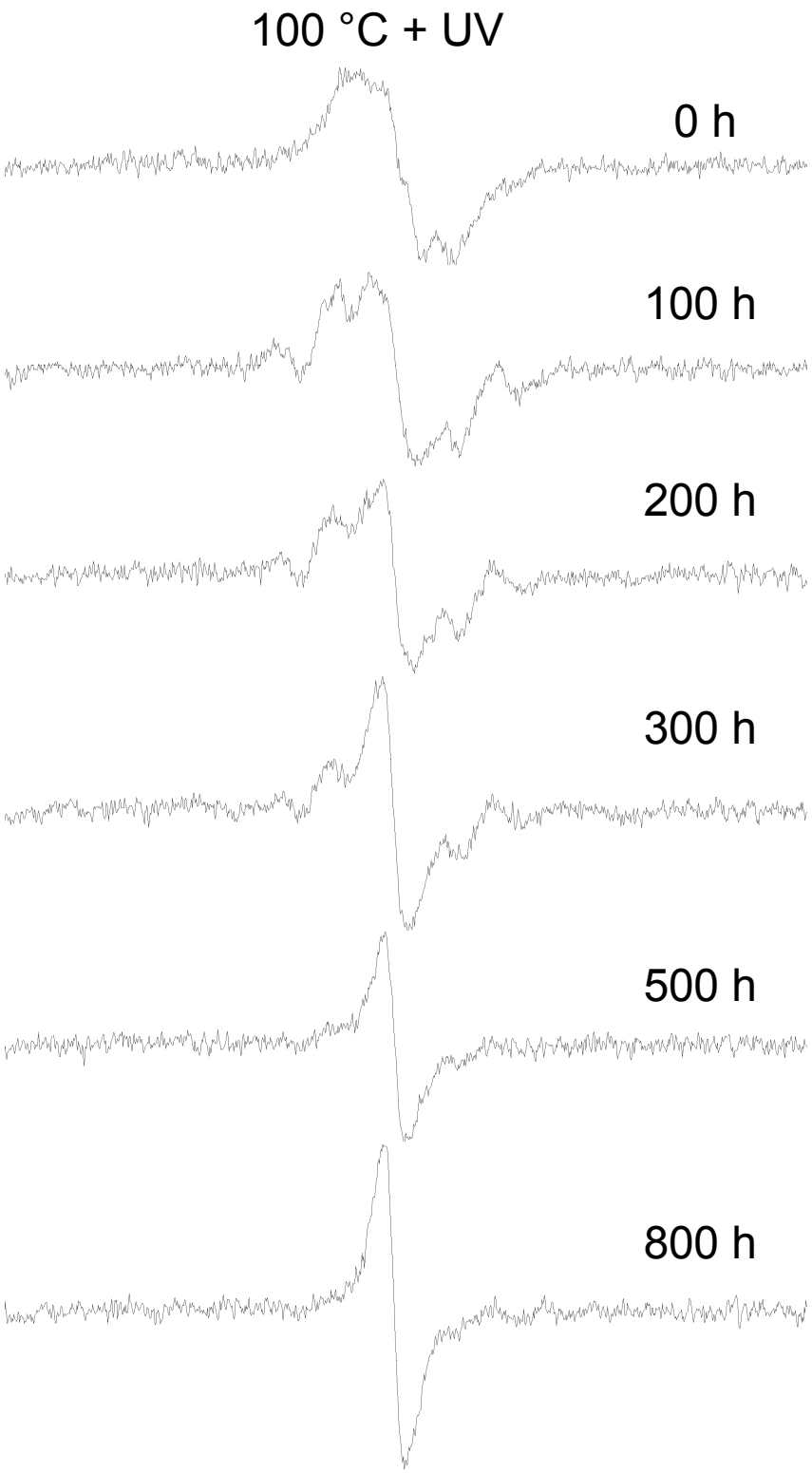

Figure 31. EPR spectra evolution upon exposure to air for samples that were sequentially annealed at 100 °C and treated with unfiltered UV light.

6.3.3 UV-Vis Spectra

The change in UV spectra upon exposure to air can be seen in Figure 32. It is clear that all free radicals and unsaturations, except for diene unsaturations, decay upon exposure to air. The decay of unsaturations other than diene is surprising and is discussed in section 7.4.2. Regardless of starting free radical concentration and type, almost all of the decay seems to have occurred after 50 hours of exposure to air. Aside from the UV treated sample, which still had some absorbance at 323 nm which corresponds to trienyl, after 300 hours of exposure to air, there is no longer a detectable signal for any species except for diene unsaturations.

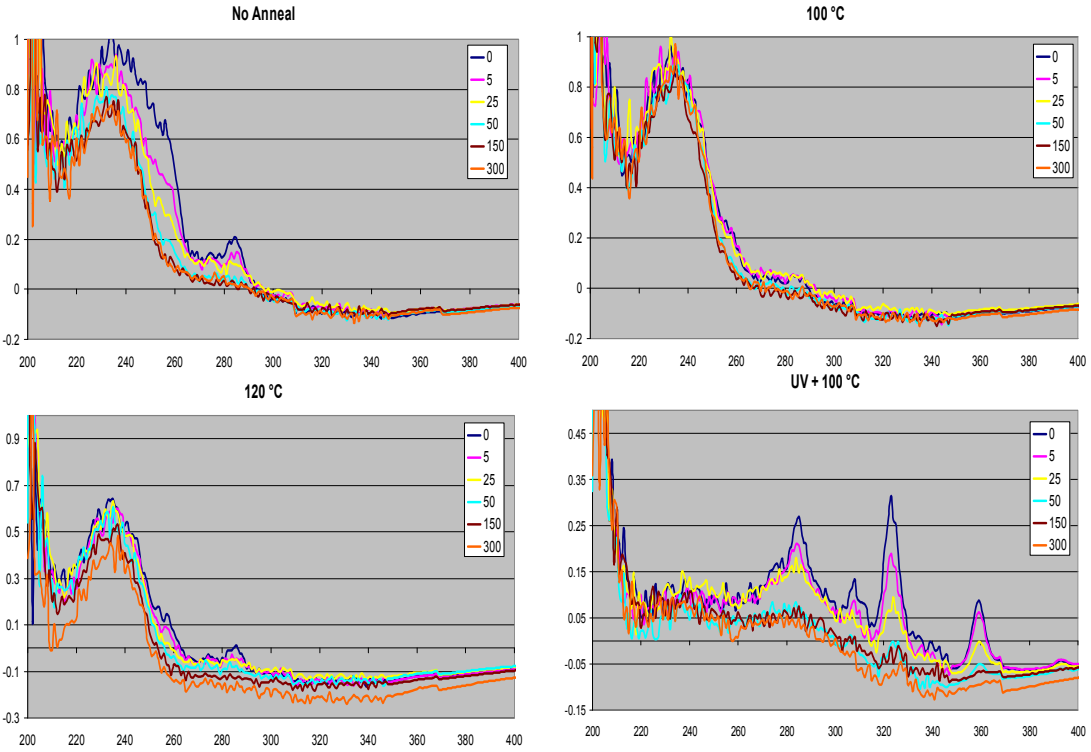

Figure 32. UV spectra showing the decrease in free radicals upon increasing exposure to air for samples with different starting thermal histories. For annealed samples a decrease of allyl and dienyl free radicals, but not of diene unsaturations, is observed. For UV treated samples all polyenyl radicals and polyene unsaturations decrease.

6.3.4 Oxidation

The increase in oxidation index upon exposure to air can be seen in Figure 33. As expected, the samples that were not annealed had the fastest growing oxidation. However, despite having different starting free radical concentrations, the sequentially annealed at 100 °C and UV treated samples and the 100 °C annealed samples had comparable oxidation. The samples annealed at 120 °C had slightly lower oxidation. Overall, the oxidation pattern is similar for all samples, starting off quickly and slowing at longer times. This implies that hydroperoxides are relatively stable at room temperature.

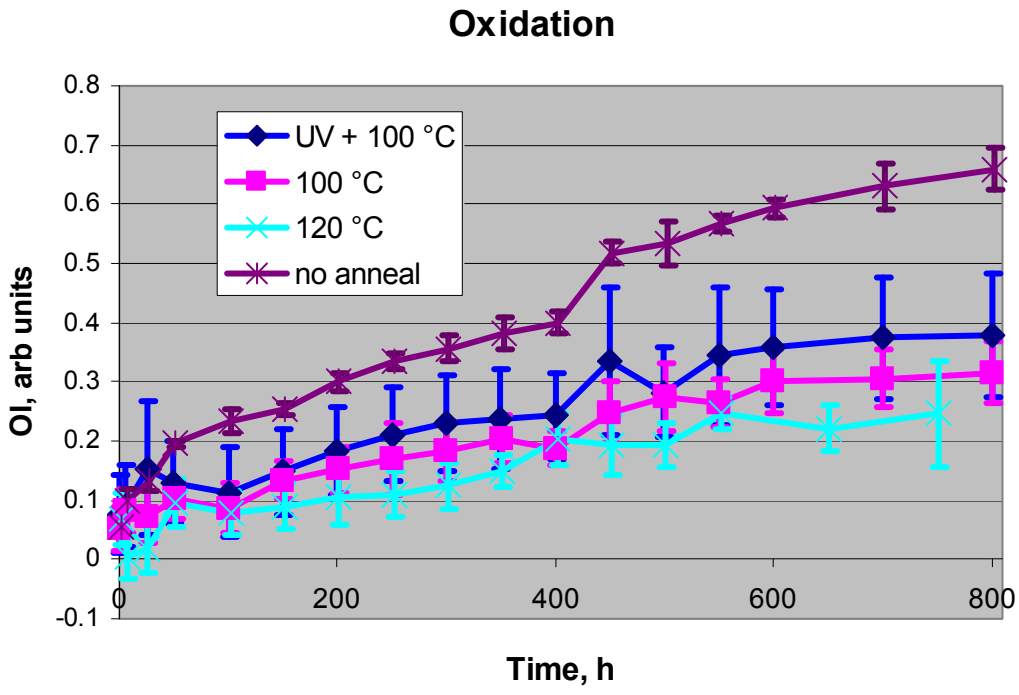

Figure 33. Change in oxidation index upon exposure to air at room temperature for samples with different thermal histories. The sharp increase in oxidation at 450 hours is an artifact caused by roughening the film's surface to reduce Fourier rippling. Oxidation index is computed by dividing the oxidation peak (1675 - 1765 cm^{-1}) by the CH_2 peak (1330-1390 cm^{-1}).

The increase in oxidation index upon accelerated aging at 80 °C for 18 days can be seen in Figure 34. The oxidation index approximately doubles for all samples. The relative extent of oxidation for different samples is similar to that of non-accelerated oxidation. Despite having similar starting free radical concentrations, it is clear the UV treated sample oxidized to a greater extent than the sample annealed at 120 °C.

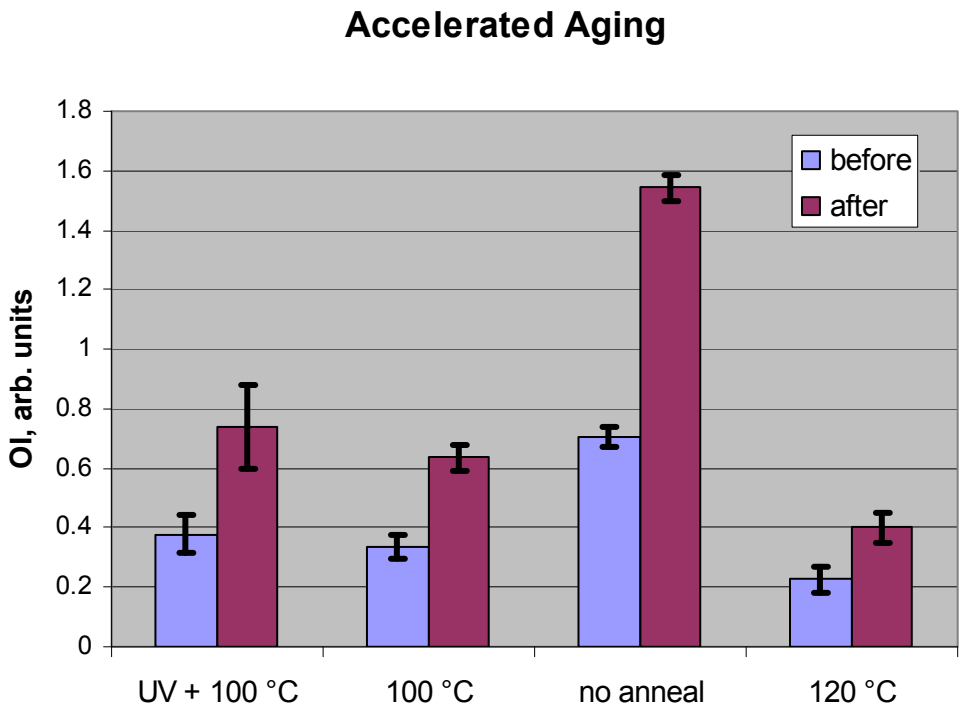

Figure 34. Change in oxidation index after accelerated aging for 18 days at 80 °C. Oxidation is equivalent to five years in vivo. Oxidation index is computed by dividing the oxidation peak (1675 - 1765 cm^{-1}) by the CH_2 peak (1330-1390 cm^{-1}).

6.4 Discussion

6.4.1 UV Treatment Effect on Oxidation

While the combination of UV and thermal treatments significantly reduces the free radical concentration, it has no effect on oxidation. From Figure 33 and Figure 34, it is clear that there is not a significant difference between the oxidation of a sample annealed at 100 °C and a sample that is UV treated and annealed at 100 °C. Further, the UV treated sample oxidized more than the 120 °C annealed sample despite having similar starting free radical concentrations. This implies that UV treatment actually leaves UHMWPE slightly more susceptible to oxidation. This may be due to the fact that the UV treatment creates unsaturations and that allylic hydrogens are more susceptible to abstraction by peroxyl radicals (see section 6.4.2). This effectively increases the propagation rate of peroxyl radicals which increases the oxidation rate.

It is interesting to note that the fastest increase in oxidation occurs during the first 50 hours of exposure to air (Figure 33). This time also corresponds to when most of the initial free radicals have decayed (Figure 32). However, the overall free radical concentration is not much reduced at this time (Figure 28). This implies that the majority of the initial free radicals are decaying by converting to peroxyl radicals via the reaction

$$R^{\bullet} + O_2 \rightarrow RO_2^{\bullet}. \qquad (2.12)$$

This reaction is fast and quickly increases the oxidation index. As all of the initial free radicals are consumed, the oxidation index increases more slowly via the peroxyl

radical abstracting hydrogen to form hydroperoxide and a carbon centered free radical via the reaction

$$ROO^{\bullet} + RH \rightarrow ROOH + R^{\bullet}. \quad (2.13)$$

The carbon center free radical can then combine with oxygen to form a peroxyl radical and further increase the oxidation index.

6.4.2 Effect of Starting Free Radical Species on Oxidation

It is interesting to note that despite the UV treated samples having a different starting free radical species and concentration, all samples underwent a similar EPR progression, i.e. the decay of a pentet component and an increase of a singlet component. A single spectrum, clearly depicting the five peaks of the pentet, can be seen in Figure 35. The five peaks are approximately 20 G apart and likely corresponds to the five strongest peaks of the allyl free radical[149, 150]. While all five peaks correspond to the pentet, the singlet is located only at P3. Close examination of the spectral evolution, Figure 29 through Figure 31, reveals that as time progresses, P1, P2, P4, and P5 decrease while P3 increases. This is due to the simultaneous decay of the pentet spectra and an increase of the singlet spectra. This observation can be made more quantitative by taking the ratio of P3 to P2 which is done in Figure 36. The increase in the ratio is due to both the decrease of P2 and an increase of P3. The ratio for the three non-UV treated samples is nearly identical despite significant differences in their free radical concentration. However, the ratio for the UV treated sample is significantly higher and is never less than one. This is may be due to the fact that, unlike the other samples, at the time of exposure to air, the UV treated

sample contains almost no allyl radical. Allyl radicals are then formed during the formation of hydroperoxide from a peroxyl radical via the reaction

$$ROO^{\bullet} + RH \rightarrow ROOH + R^{\bullet}. \quad (2.13)$$

It is possible that peroxyl radicals preferentially abstract allylic hydrogen which have lower bond energies than saturated hydrocarbons[151], resulting in direct formation of allyl radicals. Alternatively, reaction (2.13) can result in the formation of alkyl radicals which quickly migrate to unsaturations and become allyl radicals, but this is deemed less likely since no evidence of alkyl radicals was seen in the EPR spectra.

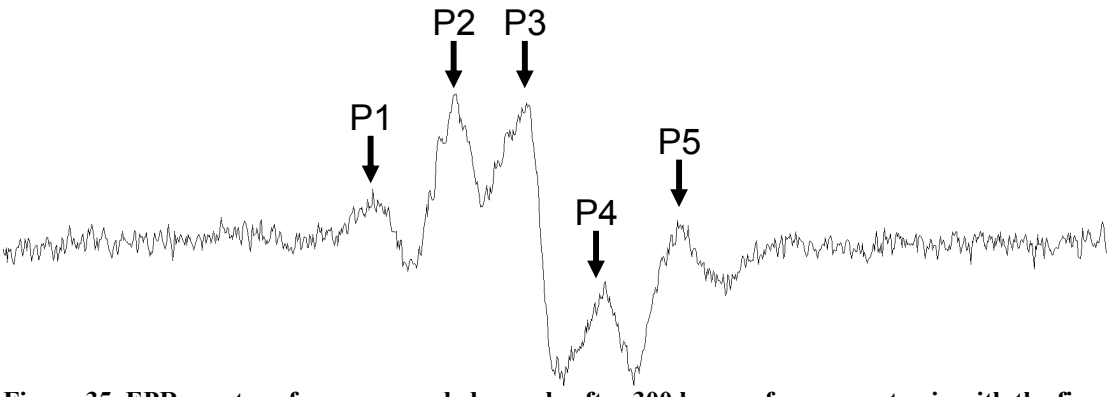

Figure 35. EPR spectra of a non-annealed sample after 300 hours of exposure to air with the five prominent peaks clearly labeled. The peaks are approximately 20 G apart, likely corresponding to the allyl radical.

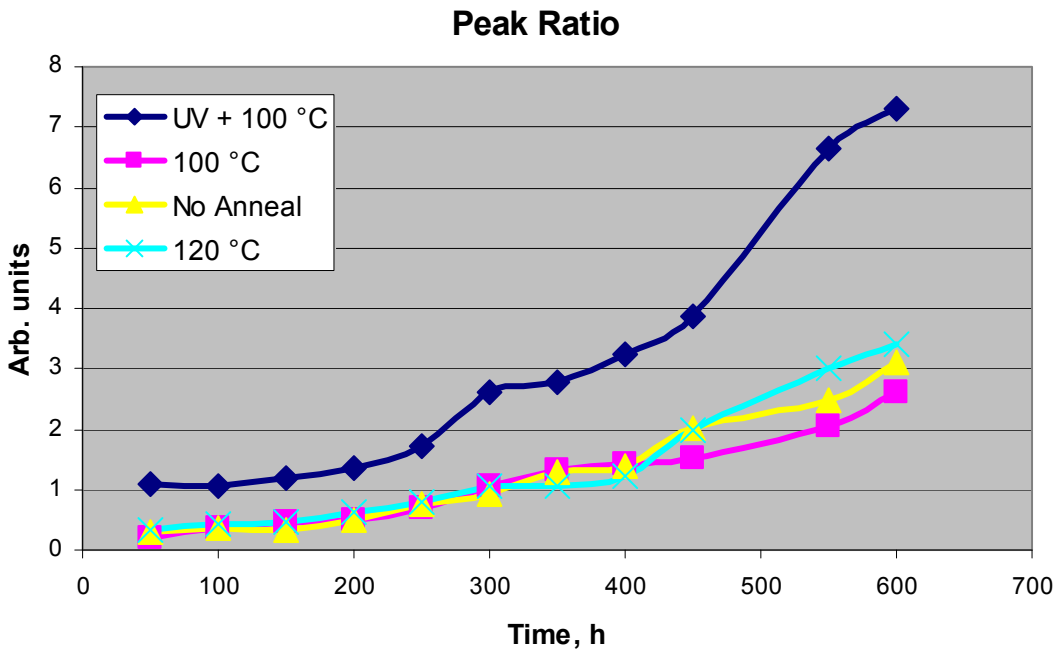

Figure 36. Change in the ratio of the P3 to P2 during prolonged exposure to air for samples with different thermal histories.

One of the objectives of this study was to determine the kinetics of oxidative decay of individual free radical species. The oxidative decay of various free radical species can be seen in Figure 37. The relative concentration of polyenyl radicals was measured by manually measuring the peak height from a linear baseline. Only samples and exposure times (≤50 hours) containing an adequate amount of free radicals to allow accurate measurement were included. Since the allyl radical only appears as a shoulder on the diene unsaturation peak, its concentration was calculated by monitoring the change in absorbance at 258 nm after correcting for absorbance at 258 nm due to diene unsaturations. This resulted in the measured allyl radical concentration having larger uncertainties that the other radicals which have well-resolved peaks.

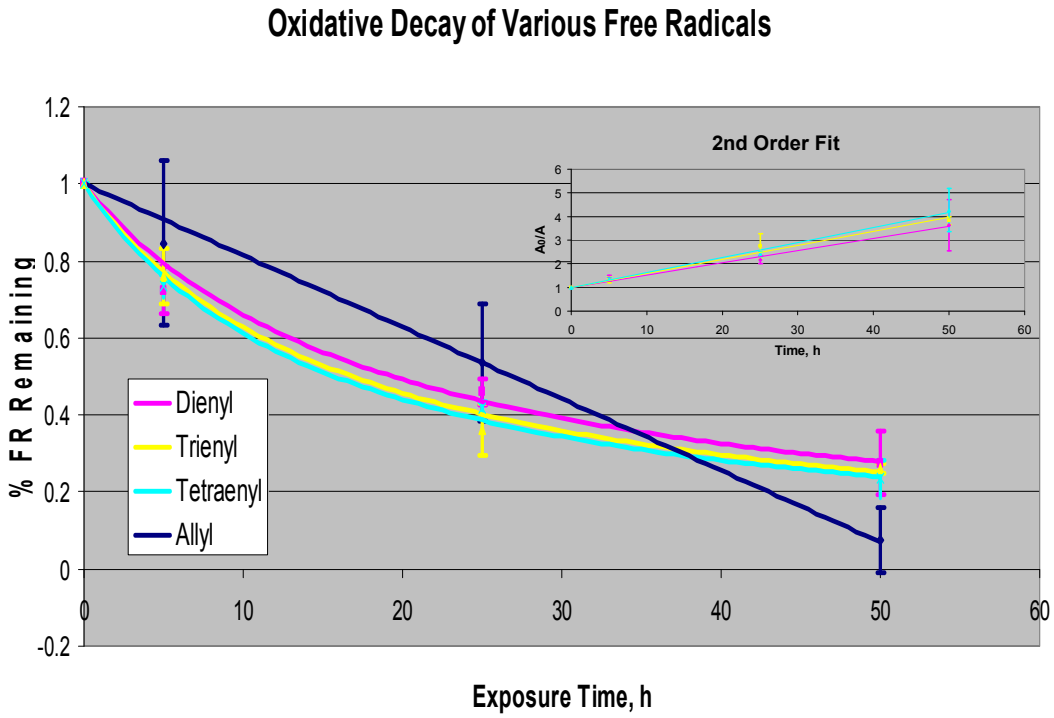

Figure 37. Oxidative decay of various free radicals upon exposure to air. Allyl radical decay shows a linear, zero-order decay while all polyenyl radicals decay via second order kinetics with similar reaction rates. Inset: Plot of inverse absorbance versus time for polyenyl radicals with linear trendlines used to determine rate constants.

The allyl radical's decay is linear, a gives an excellent fit ($R^2 = 0.99$) to a zero-order decay with a decay rate of 0.44 mole L^{-1} s^{-1}. In contrast, the decay of all polyenyl radicals fit ($R^2 = 0.99$) a second-order decay with similar rate constants, 8.8, 10 , and 11 x 10^4 ε^{-1} s^{-1}, where ε is each radical's molar absorptivity, for the dienyl, trienyl, and tetraenyl radical, respectively. The difference in rates between polyenyl radicals may lie within the margin of error of the concentration measurements. Using these values, the decay curves for the radicals were plotted in Figure 37. These results show that polyenyls containing a higher degree of conjugation are not more resistant to oxidative decay that polyenyls containing a lower degree of conjugation.

6.4.3 The Sharp Long-Lived Singlet

All samples have a similar EPR free radical evolution and, after an extended exposure to air, contain a sharp singlet. However, the nature of this singlet is unknown. At least two types of free radicals are known to exhibit singlet spectra in polyethylene, the peroxyl and polyenyl free radical. Power saturation experiments revealed that saturation occurred and that it is not a peroxyl free radical[51]. Therefore, the radical is most likely a polyenyl radical. Polyenyl radicals can be created during the oxidation of polyethylene by the abstraction of an allylic hydrogen of a conjugated unsaturation by a peroxyl radical.

There are several difficulties with this assignment. It is surprising that these polyenyl radicals are stable in the presence of oxygen. It is clear from Figure 32 that polyenyl radicals are transformed in the presence of oxygen into peroxyl radicals. However, polyenyl radicals can only combine with oxygen if they have access to it. It is believed that oxygen can not enter the crystalline region. It is also known that oxidation increases crystallinity[152]. Therefore, it is possible that these radicals become trapped in the newly formed crystals and are no longer accessible to oxygen.

It is also surprising that the long-lived polyenyl radicals are not seen in the UV spectra. This may be due to their low concentration. EPR is significantly more sensitive than UV spectroscopy. Additionally, the signal from different polyenyl radical species overlap (and hence are additive) in EPR spectra but are well resolved in UV spectra.

Finally, it is surprising that this polyenyl radical spectrum should be considerably sharper than the polyenyl radical spectra observed in the other

experiments (Figure 18 and Figure 39). This effect has been previously observed by others[51], and was attributed to the selective oxidation of lower order polyenyl radicals, the assumption being that lower order polyenyl radicals are more reactive and have larger linewidths. However, both of these assumptions are challenged in this dissertation (section 6.4.2 and section 7.4.1). Instead, I believe the sharper linewidth is due to the radicals being located in the crystalline region. Linewidth broadening is due to variations in the distance between the free radical and neighboring protons. In the crystalline region, chains are held more rigidly in place and there is less variation. This effect has previously been used to explain the sharpening of an alkyl radical EPR signal in polyethylene[46].

6.4.4 Kinetics Analysis

There are many interesting points that arise from the kinetic analysis of the total free radical decay (Figure 28) and individual specie decay (Figure 37). It is surprising that the thermal and UV treated sample, which consisted of mostly polyenyl radicals, should decay via first-order kinetics, while individual polyenyl radical species decay via second-order kinetics. The resolution to this seeming contradiction likely lies in the different characterization techniques used. Figure 28 is an EPR measurement which shows the decrease in *total* free radical concentration. When polyenyl radicals combine with oxygen, they are converted to peroxyl radicals and do not contribute to the decrease in total free radical concentration. Only when peroxyl radicals recombine with each other or with carbon centered free radicals does the free radical concentration decrease. Figure 37, which is a UV measurement, is

very sensitive to the oxidation of polyenyl radicals to peroxyl radicals since this conversion shifts the absorbance peak and dramatically lowers the molar absorptivity.

It is surprising that the total free radical concentration should decay via first-order kinetics. Since total free radical concentration can only decrease via radical-radical recombination, one would expect the decay to be second-order. There are several possible solutions to this dilemma. (1) It is possible that this decay is pseudo first-order. (2) It is possible that the recombination is limited by an intermediate, first-order reaction. For example, in order for the radical site to be mobile it must be transferred to a new chain via the reaction

$$PEO_2^{\bullet} + PE \rightarrow PEOOH + PE^{\bullet} \qquad (2.13)$$

which is expected to be a first-order reaction. (3) It is also possible that the overall decay is a combination of more than one reaction, such as the recombination of peroxyl radicals with each other and with carbon centered radicals. Overall, one must keep in mind that attempting to fit the complicated decay of the overall free radical concentration to simple first- or second-order is a crude approximation. Radical decay depends on sample morphology and radical reactivity. Accurate models attempt to correct for crystalline content[45], different radical reactivity[153], time varying reaction constants[49], or the possibility of multiple reactions[47, 48].

Another surprise is that the combination of allyl radicals with oxygen is a zero-order reaction, while the combination of polyenyl radicals with oxygen is a second-order reaction. Since, until the start of measurements, the samples were irradiated and stored in a low oxygen environment it is reasonable to assume that the starting oxygen concentration is effectively zero. Therefore, the oxygenation of allyl

radicals is expected to be limited by the diffusion of oxygen into the polyethylene film. Since the in-diffusion of oxygen is expected to be considerably slower than the oxygenation of allyl radicals[29], this reaction will be zero-order with respect to the allyl radical concentration. It is unclear why polyenyl radicals decay via second-order kinetics. Their oxidation may be considerably slower than the allyl radical's due to their greater stability or their surrounding morphology. It is also possible that they primarily decay via recombination with an oxygenated polyenyl radical which would result in second-order decay.

6.5 Conclusion

While the combination of thermal and UV treatments can reduce free radical concentrations significantly, this does not have a significant effect on its subsequent oxidation. This may be due a tradeoff between reduced starting free radical concentration and increased oxidation susceptibility induced by an increased concentration of easily abstracted allylic hydrogens. During the oxidation process, a combination of allyl, polyenyl, and peroxyl free radicals are present. After hundreds of hours of exposure to air, only a sharp singlet is present regardless of starting free radical concentration and type. This singlet is likely attributed to a polyenyl radical trapped in the crystalline region. These radicals either start in the crystalline region (as is the case with the UV treated samples), or become trapped in the crystalline region during oxidation induced crystallization. Additionally, there does not seem to be a significant difference in the oxidation rate of different polyenyl free radicals.

Chapter 7: Effect of Photoirradiation Environment

7.1 Objectives

In previous work[36, 86] involving the photoirradiation of polyethylene containing free radicals, it was observed that diene unsaturations were consumed and higher order polyene unsaturations and polyenyl radicals were produced. A possible mechanism for the conversion of lower order polyene unsaturations and polyenyl radicals to higher order is the sequential addition of alkyl radicals, i.e. reaction (3.4). However, if the overall free radical concentration does not significantly decrease during this conversion, a continuous supply of alkyl radicals from an unknown source is required for this mechanism to be plausible. Previously (section 3.2.3), it was suggested that a continuous supply of alkyl radicals could be produced via the photodecay of hydroperoxides. The first objective of this experiment is to investigate if this is indeed the source of alkyl radicals. Since this mechanism requires a constant supply of oxygen, this mechanism can be tested by photoirradiating in an oxygen rich and oxygen poor environment. It is expected that the overall increase in degree of unsaturation will proceed faster and farther in the presence of air.

It was noted above (section 3.2.2) that in order to increase the degree of conjugation, an intramolecular recombination between radicals is required. While, in general, intermolecular recombination is significantly faster than intramolecular recombination, it was postulated that this might not be the case for polyenyl free radicals due to steric hindrances resulting from stiff unsaturations. Hydrogen gas is known to increase the rate that alkyl radicals convert to allyl radicals[125]. It is believed that hydrogen catalyzes intramolecular migration along the chain by helping to bridge

the 1.93 Å distance between adjacent hydrogen atoms along the chain via a concerted mechanism during which the hydrogen atom is never completely free[42].

$$R^{\bullet} + H_aH_b + RH_c \rightarrow RH_a + H_bH_c + R^{\bullet} \quad (7.1)$$

Thus, hydrogen gas has a marked effect on the *rate* of alkyl radical decay but has no effect on the *extent* of the decay[38, 104]. The second objective of this study is to investigate the validity of reaction (3.4) as the mechanism for the increase in the overall degree of conjugation. Since hydrogen gas increases intramolecular migration, it is expected to increase the rate at which this increase occurs.

Finally, as noted above (section 3.2.4), reaction (3.4) suggests a one-to-one increase/decrease of polyene unsaturations/polyenyl radicals. The third objective of this study is to see if such an increase can be experimentally observed.

7.2 Procedure

Three 200 μm films were placed in EPR tubes and irradiated to a dose of 100 kGy. Two films were irradiated while in a nitrogen environment while one film was irradiated in 150 torr of hydrogen gas. One of the nitrogen films was opened to air and all three films were simultaneously photoirradiated, ensuring even photoirradiation of all three samples. At various time intervals, the films were removed for measurements. EPR measurements were performed while the samples were still in their tubes. Three measurements were averaged for each data point. UV spectra were measured for the air sample in air while the UV spectra for the nitrogen sample were performed with the film in a nitrogen filled cuvette (as described in section 4.2.2). It was not possible to measure the UV spectra for the hydrogen sample without destroying the hydrogen environment so only a final measurement at the

conclusion of photoirradiation was performed. Three measurements were averaged for each data point. Because of inevitable exposure to air during transfer in and out of the instrument, FTIR measurements were performed for the air sample only. However, to allow accurate UV spectra measurements, the film could not be roughened and peaks occurring at lower wavenumbers were masked by Fourier rippling. At the conclusion of the experiment, the films were roughened and the peaks at lower wavenumbers could be clearly observed. Three measurements were averaged for each data point.

In order to investigate the effect of photon flux, the experiment was repeated in an air and nitrogen environment using a lower power compact short arc xenon lamp at a distance of 60 cm. It is estimated that the light power was reduced by a factor of four.

7.3 Results

7.3.1 Free Radical Concentration

The decrease in free radical concentration upon continuous photoirradiation with unfiltered UV light can be seen in Figure 38. Initially, the free radical concentration quickly decreases to a plateau level after four to six hours of photoirradiation. This plateau level is significantly higher (~30%) than levels reached by using thermal or thermal and UV treatments (>10%). The decay did not fit first- or second-order kinetics. It is interesting to note that the radical decay is almost identical in an air or nitrogen environment but results in a higher ultimate free radical concentration in a hydrogen environment.

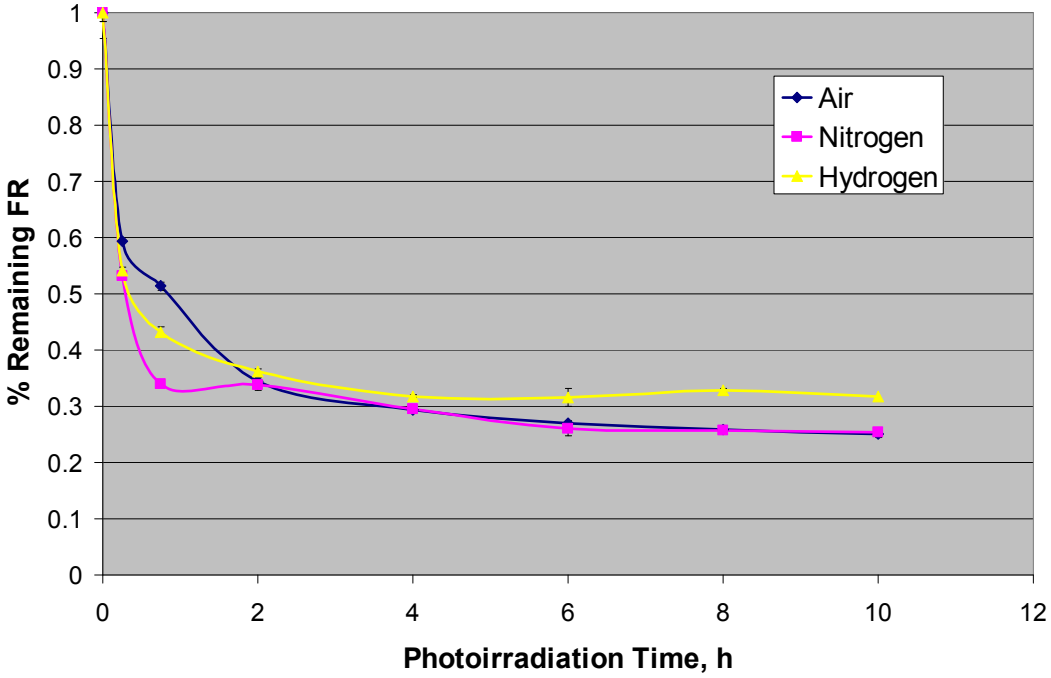

Figure 38. The decrease in free radical concentration upon photoirradiation with unfiltered UV light in various environments.

7.3.2 EPR Spectra Evolution

The evolving EPR spectra for unfiltered photoirradiation in an air, nitrogen, and hydrogen environment can be seen in Figure 39, Figure 40, and Figure 41, respectively. A similar progression is seen for all environments. The initial alkyl spectrum converts to a singlet with nine gauss hyperfine separation although some alkyl radical still remains. The singlet has already been assigned to the dienyl free radical. With increasing photoirradiation, the hyperfine structure and the presence of alkyl radicals diminished until only a smooth singlet remains. The singlet does not significantly decrease in height or linewidth during this process. Similar to the free radical decay results, the spectral evolution is nearly identical in an air and nitrogen environment, but the progression is considerably slower in a hydrogen environment.

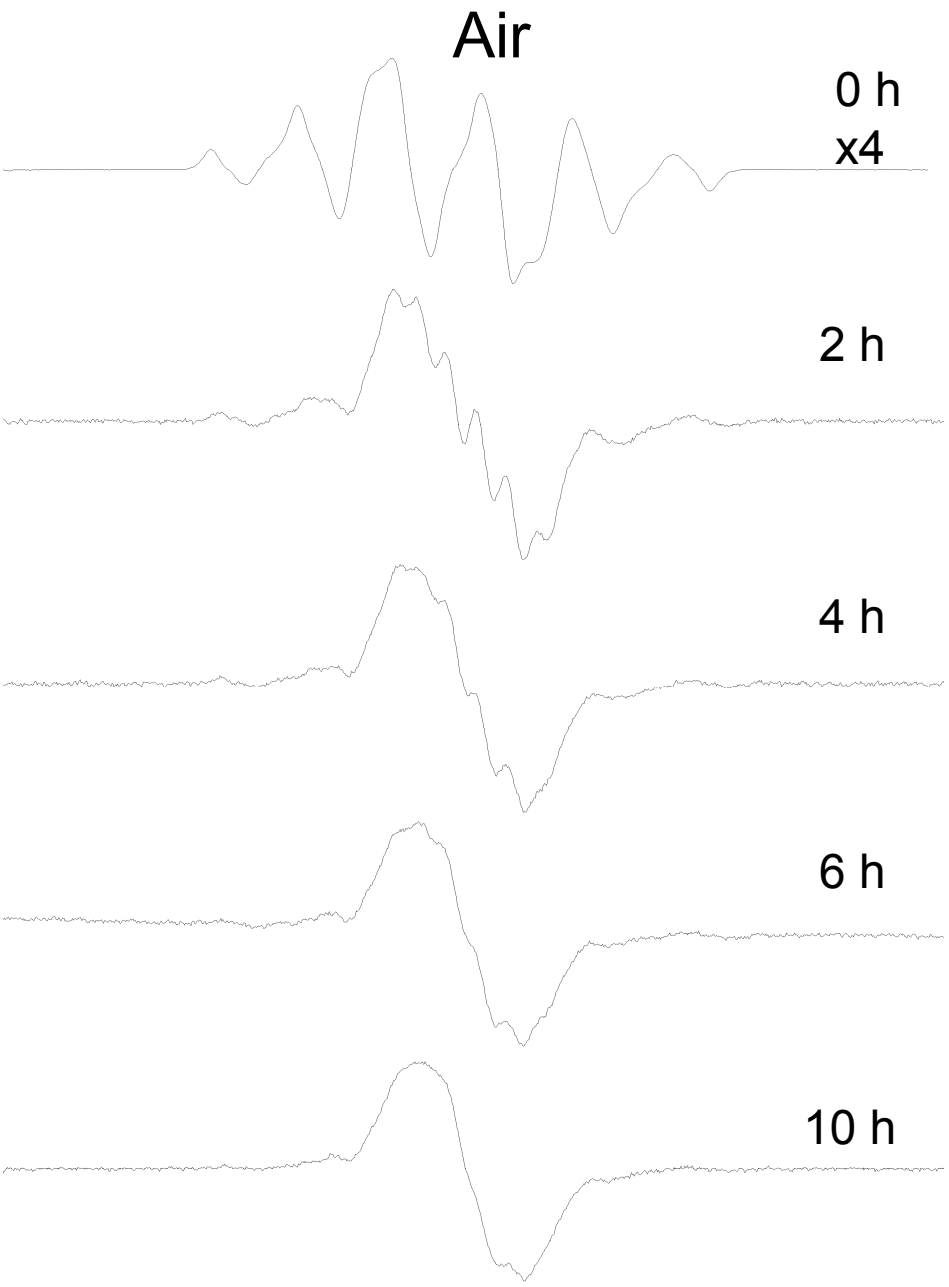

Figure 39. Evolution of the EPR spectra with increasing photoirradiation time in air.

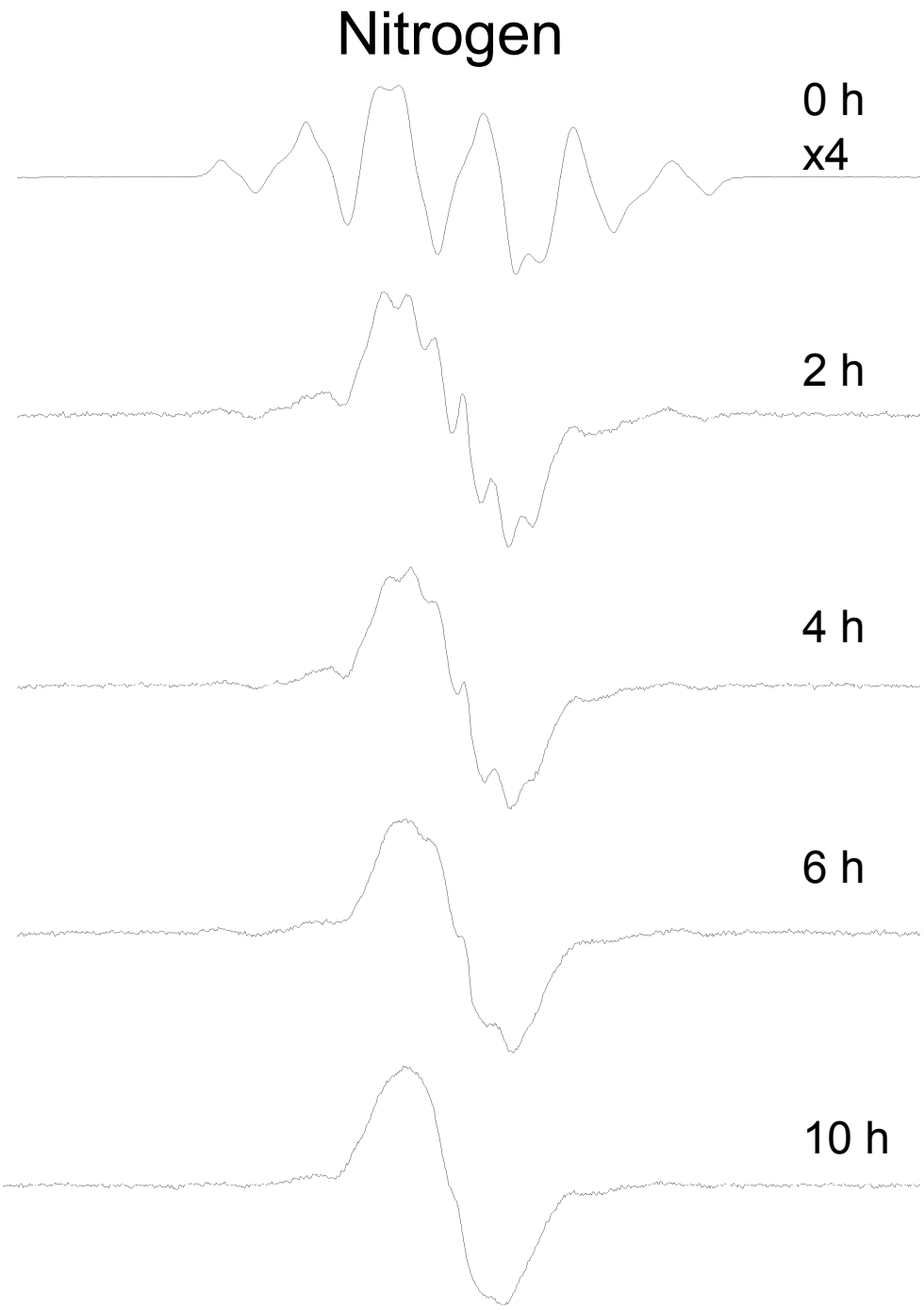

Figure 40. Evolution of the EPR spectra with increasing photoirradiation time in nitrogen.

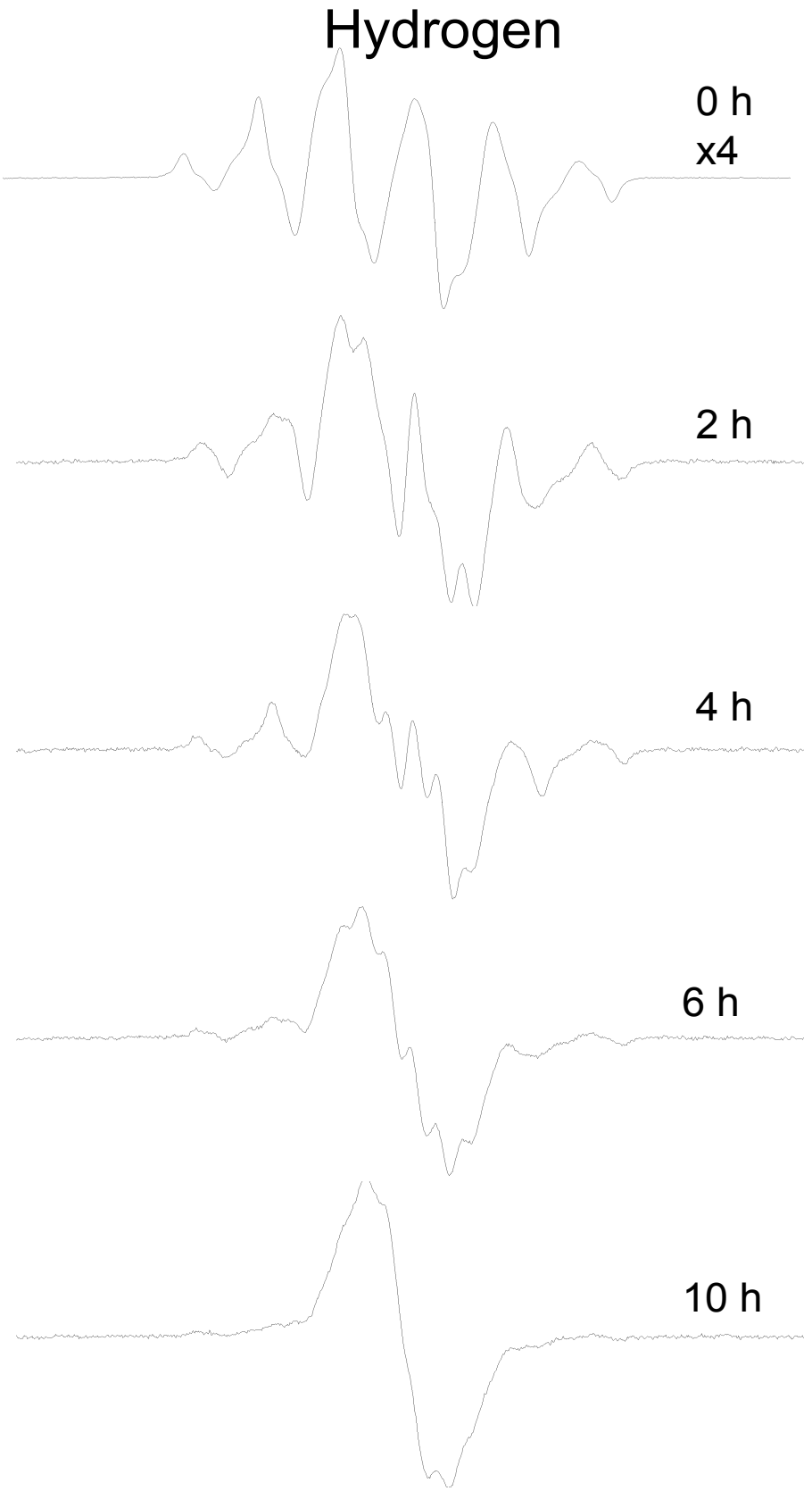

Figure 41. Evolution of the EPR spectra with increasing photoirradiation time in hydrogen.

7.3.3 UV Spectra

The change in the UV spectra upon increasing unfiltered photoirradiation in a nitrogen and air environment can be seen in Figure 42 and Figure 43, respectively. While these spectra are very complex, it is clear that with increased photoirradiation, lower order polyene unsaturations and polyenyl radicals are consumed and higher order ones are produced. To make this observation more quantitative, peak heights were manually measured from a linear baseline. Unfortunately, it was impossible to measure the change in the allyl radical because it only appeared as a subtle shoulder on the diene unsaturation peak and the diene unsaturation peak underwent severe reductions. Additionally, the triene peak also only appears as a shoulder on the dienyl radical peak and was often difficult to accurately measure. Also, due to increased noise at lower wavelengths, baseline selection for diene unsaturations was difficult. A comparison of the evolution of polyene unsaturations and polyenyl radicals in a nitrogen and air environment can be seen in Figure 44 and Figure 45, respectively. Concentrations were calculated using assumed molar absorption coefficients when known coefficients were not available, see section 7.4.5 for more details.

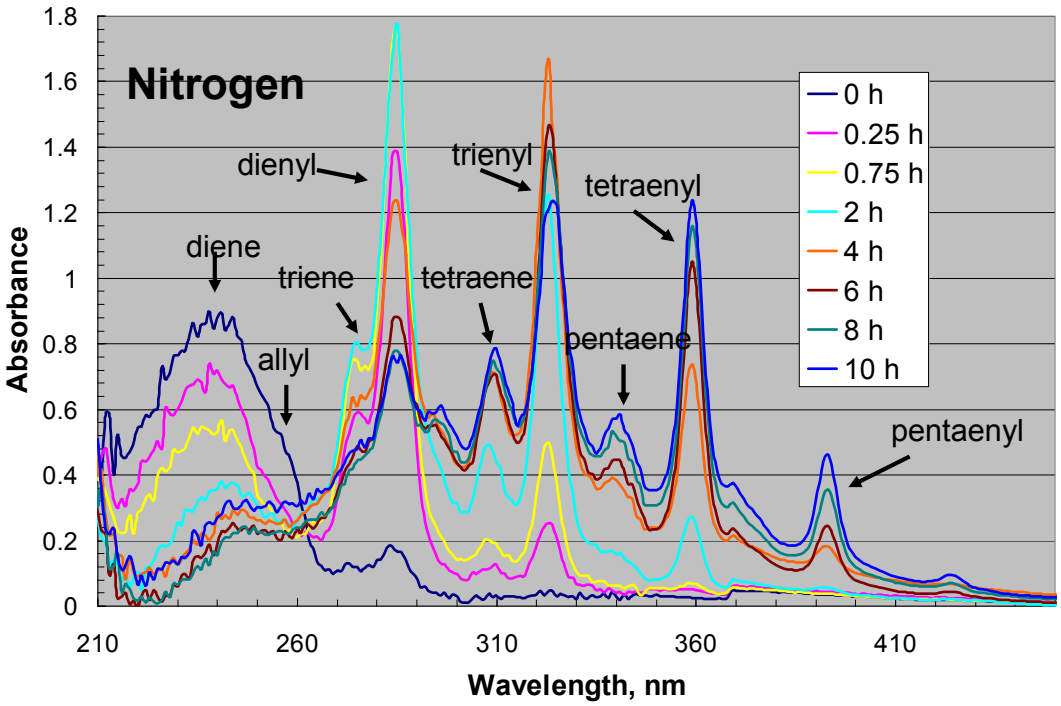

Figure 42. Change in UV spectra upon continuous unfiltered UV photoirradiation in a nitrogen environment. Spectra are an average of three scans.

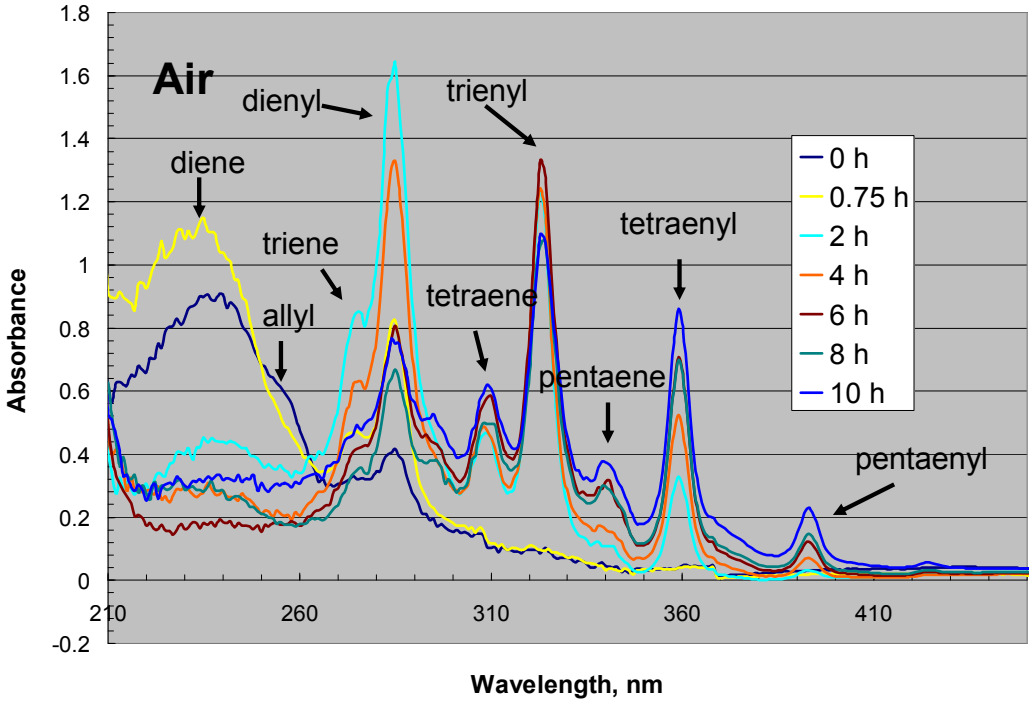

Figure 43. Change in the UV spectra upon continuous unfiltered UV photoirradiation in an air environment. Spectra are an average of three scans.

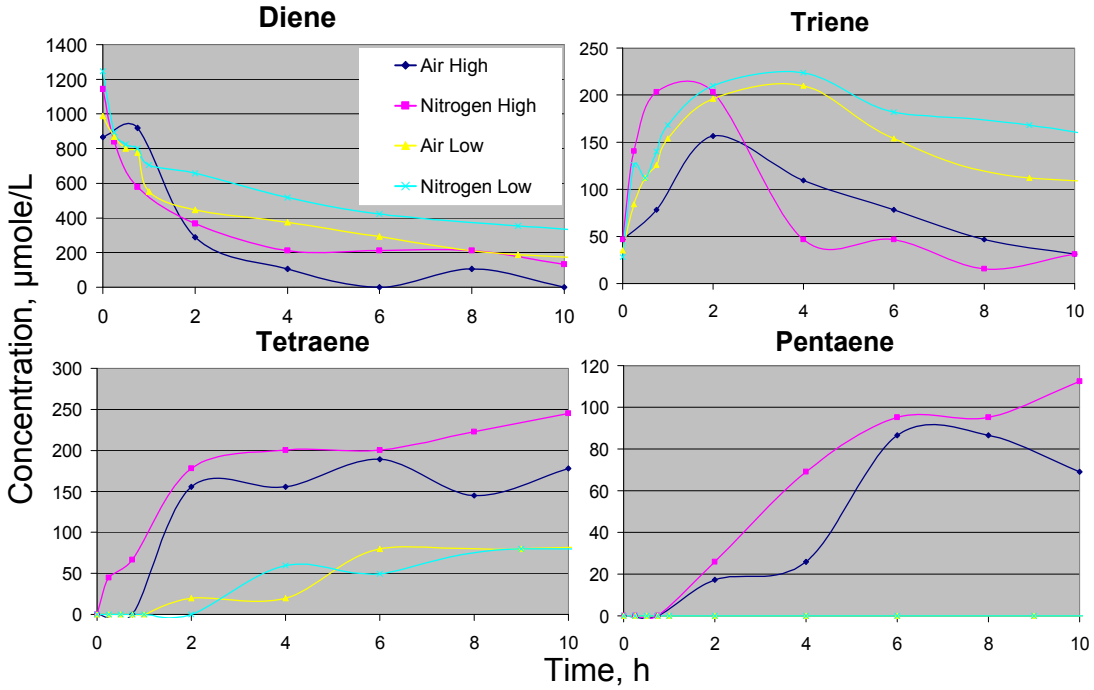

Figure 44. Change in the concentration of polyene unsaturations upon unfiltered irradiation at high and low light fluence in an air and nitrogen environment. Please note the difference in scale for the graphs.

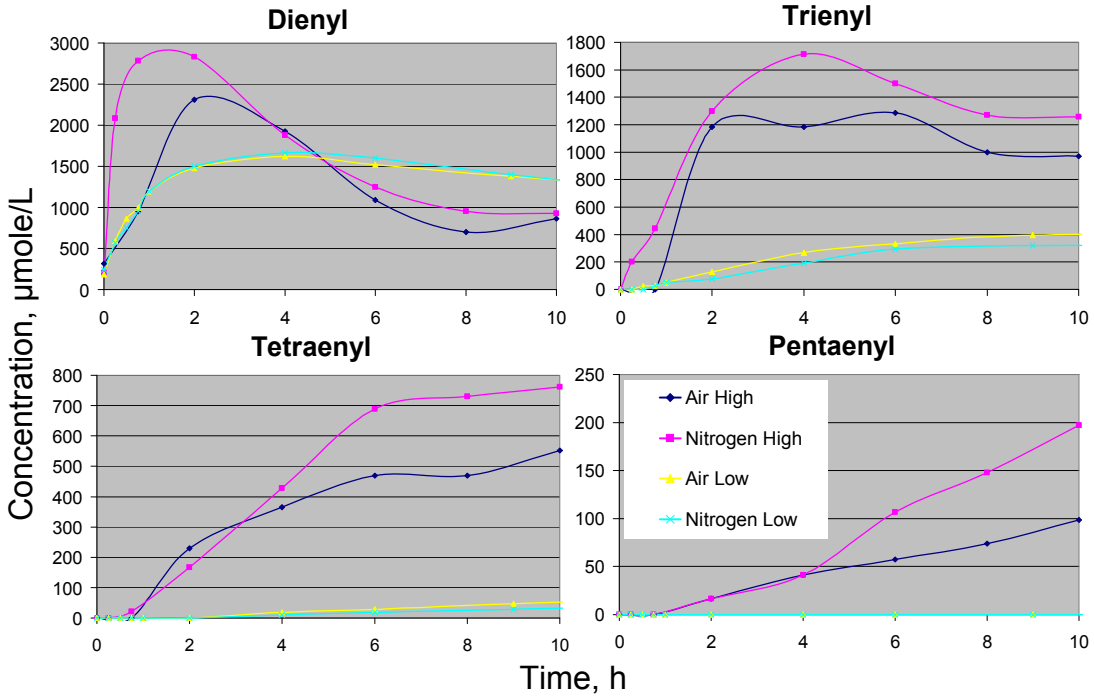

Figure 45. Change in concentration of polyenyl radicals upon unfiltered photoirradiation at high and low light fluence in an air and nitrogen environment. Please note the difference in scale for the graphs.

Overall, the change in UV spectra does not seem to depend on photoirradiation environment but strongly depends on light fluence. After about two hours of photoirradiation at high fluence, the diene unsaturation concentration is sharply reduced while the dienyl and other radical concentrations are increased. After four hours, the concentration of dienyl radicals begins to decrease and the trienyl's concentration peaks. Continued irradiation reduces the concentration of dienyl and trienyl radicals while tetraenyl and pentaenyl radicals continue to increase. A similar pattern is seen at low fluence except that the increases and decreases occur more slowly. Also, higher order free radicals like tetra and pentaenyl are substantially suppressed.

The UV spectra after ten hours of photoirradiation in an air, nitrogen and hydrogen environment can be seen in Figure 46 and a comparison of the species content can be seen in Figure 47. It is clear that the formation of higher order polyenyl radicals is reduced but not completely suppressed in a hydrogen environment. Additionally, there is a much stronger presence of diene unsaturations in the hydrogen sample.

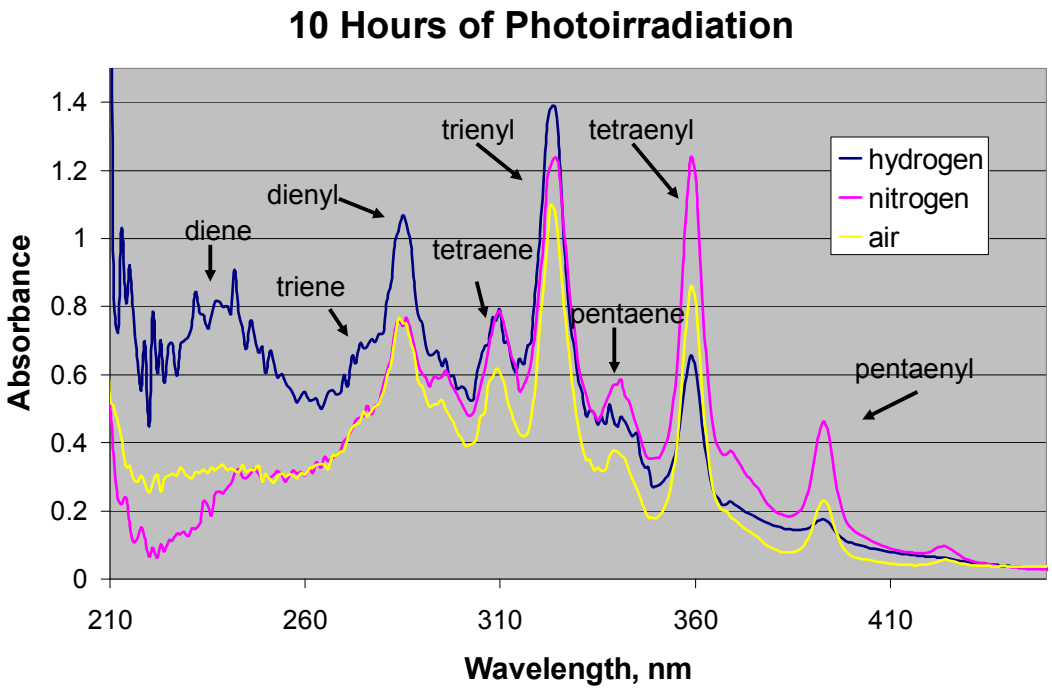

Figure 46. UV spectra after ten hours of unfiltered UV photoirradiation in a hydrogen, nitrogen, and air environment. Spectra are an average of three scans.

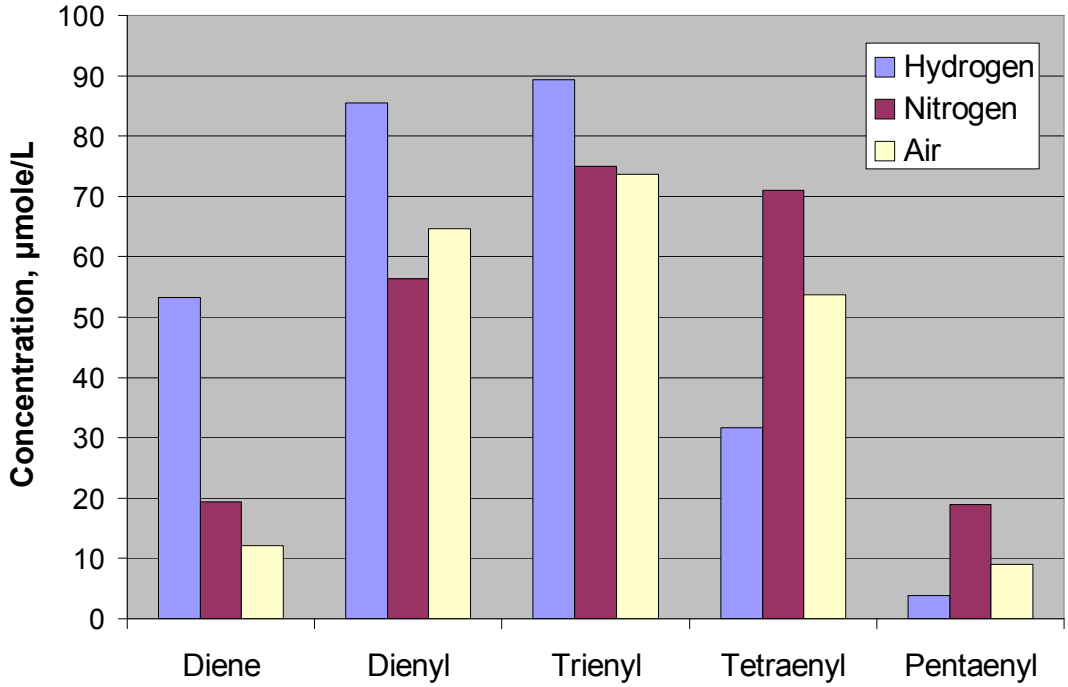

Figure 47. Comparison of diene unsaturation and polyenyl radical concentration after ten hours of unfiltered photoirradiation in different environments.

7.3.4 FTIR Results

The increase in oxidation index with photoirradiation time in air can be seen in Figure 48. The oxidation index quickly increases but starts to level off at longer photoirradiation times. This may be the result of the decreasing free radical concentration (Figure 38). The increase in oxidation index occurs more quickly than non-photoirradiated oxidation (Figure 33).

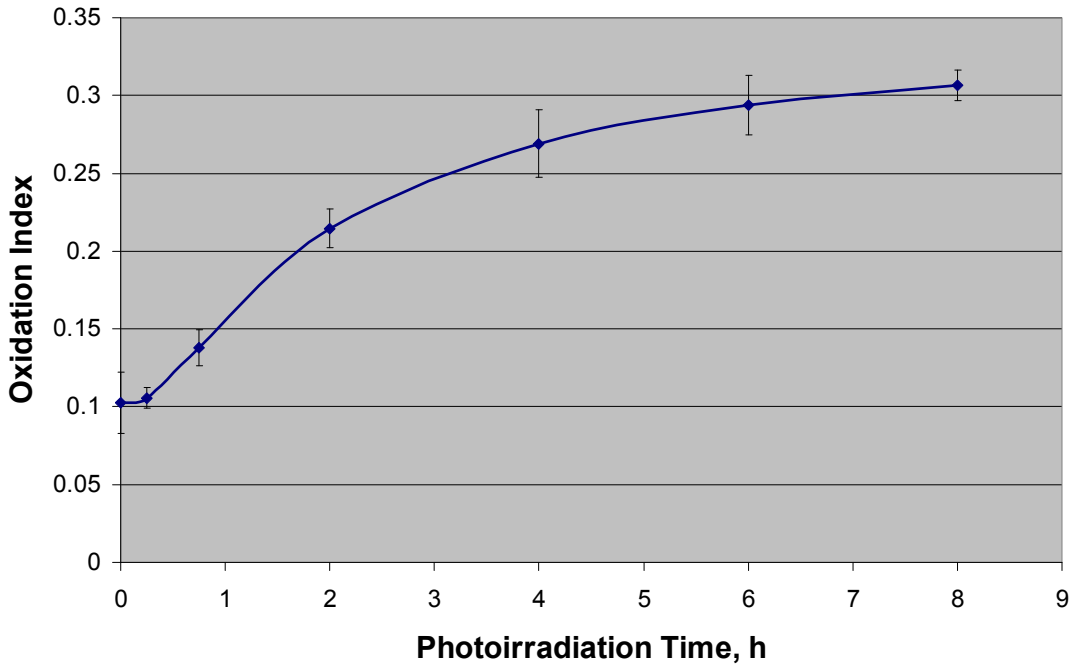

Figure 48. The increase in the oxidation index with unfiltered UV photoirradiation. Oxidation index is computed by dividing the oxidation peak (1675 - 1765 cm^{-1}) by the CH_2 peak (1330-1390 cm^{-1}).

The FTIR spectra after unfiltered photoirradiation in different environments can be seen in Figure 49. All of the samples have similar *trans*-vinylene concentrations since they received a near identical 100 kGy dose. The hydrogen sample possessed almost no vinyl while the nitrogen and air sample had approximately equal amounts. The vinyl is formed via the photodecomposition of

ketones via reaction (4.3). The hydrogen sample showed very little oxidation, whereas the nitrogen sample had some and the air sample had the most oxidation.

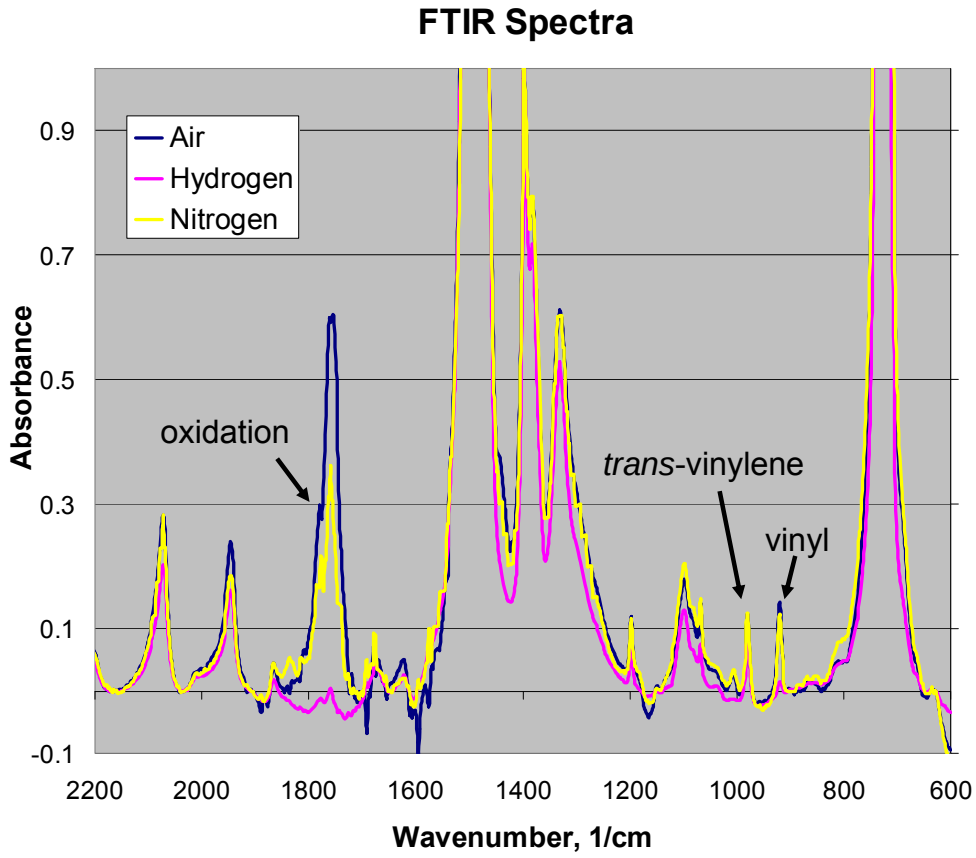

Figure 49. FTIR spectra after unfiltered photoirradiation in different environments. Please note that the hydrogen sample was photoirradiated for half the time (10 hours) and at a higher power than the other two samples. Spectra were baseline corrected and normalized to the 1330 1/cm peak.

7.4 Discussion

7.4.1 Higher Order Polyenyl Radical EPR Spectra

From Figure 39 through Figure 41 it is clear that the EPR spectra starts as a mostly alkyl sextet and evolves into a mostly dienyl singlet with 9 G hyperfine separation. Upon increased photoirradiation, the hyperfine structure is slowly lost

until only a smooth singlet remains. A similar, but slower, progression is seen in a hydrogen environment. From the UV spectra, Figure 42 through Figure 45, it is clear that during photoirradiation lower order polyenyl radicals are converted to higher order polyenyl radicals and that this process is somewhat suppressed in a hydrogen environment. Therefore, it can be concluded that the loss in hyperfine separation is the result of lower order polyenyl radicals converting to higher order polyenyl radicals. This loss of hyperfine structure likely corresponds to a decrease of the hyperfine coupling constants to a point where their splitting can no longer be resolved[110]. Unfortunately, attempts to accurately simulate the spectra were unsuccessful due to the presence of many species, and accurate simulation parameters for higher order polyenyl radicals could not be determined. It is worthwhile to note that the conversion to higher order polyenyl radicals does not result in a decrease in the overall linewidth of the spectra.

7.4.2 Polyene Unsaturations

One of the first points that requires clarification is the ratio of polyene unsaturations to polyenyl radicals. By comparing the molar absorptivity of the diene unsaturation, ~25,000 L mole^{-1} cm^{-1} [36], to the dienyl radical, 29,000 L mole^{-1} cm^{-1} [89], it seems reasonable to assume that the molar absorptivity for higher order polyenyl radicals should be only moderately higher than their polyene unsaturation counterpart. If this is the case, by comparing Figure 44 and Figure 45, it becomes obvious that there are substantially more free radicals than unsaturation for any given degree of unsaturation. This possibility has already been previously addressed (section 3.2.1), and may be attributed to polyene unsaturations converting to polyenyl

radicals much faster than polyenyl radicals convert to polyene unsaturations. Indeed, aside from the starting diene unsaturation concentration, it may be that there are very few polyene unsaturations. Evidence for this conclusion can be found by examining the oxidation of polyenyl radicals upon exposure to air, Figure 50. Note that upon increasing exposure to air, both the polyenyl radicals and polyene unsaturations decay. The decay of polyenyl radicals is expected, and occurs via the combination with oxygen to form peroxyl radicals. However, the decay of polyene unsaturations is unexpected as unsaturations should be stable upon exposure to air. This effect has been previously observed, and attributed to free radical initiated oxidation of the polyene unsaturations[91]. However, preliminary experiments have shown that UV peaks attributed to polyene unsaturations disappear upon annealing at 150 °C for four hours in a nitrogen environment. Further, it is clear that diene unsaturations do not oxidize upon exposure to air even when free radicals are present (Figure 32). Therefore, the reduction in polyene unsaturations cannot be attributed to their oxidation. A more plausible explanation is that polyenyl radicals have multiple absorption peaks, some of which coincide with polyene unsaturations. Polyene unsaturations are also known to have multiple absorption peaks, a fact which has been attributed to different C=C stretching[154]. This may also be the case for polyenyl radicals. Therefore, it is possible that the seeming decay of polyene unsaturations is, in reality, simply the decay of polyenyl radicals. This does not mean that no polyene unsaturations are present, just that their concentration is significantly lower than initially suspected.

Further support to the assignment of polyene unsaturation absorption to polyenyl radicals can be seen by comparing the change in concentration of trienes to dienyls, tetraenes to tetraenyls, and pentaenes to tetraenyls in Figure 44 and Figure 45, respectively. It is clear that the two curves have similar shapes for both photoirradiated in air or nitrogen, implying that they are, in fact, the same species. This supports the conclusion that both polyene unsaturation and polyenyl radical absorption peaks are due to the same species, i.e. polyenyl radicals.

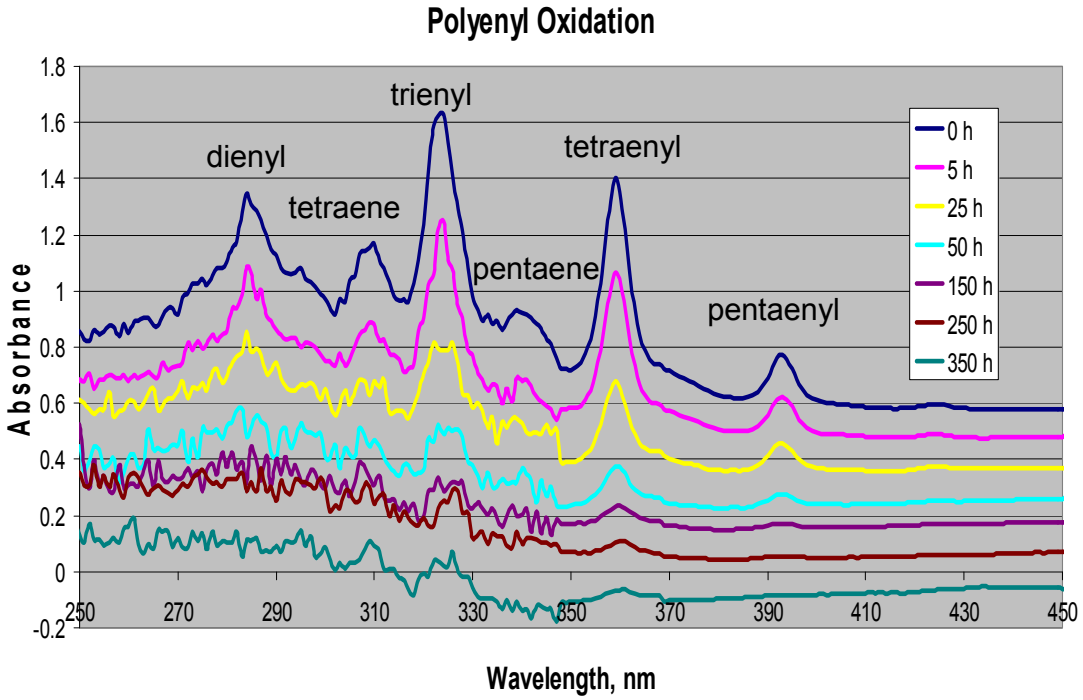

Figure 50. UV spectra showing the decay of polyenyl radicals and polyene unsaturations upon exposure to air. Please note that curves have been offset from each other for clarity.

7.4.3 The Effect of Hydrogen Gas

According to reaction (3.4), in order for the degree of conjugation to increase, free radicals need to recombine intramolecularly. Hydrogen gas, which catalyzes intramolecular movement of radical sites might be expected to increase the rate that

the degree of conjugation increases. However, from Figure 47, it is clear that the opposite is true. The sample photoirradiated in a hydrogen environment had more dienyl and trienyl radicals and less tetraenyl and pentaenyl radicals than samples that received identical photoirradiation in a non-hydrogen environment. Similar results are also seen in Figure 41, where the hydrogen sample has a similar, but slower evolving, EPR spectrum as compared to the non-hydrogen samples. Thus, it is clear that hydrogen gas suppresses, not enhances, the rate that the degree of conjugation increases. This questions the validity of reaction (3.4) as the mechanism for the increase in the degree of conjugation.

Examination of the EPR spectra for the sample photoirradiated in a hydrogen environment, Figure 39 through Figure 41, reveals that it contains more alkyl radicals than the other samples. Since the two outermost peaks of the alkyl radical do not overlap with the polyenyl radical's spectrum, it is possible to accurately track their decay with photoirradiation time by measuring the change in height of those peaks. The decay of the alkyl radical can be seen in Figure 51. An attempt was made to fit the decay to second-order kinetics, (solid lines in Figure 51) but the fit is not good for the first two hours of photoirradiation. Note that the initial decay of the alkyl radicals, almost all of which takes place between the first two hours, closely parallels the overall decay of free radicals, Figure 38. Upon further photoirradiation, the alkyl and overall free radical concentration stays roughly constant. This strongly implies that the alkyl radicals are responsible for majority of the radical decay.

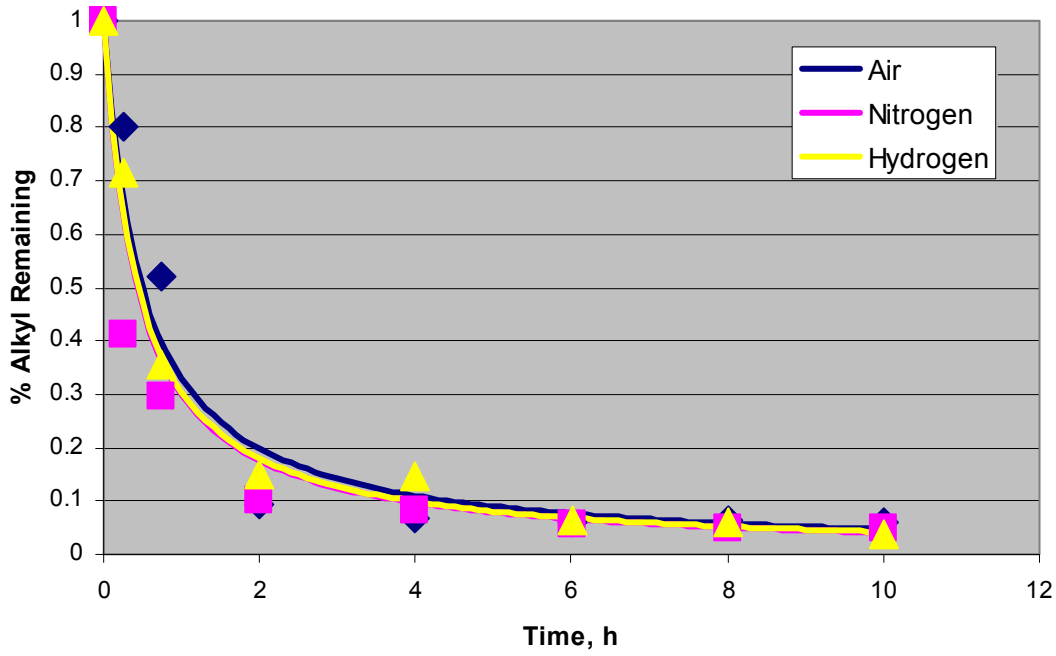

Figure 51. The decay of the alkyl radical in different environments upon continuous photoirradiation from an unfiltered UV lamp. Solid lines are best fit to second-order decay.

In between two to four hours of photoirradiation there are significantly more alkyl radicals in the hydrogen sample. This is also when the hydrogen EPR spectra most strongly differs from the other spectra (Figure 39 through Figure 41). The hydrogen sample also has a higher final free radical concentration than the other samples. An explanation for these results may be as follows. Upon photoirradiation, allyl radicals are quickly converted to alkyl radicals via reaction (3.1). However, due to its close proximity to the unsaturation, the alkyl radical can easily intramolecularly migrate back to the allylic position, reforming the allyl free radical. This back reaction has been readily observed at room temperature[86]. UV light can then reconvert the allyl radical back to an alkyl radical and this process can continue almost indefinitely. Thus, effectively, the alkyl radicals are "trapped" by the unsaturation. In order to escape the trap, the alkyl radical needs to migrate

intermolecularly to another chain after which it will freely be able to continue to migrate and decay by recombining with another radical. Since hydrogen gas increases the rate of intramolecular migration, it effectively increases the efficiency of the unsaturation trap. This results in increased alkyl radical stability. Additionally, since alkyl radicals are escaping the trap more slowly, at any point in time, there are less alkyl radicals that are free to recombine. Therefore, upon escaping, less alkyl radicals decay by recombination as compared to the other samples, resulting in a higher ultimate free radical concentration.

It is also worthwhile to note that there is significantly more diene unsaturations remaining in the hydrogen sample after ten hours of photoirradiation (Figure 47). This difference may be due to its being photoirradiated in an environment that had a lower oxygen content than the air and nitrogen sample. Evidence for this assumption can be seen in Figure 49, where the FTIR spectrum clearly shows that almost no oxidation occurred in the hydrogen sample but not in the nitrogen sample. This difference in environment may be due to difference in sample fabrication (see section 4.1.2). The presence of oxygen may lead to the decay of diene unsaturations since photoexicted diene unsaturation in a triplet state is known to react with oxygen[91]. This could explain the difference in diene unsaturation concentration for the air, nitrogen and hydrogen samples.

7.4.4 Air vs. Nitrogen

Comparison of Figure 42 and Figure 43 with Figure 38 shows that upon unfiltered photoirradiation the overall degree of conjugation of the system increases even though the free radical concentration stays the same. However, reaction (3.4)

predicts that for every degree of increase, the free radical concentration should be halved. It was previously postulated (section 3.2.3) that the free radical concentration would remain constant if there was a constant supply of alkyl radicals and that, in the presence of oxygen, the photodecay of hydroperoxides could supply such a source. Therefore, it was expected that the rate of the increase in the degree of conjugation would be faster in air as compared to in nitrogen. However, from Figure 45 it is clear that there is not a significant difference between the two environments. This implies that alkyl radicals generated from the photodecomposition of hydroperoxides do not play a significant role. This may be because the peroxyl radical is converted back to an alkyl radical and oxygen before it has a chance to abstract an oxygen and become a hydroperoxide (Figure 7). This photoreaction is known to have a quantum efficiency of 0.3 and is, therefore, expected to occur quite readily[85].

As mentioned above (section 3.2.3), another source of alkyl radicals is the photodecay of ketone groups via the Norrish type-I reaction (Figure 7). It is known that at room temperature, the Norrish type-II reaction, which results in a vinyl group and does not generate free radicals, has a significantly higher quantum yield than the Norrish type-I reaction[155]. Since an increase in the degree of conjugation has been observed in photoirradiated samples in which little, if any, vinyl groups were formed, ketones are not likely to be a significant alkyl radical source.

During the first two hours of photoirradiation there are many alkyl radicals, either surviving from the initial irradiation or generated by the photoconversion of allyl radicals. However, a majority of these radicals decay during the first two hours and then their concentration remains approximately constant (Figure 51). Therefore,

these radicals do not likely play a significant role in the increase of the degree of conjugation.

Another possible source of alkyl radicals is the photoconversion of polyenyl radicals into alkyl radicals (reaction 3.3). However, this mechanism is discounted in section 8.4.3.

Overall, this experiment has raised serious doubts about several possible sources of alkyl radicals. Either there is an unconsidered source or the validity of the alkyl radical addition mechanism must be questioned.

7.4.5 One-to-One Conversion

As mentioned above (section 3.2.4), reaction (3.4) should result in a one-to-one conversion of unsaturations to free radicals and vice versa. In practice, the polyene unsaturations appear to be short-lived and quickly convert to polyenyl radicals of the same order. Thus, a one-to-one conversion of lower order to higher order polyenyl radicals is expected. An attempt was made to investigate if a one-to-one conversion can be detected from the UV spectra using two assumptions. It is assumed that the molar absorptivity for polyenyl radicals will follow a similar pattern as the polyene unsaturations. For example, the difference between the molar absorptivity for diene, triene, and tetraene unsaturations is about 17,000 L cm^{-1} $mole^{-1}$ (Table II). The molar absorptivity of the dienyl radical is also 4,000 L cm^{-1} $mole^{-1}$ greater than the molar absorptivity of the diene unsaturation. Therefore, it assumed that the trienyl, tetraenyl, and pentaenyl radicals' molar absorptivity are 46,000, 63,000, and 80,000, L cm^{-1} $mole^{-1}$, respectively.

It is also assumed that no diene unsaturations are created. Two likely pathways for diene unsaturations to be created are the addition of an alkyl radical to an allyl radical and the photodecay of allyl radicals via reaction (3.2). However, these pathways are not expected to be significant. The slow intramolecular addition of an alkyl radical to an allyl radical is not deemed likely due to the fast photoconversion of allyl to alkyl radical via reaction (3.1). As discussed above (section 3.3), reaction (3.1) is expected to be much more important than reaction (3.2) since the allyl radical's molar absorptivity coefficient at 258 nm is 280 times greater than it is at 365 nm.

If all diene unsaturations are consumed to make dienyl radicals (as is assumed in reaction 3.4) and, aside from this increase, the total number of polyenyl radicals does not change, the sum of the concentration of diene unsaturations, dienyl, trienyl, tetraenyl, and pentaenyl radicals should remain constant. Numbers greater than the starting concentration imply that polyenyl radicals are being created, possibly through the conversion of allyl to dienyl radicals (section 8.3.4) or some other, unknown reaction. Numbers smaller than the starting concentration imply that free radicals are recombining and forming non-radical products like crosslinks.

Using the analysis above, the overall concentration of polyenyl radicals can be seen in Figure 52. It is clear that polyenyl radicals are being created during the first few hours of photoirradiation and decaying during later hours. From Figure 51, it is clear that majority of alkyl radicals decay during the first few hours of photoirradiation. Therefore, it is possible that alkyl radicals are decaying into polyenyl radicals through some unknown mechanism other than reaction (3.4).

Alternatively, the alkyl radical decay may be completely due to the formation of crosslinks and not contribute to polyenyl radical formation at all. The formation and decay of polyenyl radicals occurs to a lesser extent when lower UV light fluences are used.

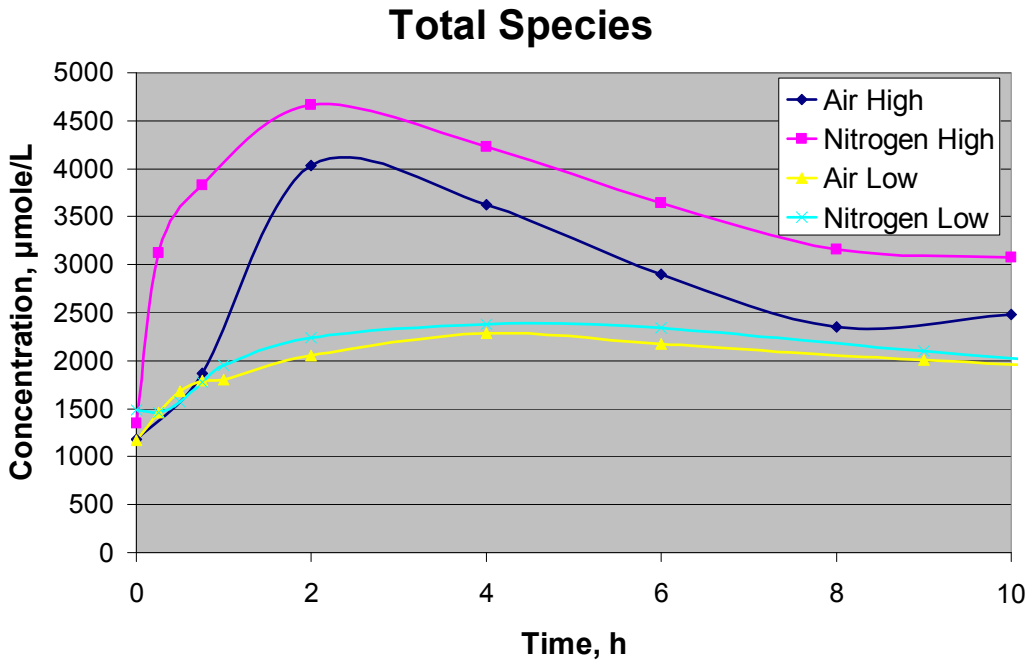

Figure 52. Change in the overall concentration of diene unsaturations and polyenyl radicals upon low and high fluence unfiltered photoirradiation in different environments. Overall concentration was calculated by summing the concentration of diene unsaturations, dienyl, trienyl, tetraenyl, and pentaenyl radicals.

7.5 Conclusion

It has been concluded that, aside from diene, the absorption peaks at wavelengths usually attributed to polyene unsaturations should be assigned to polyenyl radicals. Upon increased photoirradiation, lower order polyenyl radicals convert to higher order polyenyl radicals. The overall concentration of free radicals does not significantly change during this process, which, if reaction (3.4) is correct,

means a continuous supply of alkyl radicals is required. However, the photodecomposition of hydroperoxides and ketones can not be the source.

A one-to-one conversion from lower order to higher order polyenyl radicals was not observed. At short photoirradiation times polyenyl radicals are created while at longer times they are destroyed. However, this statement is based on two assumptions neither of which may be valid.

Overall, the validity of reaction (3.4) as the mechanism for the increase in the degree of conjugation of polyenyl radicals in photoirradiated polyethylene has been brought into serious doubt and other possibilities should be explored.

Chapter 8: Effect of Wavelength of UV Light

8.1 Objectives

In the previous experiment, the validity of reaction (3.4) as the mechanism for the increase in degree of conjugation was questioned. In order to explore the mechanism, monochromatic photoirradiation was performed at specific wavelengths. Irradiation at 235 nm was performed to explore the mechanism for the decrease in diene unsaturation. Irradiation at 258 nm was performed in order to determine the products of the photoconversion of allyl to alkyl radicals. Additionally, photoirradiations at 285 and 323 nm were performed to determine if polyenyl radicals photoconvert to alkyl radicals. Photoirradiations at 275 and 310 nm were performed to determine if these wavelengths play a significant role in the increase in degree of unsaturation. Finally, photoirradiation through a filter that removed wavelengths shorter than 320 nm was also performed to determine if longer wavelengths play a significant role in the increase in degree of conjugation of polyenyl radicals.

8.2 Procedure

200 μm films of UHMWPE were irradiated in a nitrogen environment to a dose of 100 kGy. Unless noted otherwise, the films were then annealed at 100 °C in a nitrogen environment for four hours which dramatically reduced the radical concentration and prevented non-photoinduced radical decay. The films were then subjected to monochromatic photoirradiation by passing the light from the UV lamp through a monochromator. This reduced the amount of transmitted light to levels below what could be detected by the photodetector (<100 $\mu W/cm^2$) and considerably

longer photoirradiation times were required. The wavelengths investigated were 235, 258, 275, 285, 310 and 323 nm corresponding to peak absorbance of diene, allyl, triene, dienyl, tetraene, and trienyl, respectively. Additionally, photoirradiation through a Corning glass filter #3965 was performed to determine the effect of longer wavelengths (>320 nm). For all samples, a non-photoirradiated control was also created to verify that all radical changes were photoinduced. ESR and UV-Vis spectra were taken at various time intervals. All photoirradiations and measurements were performed in a nitrogen environment.

8.3 Results

8.3.1 235 nm

The change in UV spectra upon 68 hours of photoirradiation at 235 nm can be seen in Figure 53. It is clear that some diene unsaturations are consumed and some dienyl radicals are produced during this time. This change is not observed in the non-photoirradiated control. During photoirradiation, a significant change in free radical concentration or EPR spectral shape was not observed.

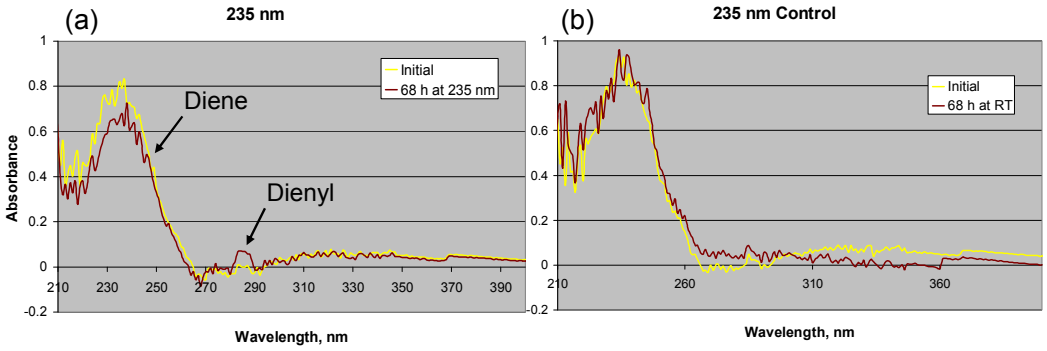

Figure 53. (a) Change in UV spectra after 68 photoirradiation at 235 nm. Note the slight decrease in diene unsaturations and increase in dienyl radical absorbance. (b) Change in the UV spectra

of control sample that received identical electron beam irradiation and thermal history but was not photoirradiated. Note the lack of change in the spectra.

8.3.2 258 nm

The change in UV spectra upon photoirradiation with 258 nm UV light can be seen in Figure 54. During the first 23 hours of photoirradiation there is a decrease in allyl radicals and a small increase in dienyl radicals. It is clear from difference spectra in the inset of Figure 54 that continued photoirradiation leads the creation of more dienyl radicals but not to a further reduction in allyl radicals. During the photoirradiation, there was not a measurable change in the concentration of diene unsaturations.

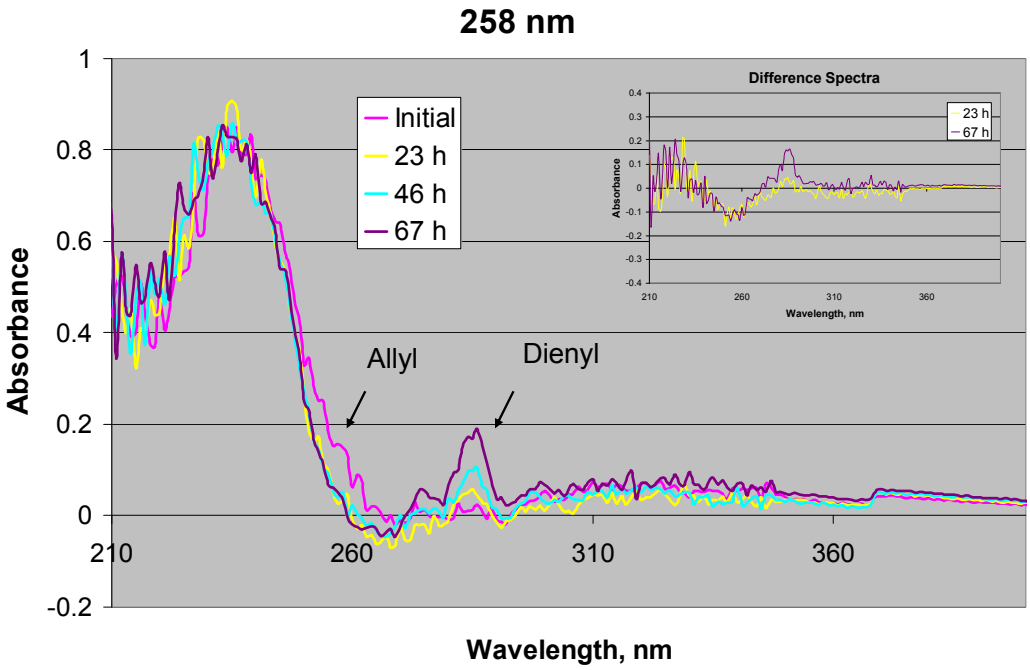

Figure 54. Change in UV spectra upon continuous photoirradiation with 258 nm light. Inset: Difference spectra wherein the UV spectra after 23 and 67 hours of photoirradiation were subtracted from the initial spectra. It is clear that all allyl radical decay occurs in the first 23 hours whereas the dienyl radical concentration continues to increase throughout 67 hours of photoirradiation.

The change in EPR spectra upon photoirradiation with 258 nm UV light can be seen in Figure 55. The gradual development into singlet containing 9 G hyperfine separation can be seen. This spectra has previously (section 5.4.3) been assigned to the dienyl radical. There was not a measurable decrease in free radical concentration throughout the photoirradiation.

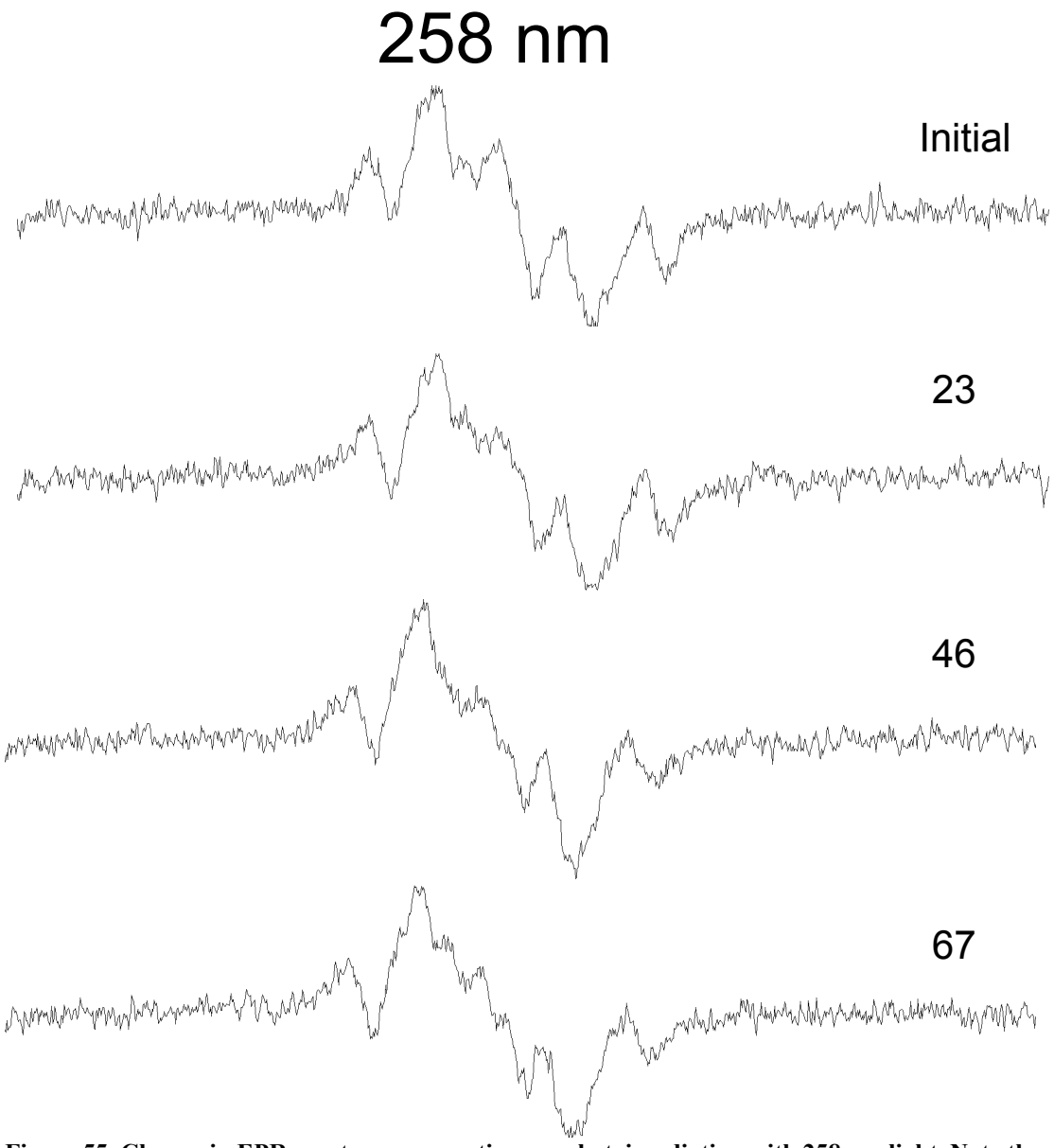

Figure 55. Change in EPR spectra upon continuous photoirradiation with 258 nm light. Note the gradual development of a singlet with 9 G hyperfine separation.

8.3.3 285 and 323 nm

In order to determine if photoirradiation with 285 and 323 nm light creates dienyl and trienyl radicals, respectively, samples that were annealed and contained a low starting free concentration were photoirradiated. The change in UV spectra can be seen in Figure 56. It is clear that no significant changes occur. A similar lack of change was also seen in the EPR spectra (not shown).

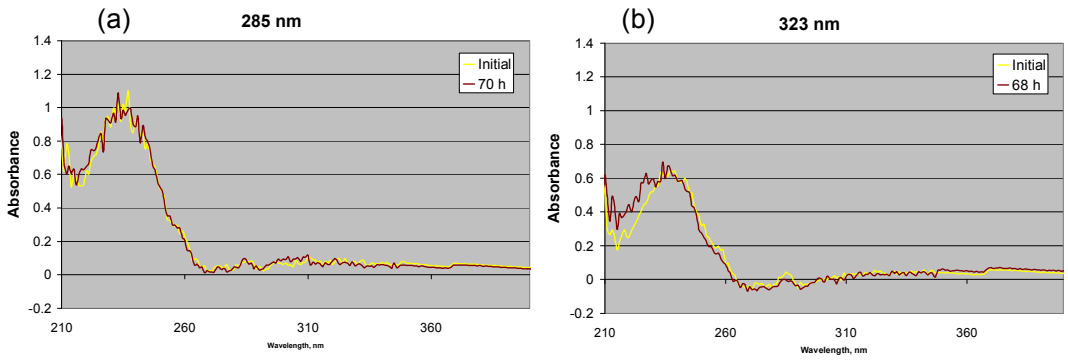

Figure 56. UV spectra before and after a long photoirradiation with (a) 285 and (b) 323 nm light. Note the lack of change in the spectra.

In order to determine if photoirradiation with 285 light causes dienyl radicals to photoconvert to alkyl radicals samples that were not annealed and contained a large starting free concentration were photoirradiated. The change in UV spectra can be seen in Figure 57. It is clear that a measurable amount of decay did not occur.

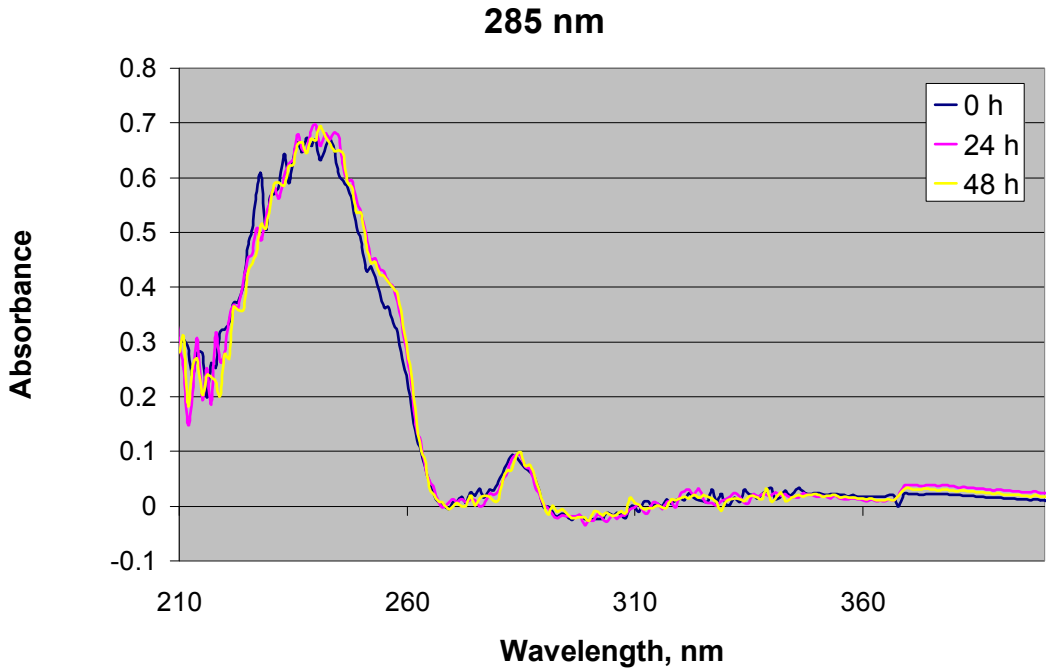

Figure 57. UV spectra of non-annealed sample before and after photoirradiation with 285 nm light.

8.3.4 275 and 310 nm

For both the 275 and 310 nm samples, the samples were not annealed prior to photoirradiation in order to maximize the number of radicals present before photoirradiation. The change in UV spectra after photoirradiation with 275 nm light can be seen in Figure 58. It is clear that allyl radicals are consumed and dienyl radicals are produced. No change in the allyl and dienyl radical concentration could be detected in the control sample, (Figure 59). No change in the spectra could be detected after photoirradiation at 310 nm (data not shown).

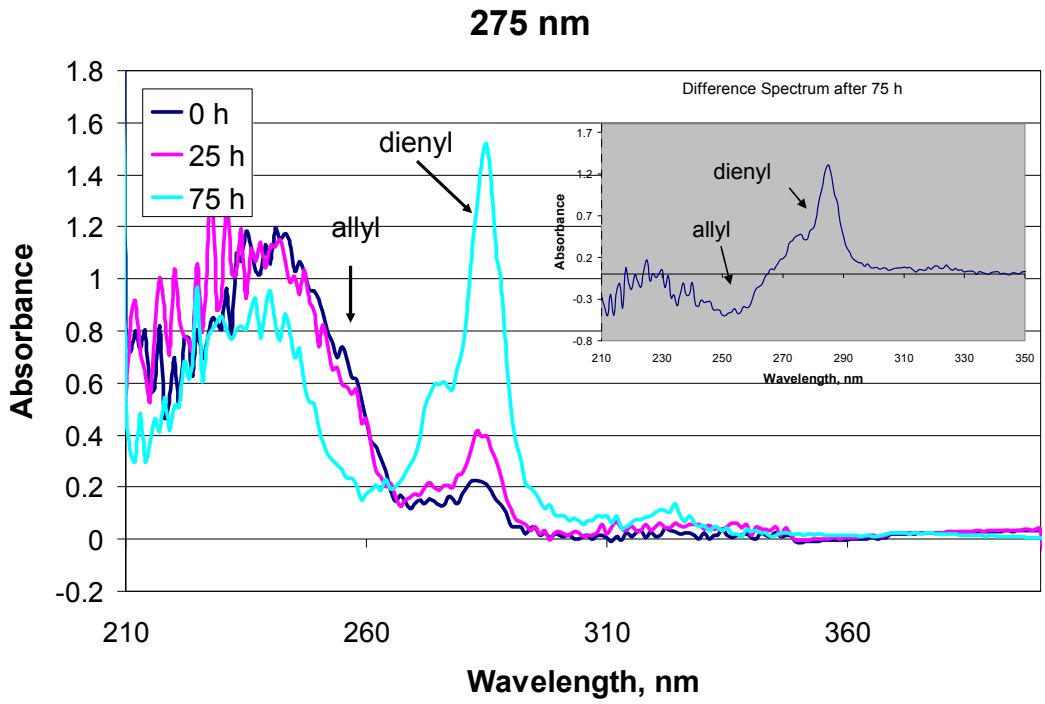

Figure 58. Change in the UV spectra of a non-annealed sample after photoirradiation at 275 nm. A large decrease at 258 nm and increase in 285 nm, corresponding to the allyl and dienyl free radicals, respectively, is seen. Inset: the difference spectra attained by subtracting the initial spectra from the spectra attained after 75 hours of photoirradiation. It is clear that the decrease at lower wavelengths is centered at 258 nm and corresponds to a decrease in allyl radicals and not diene unsaturations which would be centered at 235 nm. Spectra are an average of three scans.

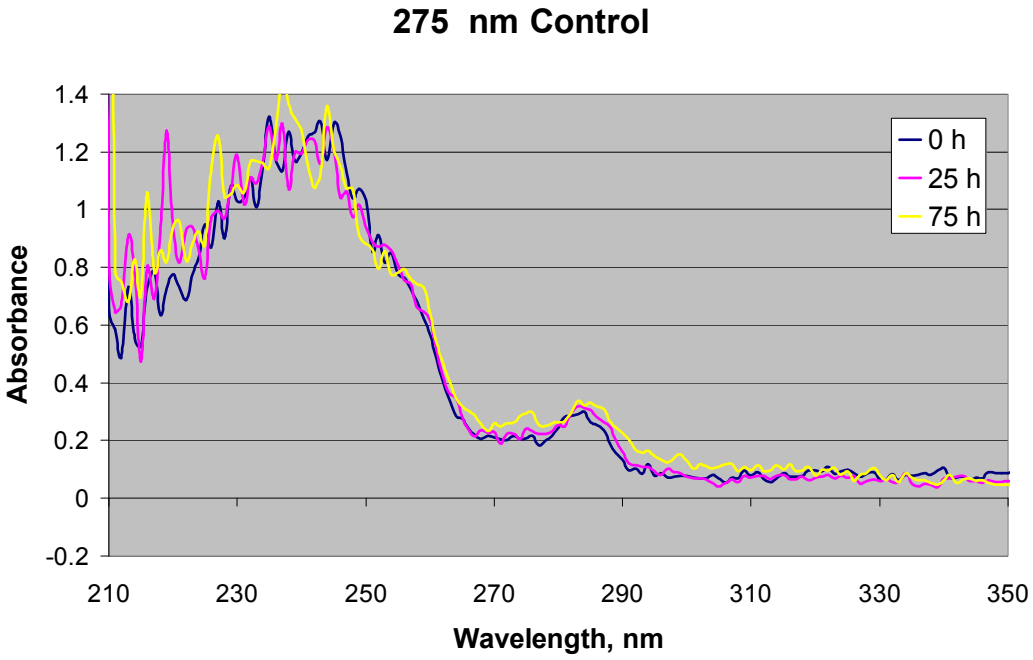

Figure 59. UV spectra of the 275 nm control sample which was electron beam irradiated simultaneously with the photoirradiated sample and then left at room temperature in a nitrogen environment. Note the lack of change in the allyl and dienyl radical concentration. Spectra are an average of three scans.

8.3.5 Longer Wavelengths

The change in the UV spectra upon photoirradiation with light whose wavelength is greater than 320 nm can be seen in Figure 60. The change in EPR spectra has already been shown in Figure 16. It is clear that longer wavelengths do not play a significant role in the photochemistry of polyenyl radicals.

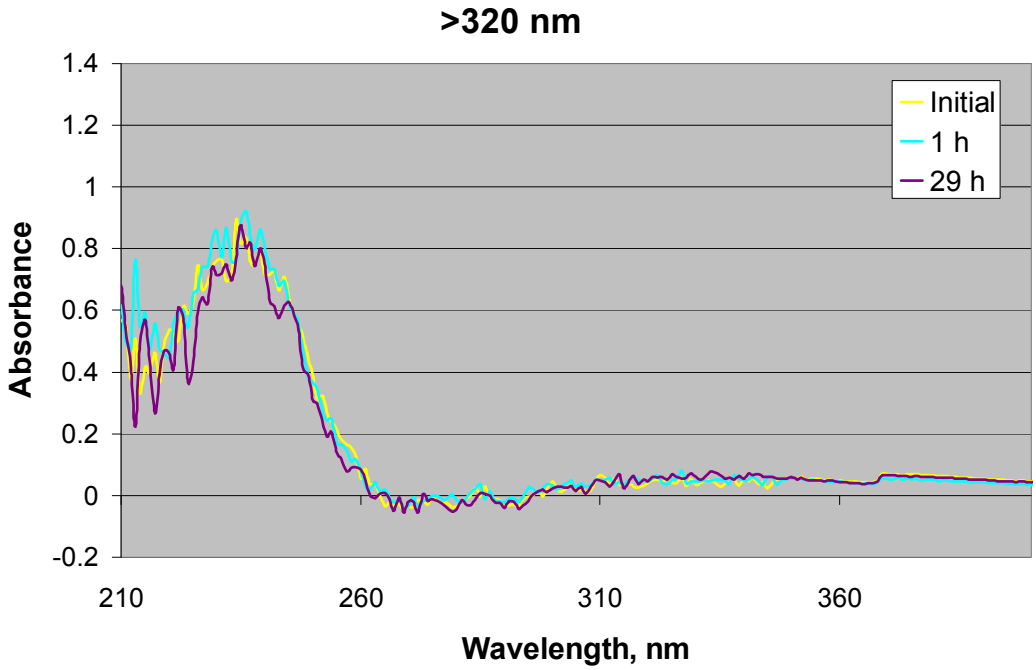

Figure 60. Change in the UV spectra upon photoirradiation with light whose wavelength is greater than 320 nm. Note the lack of change in the spectra.

8.4 Discussion

8.4.1 235 nm

From Figure 53, it is clear that upon photoirradiation with 235 nm light the concentration of diene unsaturations decreases and dienyl free radical concentration increases. This strongly suggests that diene unsaturations are converted into dienyl radicals. However, it is unclear if this conversion is caused by the migration of an alkyl radical to the unsaturation, as suggested in reaction (3.4), or caused directly by the UV light. The fact that this conversion only occurs under photoirradiation suggests the latter.

It is unclear if this mechanism is the sole cause for the decrease in diene unsaturations. Despite an extremely long photoirradiation time, only a slight decrease

in diene unsaturations was observed, although this may simply be the result of low light power exiting the monochromator. Additionally, as mentioned above (section 7.4.5), a quantitative conversion of diene unsaturations to dienyl radicals was not observed. Another possible mechanism for diene unsaturation decay is a reaction with oxygen when in an excited triplet state[91]. This reaction may be the cause for reduced concentration of diene unsaturations in samples that were photoirradiated in air (Figure 47).

8.4.2 258 nm

From Figure 54, it is clear that photoirradiation with light whose wavelength is 258 nm leads to a decrease in the concentration of allyl radicals and an increase in dienyl radicals. However, it seems unlikely that the mechanism for this increase is the photoconversion of allyl radicals to alkyl radicals which then migrate to diene unsaturations, forming dienyl radicals, for two reasons. One, there was not a measurable decrease in the diene unsaturation concentration, although this may be due to the large signal to noise ratio prevalent at lower wavelengths. Two, the concentration of dienyl radicals continued to increase after allyl radicals were no longer photoconverting to alkyl radicals. The delayed increase of dienyl radicals can not be attributed to a delay in the migration of the photoconverted alkyl radicals to diene unsaturations since, in a similar experiment where no further photoirradiation was performed after photoirradiation at 258 nm, it was observed that the concentration of dienyl radicals slightly decreased instead of increasing. Rather, it seems that dienyl radicals are formed only upon photoirradiation with 258 nm light and may be produced directly by UV light.

It is interesting to note that 258 nm light reduced the allyl radical concentration for only the first 23 hours of photoirradiation. This effect cannot be due to the complete consumption of the allyl radical since there is clearly allyl radical still present in the EPR spectra (Figure 55). Comparison of Figure 55 with Figure 17 shows that two outer peaks still remain after photoirradiation with 258 nm light. Comparison of the initial and final spectra in Figure 55 shows that the outer peaks occur at the same location for both spectra and should be attributed to the same radical. Since the initial spectra was taken after a four hour anneal at 100 °C, it is composed of mostly allyl radicals. This conclusion is also supported by the UV spectra (Figure 54). Thus, it would seem that while photoirradiation quickly reduces the allyl radical concentration, it does not entirely eliminate all allyl radicals.

8.4.3 285 and 323 nm

From Figure 56 it is clear that photoirradiation with 285 and 323 nm light does not create dienyl and trienyl radicals. From Figure 57 it appears that 285 nm light does not photoconvert dienyl radicals to alkyl radicals. While it is possible that the lack of observed reduction is due to low light power and quick back-conversion, this is not deemed likely since a noticeable reduction was observed with allyl radicals during a shorter photoirradiation (Figure 54) and lower light power, (Figure 10). While the photoconversion of trienyl and higher order radicals was not experimentally tested, it is reasonable to assume that photoconversion does not occur since they are known to be more stable than the dienyl radical which did not convert.

8.4.4 275 and 310 nm

From Figure 58 it is clear the photoirradiation at 275 nm results in a decrease in allyl and an increase in dienyl radicals. A significant change in the diene unsaturation concentration was not observed at this wavelength. This suggests a direct photoconversion of allyl to dienyl radicals, possibly via the reaction

$$\sim CH_2\text{-}CH_2\text{-}CH_2\text{-}CH{=}CH\text{-}C^{\bullet}H\text{-}CH_2\sim \xrightarrow{275\ nm} \sim CH_2\text{-}CH{=}CH\text{-}CH{=}CH\text{-}C^{\bullet}H\text{-}CH_2\sim + H_2 \quad (8.1)$$

This reaction implies a one-to-one conversion of allyl to dienyl radicals. Indeed, after correcting for differences in the molar absorptivity, comparison of the change in peak height corresponding to the allyl and dienyl radical in the difference spectrum (inset of Figure 58) imply that approximately the same amount of dienyl radical are created as the amount of allyl radicals destroyed. It is interesting to note that the analogous photoconversion of dienyl to trienyl radicals at 310 nm was not observed.

8.5 Conclusion

It was determined that polyenyl radicals do not photoconvert to alkyl radicals upon photoirradiation with UV light of the appropriate wavelength and that polyenyl radicals are not a source of alkyl radicals. Therefore, all likely sources for the supply of alkyl radicals have been investigated and discounted. This questions the validity of reaction (3.4) as the source for the increase in degree of conjugation.

It was determined that dienyl radicals are created upon photoirradiation of 235, 258, and 275 nm light. In all cases, the dienyl radical seemed to be a direct product of UV light and not created by the migration of an alkyl radical to a diene unsaturation. In the first case, a concurrent decrease in diene unsaturations was

observed. Therefore, it is possible that diene unsaturations are converted into dienyl radicals via the absorption of UV light which results in the breaking of the allylic carbon-hydrogen bond. However, the mechanism for the creation of higher order polyenyl radicals remains unclear. It is possible that it involves wavelengths not explored in this study and/or is a multiphotonic process which does not occur during monochromatic photoirradiation or low light fluences. It is clear that wavelengths longer than 320 nm do not play a significant role.

Chapter 9: Summary and Future Work

9.1 Reducing Free Radicals in Surface Irradiated UHMWPE

Overall, sequential thermal and UV treatments are not an effective way to remove free radicals from surface irradiated UHMWPE. While a moderate reduction in free radical concentration can be achieved, it does not have a significant effect on long-term oxidation. The ultimate goal of complete removal of all free radicals can not be achieved because UV light does not convert stable polyenyl radicals into unstable alkyl radicals.

However, this does not mean that the surface irradiation approach to improving wear resistance without decreasing fatigue or oxidation resistance should be abandoned. Rather, an alternate way to remove surface free radicals should be employed. Currently, replacement joint manufacturers are attempting to improve wear resistance without decreasing fatigue or oxidation resistance by incorporating α-tocopherol (Vitamin E), a natural antioxidant, into UHMWPE. Due to poor diffusivity in UHMWPE, α-tocopherol cannot easily be absorbed into molded UHMWPE[156, 157], and is instead mixed in with UHMWPE powder. The α-tocopherol coated powder is then consolidated via compression molding or ram extrusion into bar or sheet stock and gamma or electron beam irradiated. It has been reported[158, 159] that α-tocopherol preferentially reacts with peroxyl radicals and is relatively unreactive with carbon centered free radicals. Thus, it will prevent oxidation but will not significantly suppress crosslinking. α-tocopherol-doped UHMWPE has recently received FDA approval and will begin to be used in replacement joints. However, there are two possible problems with α-tocopherol-doped UHMWPE. One, because α-tocopherol is

introduced before consolidation, it is preferentially located a grain boundaries and may affect the ability of the powder to consolidate effectively. Poor consolidation has previously been attributed to early implant failure[160]. Two, because α-tocopherol only reacts with peroxyl radicals, in order to be effective, high concentrations must remain within the component throughout its entire lifetime. However, the long-term stability of α-tocopherol in UHMWPE is still largely unknown.

An alternate technique that has all of the advantages of surface-only modification and none of the drawbacks of α-tocopherol is the incorporation of an antioxidant, such as nitroxyl, that reacts with carbon centered free radicals into surface irradiated polyethylene. This technique should have many advantages. One, since the bulk of the material remains unmodified, it does not suffer the decrease in fatigue resistance[66] and possible increase in impingement rate[70] associated with crosslinking. Two, since free radicals are located only at the surface, nitroxyl can be diffused in instead of incorporated during consolidation. Thus, it should have no effect on material consolidation. Three, since nitroxyl combines with carbon centered free radicals and thereby eliminates them, long-term out diffusion of the antioxidant will have no effect on oxidation. The preliminary effectiveness of this technique has been accidentally demonstrated in our lab when all the free radicals in 200 μm UHMWPE films that were irradiated to a dose of 100 kGy were eliminated by nitroxyl that was absorbed in the films by being stored for a prolonged time in the same glovebox as UHWMPE samples that contained a high concentration of nitroxyl. My colleague is currently investigating this technique in a more systematic manner.

9.2 Polyenyl Radical Mechanism

It would seem that the alkyl radical addition scheme, reaction (3.4) is not the mechanism for the conversion of lower order to higher order polyenyl radicals. It is clear that this conversion occurs without a significant reduction in free radical concentration. For reaction (3.4) to be valid, this would require a constant supply of alkyl radicals. Several plausible alkyl radical sources were investigated, and none were found to affect the conversion rate. Additionally, reaction (3.4) predicts a one-to-one conversion of lower to higher order polyenyl radicals, which was not observed. However, this measurement is not deemed completely reliable due to difficulties in measuring the diene unsaturation concentration and uncertainties in absorption coefficients.

Creation of dienyl radicals via photoirradiation at 235 and 258 nm was observed. It is believed that dienyl radicals are created directly by UV light and do not involve an alkyl radical intermediate. The creation of higher order polyenyl radicals was not observed during monochromatic radiation. This may be due to low light power, because their creation is a multiphotonic process, or because the appropriate wavelengths were not explored.

Given the above experimental results, I tentatively believe the most likely mechanism for the creation of higher order polyenyl radicals to be the direct conversion from lower order to higher order via the reaction

$$\sim CH_2\text{-}CH_2\text{-}CH_2\text{-}(CH{=}CH\text{-})_n\text{-}C^{\bullet}H\text{-}CH_2\sim \xrightarrow{UV} \sim CH_2\text{-}CH{=}CH\text{-}(CH{=}CH\text{-})_n\text{-}C^{\bullet}H\text{-}CH_2\sim + H_2 \qquad (9.1)$$

There are several observed experimental results that support this reaction. One, it allows for an increase in degree of conjugation without a decrease in the number of

free radicals. Two, it does not involve polyene unsaturations. Three, the fact that hydrogen gas is a product suggests that the presence of hydrogen gas would suppress the reaction. Four, it predicts an increase in conversion rate with increasing light fluence. The fact that higher order polyenyl radical production was severely suppressed at lower light fluences (Figure 45) suggests that reaction (9.1) is a multiphotonic process. Five, its direct analog for the allyl radical was observed to occur at 275 nm. One criticism to this mechanism is that it also predicts a one-to-one conversion from lower to higher order polyenyl radicals which was not observed. However, as discussed above, this observation is not deemed completely reliable. Future work involving bandpass filters that will allow greater light power and range of wavelengths to pass may help confirm or disprove this mechanism. Also, photoirradiation with a well-characterized UV source will allow the determination of the quantum efficiency of the reactions discussed in this dissertation. Additionally, improved UV spectroscopy instrumentation and technique that will allow more accurate measurement of diene unsaturation concentration would be helpful.

Glossary

Arb.- Arbitrary

DSC- Differential Scanning Calorimetry

EPR- Electron Paramagnetic Resonance

FR- Free radical

FTIR- Fourier Transform Infrared

G- Gauss

MCNP5- Monte Carlo N-Particle, version 5

nm- nanometer

SEM- Scanning Electron Microscopy

UHMWPE- Ultrahigh molecular weight polyethylene

μm- micrometer

UV- Ultraviolet

Bibliography

1. Hwang, L. P.; Cheng, J. T. *Journal of Polymer Science Part B-Polymer Physics* **1981,** 19, (6), 983-989.
2. Kubo, S.; Dole, M. *Macromolecules* **1973,** 6, (5), 774-777.
3. Reno, F. F. *Biomaterials* **2006,** 27, (16), 3039.
4. Ingham, E.; Fisher, J. *Biomaterials* **2005,** 26, (11), 1271-1286.
5. Kurtz, S. M.; Muratoglu, O. K.; Evans, M.; Edidin, A. A. *Biomaterials* **1999,** 20, (18), 1659-1688.
6. Kurtz, L., Zhao, Mowat, Ong, and Halpern. *73rd Annual Meeting of the American Academy of Orthopaedic Surgeons* **2006**.
7. Li, S.; Burstein, A. H. *J Bone Joint Surg Am* **1994,** 76, (7), 1080-1090.
8. Connelly, G. M.; Rimnac, C. M.; Wright, T. M.; Hertzberg, R. W.; Manson, J. A. *Journal of Orthopaedic Research* **1984,** 2, (2), 119-125.
9. Livingston, B. J.; Chmell, M. J.; Spector, M.; Poss, R. *J Bone Joint Surg Am* **1997,** 79, (10), 1529-38.
10. Santavirta, S.; Bohler, M.; Harris, W. H.; Konttinen, Y. T.; Lappalainen, R.; Muratoglu, O.; Rieker, C.; Salzer, M. *Acta Orthopaedica Scandinavica* **2003,** 74, (4), 380-388.
11. McKay, G. C.; Macnair, R.; MacDonald, C.; Grant, M. H. *Biomaterials* **1996,** 17, (13), 1339-1344.
12. Rimnac, C. M.; Kurtz, S. M. *Nuclear Instruments & Methods in Physics Research Section B-Beam Interactions with Materials and Atoms* **2005,** 236, 30-37.
13. Naidu, S. H.; Bixler, B. L.; Moulton, M. J. R. *Orthopedics* **1997,** 20, (2), 137-142.
14. Lin, L.; Argon, A. S. *Journal of Materials Science* **1994,** 29, (2), 294-323.
15. Premnath, V.; Harris, W. H.; Jasty, M.; Merrill, E. W. *Biomaterials* **1996,** 17, (18), 1741-1753.
16. Nusbaum, H. J.; Rose, R. M. *J. Biomed. Mater. Res. ; Vol/Issue: 13:4* **1979**, Pages: 557-576.
17. Roe, R. J.; Grood, E. S.; Shastri, R.; Gosselin, C. A.; Noyes, F. R. *Journal of Biomedical Materials Research* **1981,** 15, (2), 209-230.
18. Rimnac, C. M.; Klein, R. W.; Betts, F.; Wright, T. M. *J Bone Joint Surg Am* **1994,** 76, (7), 1052-1056.
19. McKellop, H.; Shen, F.-w.; Lu, B.; Campbell, P.; Salovey, R. *J Bone Joint Surg Am* **2000,** 82, (12), 1708-.
20. Collier, J. P.; Sutula, L. C.; Currier, B. H.; Currier, J. H.; Wooding, R. E.; Williams, I. R.; Farber, K. B.; Mayor, M. B. *Clinical Orthopaedics and Related Research* **1996**, (333), 76-86.
21. Coote, C. F.; Hamilton, J. V.; McGimpsey, W. G.; Thompson, R. W. *Journal of Applied Polymer Science* **2000,** 77, (11), 2525-2542.
22. Currier, B. H.; Currier, J. H.; Mayor, M. B.; Lyford, K. A.; Van Citters, D. W.; Collier, J. P. *The Journal of Arthroplasty* **2007,** 22, (5), 721-731.
23. Bartel, D. L.; Bicknell, V. L.; Wright, T. M. *J Bone Joint Surg Am* **1986,** 68, (7), 1041-1051.

24. Yeom, B.; Yu, Y. J.; McKellop, H. A.; Salovey, R. *Journal of Polymer Science Part a-Polymer Chemistry* **1998,** 36, (2), 329-339.
25. Buchanan, F. J.; White, J. R.; Sim, B.; Downes, S. *Journal of Materials Science-Materials in Medicine* **2001,** 12, (1), 29-37.
26. Lacoste, J.; Carlsson, D. J. *Journal of Polymer Science Part a-Polymer Chemistry* **1992,** 30, (3), 493-500.
27. Goldman, M.; Lee, M.; Gronsky, R.; Pruitt, L. *Journal of Biomedical Materials Research* **1997,** 37, (1), 43-50.
28. Assink, R. A.; Celina, M.; Dunbar, T. D.; Alam, T. M.; Clough, R. L.; Gillen, K. T. *Macromolecules* **2000,** 33, (11), 4023-4029.
29. Daly, B. M.; Yin, J. *Journal of Biomedical Materials Research* **1998,** 42, (4), 523-529.
30. Alam, T. M.; Celina, M.; Collier, J. P.; Currier, B. H.; Currier, J. H.; Jackson, S. K.; Kuethe, D. O.; Timmins, G. S. *Journal of Polymer Science Part a-Polymer Chemistry* **2004,** 42, (23), 5929-5941.
31. Medhekar, V.; Thompson, R. W.; Wang, A.; McGimpsey, W. G. *Journal of Applied Polymer Science* **2003,** 87, (5), 814-826.
32. McKellop, H.; Shen, F. W.; Lu, B.; Campbell, P.; Salovey, R. *Journal of Orthopaedic Research* **1999,** 17, (2), 157-167.
33. Williams, P. A.; Yamamoto, K.; Masaoka, T.; Oonishi, H.; Clarke, I. C. *Tribology Transactions* **2007,** 50, (2), 277 - 290.
34. Muratoglu, O. K.; Bragdon, C. R.; O'Connor, D. O.; Jasty, M.; Harris, W. H.; Gul, R.; McGarry, F. *Biomaterials* **1999,** 20, (16), 1463-1470.
35. Singh, A. *Radiation Physics and Chemistry* **1999,** 56, (4), 375-380.
36. Fallgatter, M. B.; Dole, M. *The Journal of Physical Chemistry* **1964,** 68, (7), 1988-1997.
37. Bhateja, S. K.; Duerst, R. W.; Martens, J. A.; Andrews, E. H. *Polymer Reviews* **1995,** 35, (4), 581 - 659.
38. Ormerod, M. G. *Polymer (England); Vol: 4* **1963**, Pages: 451-7.
39. Bodily, D. M.; Dole, M. *The Journal of Chemical Physics* **1966,** 45, (5), 1433-1439.
40. Dole, M.; Cracco, F. *J. Phys. Chem.* **1962,** 66, (2), 193-201.
41. Clough, R. L. *Journal of Chemical Physics* **1987,** 87, (3), 1588-1595.
42. Waterman, D. C.; Dole, M. *Journal of Physical Chemistry* **1970,** 74, (9), 1913-1922.
43. Dole, M.; Gupta, C.; Gvozdic, N. *Radiation Physics and Chemistry* **1979,** 14, (3-6), 711-720.
44. Fujimura, T.; Hayakawa, N.; Kuriyama, I. *J. Polym. Sci., Polym. Phys. Ed. ; Vol/Issue: 16:5* **1978**, Pages: 945-948.
45. Kusumoto, N.; Yamamoto, T.; Takayana.M. *Journal of Polymer Science Part a-2-Polymer Physics* **1971,** 9, (7), 1173-&.
46. Shimada, S.; Maeda, M.; Hori, Y.; Kashiwabara, H. *Polymer* **1977,** 18, (1), 19-24.
47. Patel, V. M.; Patel, G. N.; Gvozdic, N.; Hsu, C. S.; Dole, M. *Journal of Polymer Science: Polymer Physics Edition* **1978,** 16, (3), 467-484.

48. Dole, M.; Hsu, C. S.; Patel, V. M.; Patel, G. N. *J. Phys. Chem., v. 79, no. 23, pp. 2473-2479* **1975**.
49. Plonka, A. *Journal of Polymer Science Part B-Polymer Physics* **1983,** 21, (7), 1011-1016.
50. Bracco, P.; del Prever, E. M. B.; Cannas, M.; Luda, M. P.; Costa, L. *Polymer Degradation and Stability* **2006,** 91, (9), 2030-2038.
51. Ohnishi, S. I.; Sugimoto, S. I.; Nitta, I. *Journal of Polymer Science Part a-General Papers* **1963,** 1, (2), 605-622.
52. Knahr, K.; Pospischill, M.; Kottig, P.; Schneider, W.; Plenk, H., Jr. *J Bone Joint Surg Br* **2007,** 89-B, (8), 1036-1041.
53. Scott, M.; Morrison, M.; Mishra, S. R.; Jani, S. *Journal of Biomedical Materials Research Part B: Applied Biomaterials* **2005,** 73B, (2), 325-337.
54. Plank, G. R.; Estok, D.; Muratoglu, O. K.; O'Connor, D. O.; Burroughs, B. R.; Harris, W. H. *Journal of Biomedical Materials Research Part B: Applied Biomaterials* **2007,** 80B, (1), 1-10.
55. Wang, A.; Sun, D. C.; Yau, S. S.; Edwards, B.; Sokol, M.; Essner, A.; Polineni, V. K.; Stark, C.; Dumbleton, J. H. *Wear* **1997,** 203-204, 230-241.
56. Kurtz, S. S.; Rimnac, C. M.; Pruitt, L.; Jewett, C. W.; Goldberg, V.; Edidin, A. A. *Biomaterials* **2000,** 21, (3), 283-291.
57. Meyer, R. W.; Pruitt, L. A. *Polymer* **2001,** 42, (12), 5293-5306.
58. Chaki, T. K.; Li, J. C. M. *Journal of Applied Physics* **1984,** 56, (9), 2392-2395.
59. Zhou, J.; Chakravartula, A.; Pruitt, L.; Komvopoulos, K. *Journal of Tribology-Transactions of the Asme* **2004,** 126, (2), 386-394.
60. Harris, W. H. *Clinical Orthopaedics and Related Research* **1995**, (311), 46-53.
61. Davidson, J. A.; Schwartz, G. *Journal of Biomedical Materials Research-Applied Biomaterials* **1987,** 21, (A3), 261-285.
62. Wang, A.; Sun, D. C.; Stark, C.; Dumbleton, J. H. *Wear* **1995,** 181, 241-249.
63. Bartel, D. L.; Rawlinson, J. J.; Burstein, A. H.; Ranawat, C. S.; Flynn, W. F. *Clinical Orthopaedics and Related Research* **1995**, (317), 76-82.
64. Wright, T. M.; Bartel, D. L. *Clinical Orthopaedics and Related Research* **1986**, (205), 67-74.
65. Klapperich, C.; Komvopoulos, K.; Pruitt, L. *Journal of Tribology* **1999,** 121, (2), 394-402.
66. Gencur, S. J.; Rimnac, C. M.; Kurtz, S. M. *Biomaterials* **2006,** 27, (8), 1550-1557.
67. Oral, E.; Malhi, A. S.; Muratoglu, O. K. *Biomaterials* **2006,** 27, (6), 917-925.
68. Puertolas, J. A.; Medel, F. J.; Cegonino, J.; Gomez-Barrena, E.; Rios, R. *Journal of Biomedical Materials Research Part B-Applied Biomaterials* **2006,** 76B, (2), 346-353.
69. Baker, D. A.; Bellare, A.; Pruitt, L. *Journal of Biomedical Materials Research Part A* **2003,** 66A, (1), 146-154.
70. Huo, M. H.; Parvizi, J.; Gilbert, N. F. *J Bone Joint Surg Am* **2006,** 88, (9), 2100-2113.

71. Collier, J. P.; Currier, C. H.; Kennedy, F. E.; Currier, J. H.; Timmins, G. S.; Jackson, S. K.; Brewer, R. L. *Clinical Orthopaedics and Related Research* **2003,** 414, 289-304.
72. Wannomae, K. K.; Bhattacharyya, S.; Freiberg, A.; Estok, D.; Harris, W. H.; Muratoglu, O. *The Journal of Arthroplasty* **2006,** 21, (7), 1005-1011.
73. Jacobs, C. A.; Christensen, C. P.; Greenwald, A. S.; McKellop, H. *J Bone Joint Surg Am* **2007,** 89, (12), 2779-2786.
74. Zhou, J.; Chakravartula, A.; Pruitt, L.; Komvopoulos, K. *Journal of Tribology* **2004,** 126, (2), 386-394.
75. Grobbelaar, C. J.; Duplessis, T. A.; Marais, F. *Journal of Bone and Joint Surgery-British Volume* **1978,** 60, (3), 370-374.
76. Muratoglu, O. K.; Bragdon, C. R.; O'Connor, D. O.; Jasty, M.; Harris, W. H. *Journal of Arthroplasty* **2001,** 16, (2), 149-160.
77. Edidin, A. A.; Pruitt, L.; Jewett, C. W.; Crane, D. J.; Roberts, D.; Kurtz, S. M. *Journal of Arthroplasty* **1999,** 14, (5), 616-627.
78. Jasty, M.; Rubash, H. E.; Muratoglu, O. *Journal of Arthroplasty* **2005,** 20, (4), 55-58.
79. Wang, A. *Wear* **2001,** 248, (1-2), 38-47.
80. D'Antonio, J. A.; Manley, M. T.; Capello, W. N.; Bierbaum, B. E.; Ramakrishnan, R.; Naughton, M.; Sutton, K. *Clinical Orthopaedics and Related Research* **2005**, (441), 143-150.
81. Dorr, L. D.; Wan, Z. N.; Shahrdar, C.; Sirianni, L.; Boutary, M.; Yun, A. *Journal of Bone and Joint Surgery-American Volume* **2005,** 87A, (8), 1816-1821.
82. Bragdon, C. R.; Barrett, S.; Martell, J. M.; Greene, M. E.; Malchau, H.; Harris, W. H. *Journal of Arthroplasty* **2006,** 21, (7), 935-943.
83. Engh, C. A.; Stepniewski, A. S.; Ginn, S. D.; Beykirch, S. E.; Sychterz-Terefenko, C. J.; Hopper, R. H. *Journal of Arthroplasty* **2006,** 21, (6), 17-25.
84. Currie, C. L.; Ramsay, D. A. *The Journal of Chemical Physics* **1966,** 45, (2), 488-491.
85. Vasilenko, V. V.; Klinshpont, E. R.; Milinchuk, V. K. *High Energy Chemistry* **1976,** 10, (5), 378-381.
86. Ohnishi, S. I.; Nitta, I.; Sugimoto, S. I. *Journal of Chemical Physics* **1963,** 39, (10), 2647-2653.
87. Shimada, S.; Kashiwab.H; Sohma, J. *Journal of Polymer Science Part a-2-Polymer Physics* **1970,** 8, (8), 1291-1302.
88. Melnikov, M. Y. *International Journal of Polymeric Materials* **1996,** 32, (1-4), 1-62.
89. Waterman, D. C.; Dole, M. *Journal of Physical Chemistry* **1970,** 74, (9), 1906-1912.
90. Lawton, E. J.; Balwit, J. S.; Powell, R. S. *The Journal of Chemical Physics* **1960,** 33, (2), 405-412.
91. Vasilenko, V. V.; Klinshpont, E. R.; Milinchuk, V. K. *High Energy Chem., v. 8, no. 3, pp. 227-231; Translated from Khim. Vys. Energ.;8: No. 3, 273-278(1974)* **1974**.
92. Shimada, S.; Hori, Y.; Kashiwabara, H. *Polymer* **1977,** 18, (1), 25-31.

93. Bracco, P.; Brunella, V.; Luda, M. P.; Zanetti, M.; Costa, L. *Polymer* **2005,** 46, (24), 10648-10657.
94. Jones, R. A.; Salmon, G. A.; Ward, I. M. *Journal of Polymer Science Part B: Polymer Physics* **1993,** 31, (7), 807-819.
95. Jafri, J. A.; Phillips, D. H. *Journal of the American Chemical Society* **2002,** 112, (7), 2586-2590.
96. Tsuji, K. *Polymer-Plastics Technology and Engineering* **1977,** 9, (1), 1-86.
97. Costa, L.; Luda, M. P.; Trossarelli, L. *Polymer Degradation and Stability* **1997,** 58, (1-2), 41-54.
98. Tsuji, K. *Journal of Polymer Science Part a-Polymer Chemistry* **1973,** 11, (2), 467-484.
99. Pergushov, V. I.; Melnikov, M. Y. *High Energy Chemistry* **1995,** 29, (3), 185-188.
100. Melnikov, M. Y.; Seropegina, E. N. *International Journal of Polymeric Materials* **1996,** 31, (1-4), 41-93.
101. Tsuji, K.; Seiki, T. *Polymer Journal* **1971,** 2, (5), 606-&.
102. Muratoglu, O. K.; O'Connor, D. O.; Bragdon, C. R.; Delaney, J.; Jasty, M.; Harris, W. H.; Merrill, E.; Venugopalan, P. *Biomaterials* **2002,** 23, (3), 717-724.
103. O'Neill, P.; Birkinshaw, C.; Leahy, J. J.; Barklie, R. *Polymer Degradation and Stability* **1999,** 63, (1), 31-39.
104. Johnson, D. R.; Wen, W. Y.; Dole, M. *Journal of Physical Chemistry* **1973,** 77, (18), 2174-2179.
105. Durant, J.; Jahan, M. S. *Nuclear Instruments & Methods in Physics Research Section B-Beam Interactions with Materials and Atoms* **2005,** 236, 160-165.
106. Kuzuya, M.; Kondo, S.; Sugito, M.; Yamashiro, T. *Macromolecules* **1998,** 31, (10), 3230-3234.
107. Naheed, N.; Jahan, M. S.; Ridley, M. *Nuclear Instruments & Methods in Physics Research Section B-Beam Interactions with Materials and Atoms* **2003,** 208, 204-209.
108. Jahan, M. S.; Fuzail, M. *Nuclear Instruments & Methods in Physics Research Section B-Beam Interactions with Materials and Atoms* **2007,** 265, (1), 67-71.
109. Jahan, M. S.; Stovall, J. C.; King, M. C. *Nuclear Instruments & Methods in Physics Research Section B-Beam Interactions with Materials and Atoms* **2001,** 185, 323-327.
110. Ohnishi, S. I.; Ikeda, Y.; Sugimoto, S. I.; Nitta, I. *Journal of Polymer Science* **1960,** 47, (0149), 503-507.
111. Hori, Y.; Shimada, S.; Kashiwabara, H. *Polymer* **1977,** 18, (6), 567-572.
112. Jahan, M. S.; Durant, J. *Nuclear Instruments & Methods in Physics Research Section B-Beam Interactions with Materials and Atoms* **2005,** 236, 166-171.
113. Auerbach, I. *Polymer (England); Vol: 7* **1966**, Pages: 283-92.
114. Bodily, D. M.; Dole, M. *Journal of Chemical Physics* **1966,** 44, (7), 2821-2822.
115. Tsuji, K.; Seiki, T. *Polymer Journal* **1971,** 2, (5), 606-622.
116. Bohlmann, F. *Angewandte Chemie* **1953,** 65, (15), 385-389.
117. Lawton, E. J.; Balwit, J. S.; Powell, R. S. *Journal of Polymer Science* **1958,** 32, (125), 257-275.

118. Dole, M.; Fallgatter, M. B.; Katsuura, K. *The Journal of Physical Chemistry* **1966,** 70, (1), 62-70.
119. Lacoste, J.; Carlsson, D. J.; Falicki, S.; Wiles, D. M. *Polymer Degradation and Stability* **1991,** 34, (1-3), 309-323.
120. Dole, M.; Milner, D. C.; Williams, T. F. *Journal of the American Chemical Society* **1958,** 80, (7), 1580-1588.
121. Waterman, D. C.; Dole, M. *The Journal of Physical Chemistry* **1971,** 75, (26), 3988-3992.
122. Muratoglu, O. K.; Harris, W. H. *Journal of Biomedical Materials Research* **2001,** 56, (4), 584-592.
123. Fujimura, T.; Hayakawa, N.; Kuriyama, I. *Journal of Applied Polymer Science* **1982,** 27, (11), 4093-4100.
124. Kang, H. Y.; Saito, O.; Dole, M. *Journal of the American Chemical Society* **1967,** 89, (9), 1980-1986.
125. Cracco, F.; Dole, M.; Arvia, A. J. *Journal of Chemical Physics* **1962,** 37, (10), 2449-2457.
126. Jones, R. A. *Radiation Physics and Chemistry* **1999,** 53, (1), 19-23.
127. Chisholm, M. J.; Hopkins, C. Y. *Journal of Organic Chemistry* **1962,** 27, (9), 3137-3139.
128. Tidjani, A.; Arnaud, R. *Polymer Degradation and Stability* **1993,** 39, (3), 285-292.
129. Carlsson, D. J.; Brousseau, R.; Zhang, C.; Wiles, D. M. *Polymer Degradation and Stability* **1987,** 17, (4), 303-318.
130. Costa, L.; Luda, M. P.; Trossarelli, L.; del Prever, E. M. B.; Crova, M.; Gallinaro, P. *Biomaterials* **1998,** 19, (15), 1371-1385.
131. Harrick, N. J. *Applied Spectroscopy* **1977,** 31, (6), 548-549.
132. Medel, F. J.; Garcia-Alvarez, F.; Gomez-Barrena, E.; Puertolas, J. A. *Polymer Degradation and Stability* **2005,** 88, (3), 435-443.
133. Sobieraj, M. C.; Kurtz, S. M.; Rimnac, C. M. *Biomaterials* **2005,** 26, (33), 6430-6439.
134. Hullihen, K. *Industrial & Engineering Chemistry Research* **2006,** 45, (18), 6095-6098.
135. Partridge, R. H. *Journal of Chemical Physics* **1966,** 45, (5), 1679-1684.
136. Tsuji, K.; Nagata, H. *Journal of Polymer Science Part a-Polymer Chemistry* **1973,** 11, (4), 897-900.
137. Lundberg, L.; Sjonell, Y.; Stenberg, B.; Terselius, B.; Jansson, J. F. *Polymer Testing* **1994,** 13, (5), 441-459.
138. Pruitt, L.; Bailey, L. *Polymer* **1998,** 39, (8-9), 1545-1553.
139. Costa, L.; Luda, M. P.; Trossarelli, L. *Polymer Degradation and Stability* **1997,** 55, (3), 329-338.
140. Ohnishi, S.; Ikeda, Y.; Kashiwagi, M.; Nitta, I. *Polymer* **1961,** 2, (2), 119-141.
141. Jahan, M. S.; McKinny, K. S. In *Radiation-sterilization and subsequent oxidation of medical grade polyethylene: an ESR study*, 1999; Elsevier Science Bv: 1999; pp 207-212.
142. Hori, Y.; Shimada, S.; Kashiwabara, H. *Polymer* **1977,** 18, (11), 1143-1148.

143. Bally, T.; Hrovat, D. A.; Borden, W. T. *Physical Chemistry Chemical Physics* **2000,** 2, (15), 3363-3371.
144. Pruitt, L.; Ranganathan, R. *Materials Science & Engineering C-Biomimetic Materials Sensors and Systems* **1995,** 3, (2), 91-93.
145. Currier, J. H.; Duda, J. L.; Sperling, D. K.; Collier, J. P.; Currier, B. H.; Kennedy, F. E. *Proceedings of the Institution of Mechanical Engineers Part H-Journal of Engineering in Medicine* **1998,** 212, (H4), 293-302.
146. McKellop, H.; Shen, F.-w.; Lu, B.; Campbell, P.; Salovey, R. *J Bone Joint Surg Am* **2000,** 82, (12), 1708-1725.
147. Brunella, V.; Bracco, P.; Carpentieri, I.; Paganini, M. C.; Zanetti, M.; Costa, L. *Polymer Degradation and Stability* **2007,** 92, (8), 1498-1503.
148. Carlsson, D. J.; Dobbin, C. J. B.; Jensen, J. P. T.; Wiles, D. M. *Acs Symposium Series* **1985,** 280, 359-371.
149. Ohnishi, S.; Sugimoto, S.; Nitta, I. *The Journal of Chemical Physics* **1962,** 37, (6), 1283-1288.
150. Charlesby, A.; Libby, D.; Ormerod, M. G. *Proceedings of the Royal Society of London. Series A, Mathematical and Physical Sciences* **1961,** 262, (1309), 207-218.
151. McMillen, D. F.; Golden, D. M. *Annual Review of Physical Chemistry* **1982,** 33, (1), 493-532.
152. Goldman, M.; Gronsky, R.; Ranganathan, R.; Pruitt, L. *Polymer* **1996,** 37, (14), 2909-2913.
153. Wuensche, P.; Limburg, J.; Roth, H. K. *Journal of Macromolecular Science, Part B: Physics* **1983,** 22, (2), 169 - 183.
154. Bodily, D. M.; Dole, M. *Journal of Chemical Physics* **1966,** 45, (5), 1428-1432.
155. Hartley, G. H.; Guillet, J. E. *Macromolecules* **1968,** 1, (2), 165-170.
156. Oral, E.; Wannomae, K. K.; Hawkins, N.; Harris, W. H.; Muratoglu, O. K. *Biomaterials* **2004,** 25, (24), 5515-5522.
157. Wolf, C.; Maninger, J.; Lederer, K.; Fruhwirth-Smounig, H.; Gamse, T.; Marr, R. *Journal of Materials Science-Materials in Medicine* **2006,** 17, (12), 1323-1331.
158. Costa, L.; Brach, E. M.; Bracco, P.; Luda, M. P., Stabilisation of UHMWPE with Vitamin E. In University of Torino, 2005; pp 148-156.
159. Ridley, M. D.; Jahan, M. S. *Nuclear Instruments and Methods in Physics Research Section B: Beam Interactions with Materials and Atoms* **2007,** 265, (1), 62-66.
160. Wrona, M.; Mayor, M. B.; Collier, J. P.; Jensen, R. E. *Clinical Orthopaedics and Related Research* **1994**, (299), 92-103.